Haptic Rendering with Series Elastic Actuation: Effects of Filtering on Passivity and Fidelity of Kinesthetic Haptic Feedback

by

Özgür Taylan Kenanoğlu

Submitted to
the Graduate School of Engineering and Natural Sciences
in partial fulfillment of
the requirements for the degree of
Master of Science

SABANCI UNIVERSITY

December, 2023

Haptic Rendering with Series Elastic Actuation:
Effects of Filtering on Passivity and Fidelity of Kinesthetic Haptic Feedback

Özgür Taylan Kenanoğlu

Mechatronics Engineering, M.Sc. Thesis, 2023

Thesis Supervisor: Prof. Volkan Patoglu

Keywords: Physical human-robot interaction, series elastic actuation, velocity-sourced impedance control, haptic rendering, passivity, low-pass filtering, physical realization.

Abstract

Synergistically combining the adaptable decision-making capacity of humans with the productivity of robots, systems featuring physical human-robot interaction (pHRI) have become an indispensable component of several fields, such as surgical, rehabilitation, and service robotics, while also finding widespread uses in manufacturing, agriculture, and entertainment industries. pHRI systems are required to provide high interaction performance while ensuring the safety of the user. However, there exists a fundamental trade-off between the stability robustness and kinesthetic haptic rendering fidelity of interaction controllers.

One commonly used approach to relax coupled stability conditions during physical interactions is to intentionally introduce a compliant element between the actuator and the interaction point. The interaction control paradigm, called series elastic actuation (SEA), can be implemented by complementing such a plant with a compliant power transmission with a closed-loop force controller that relies on the model of the compliant element. A cascaded controller, called velocity-sourced impedance controller (VSIC), is commonly utilized for the closed-loop force control of SEA, to achieve natural and responsive interactions. VSIC is preferred due to its easy-to-tune controllers that can ensure robust performance while rendering a wide range of virtual environments (VEs).

In this thesis, we study the effects of utilization of filters on the stability robustness, and kinesthetic haptic rendering performance of SEA under VSIC and investigate the underlying trade-offs while rendering linear VE models. We analyze the stability robustness by deriving the necessary and sufficient conditions for

the passivity of, while we study the fidelity of haptic rendering by deriving passive physical equivalents of closed-loop control of SEA under VSIC. We explore the underlying trade-offs through rigorous comparisons of the passivity bounds and physical equivalents of SEA under VSIC, with and without filters.

We explore the effects of three distinct uses of filters during haptic rendering of VEs wıth SEA under VSIC; (i) to attenuate high-frequency sensor noise, (ii) to serve as a compensator to improve the phase response of the system, and (iii) to shape the dynamics of the reference model to ensure its trackability and causality by introducing high-frequency roll-off characteristics.

We study the use of filters to attenuate high-frequency sensor noise by introducing a low-pass filter to the motor feedback of the inner motion control loop of VSIC while rendering linear springs with SEA. If motor velocity is measured by an analog sensor, the low-pass filter attenuates the sensor noise. On the other hand, if the motor position is measured by a digital encoder, the low-pass filter not only attenuates the quantization noise amplified by differentiation but also ensures the causality of numerical differentiation. Our results indicate that the passivity of the system is not negatively affected by the noise attenuation, while haptic rendering performance is improved since low-pass filtering decreases parasitic damping effects; hence, enhances the spring rendering performance. On the other hand, if the actuator velocity feedback of the inner motion controller is low-pass filtered, then the force controller should also feature compensators with noise attenuation properties.

Next, we analyze the effect of utilizing lag or lead compensators in the force control loop during spring rendering with SEA under VSIC. Through comparisons of passive physical equivalents, we show that the utilization of lag compensators can increase the spring rendering performance by decreasing the parasitic damping effects, while the utilization of lead compensators increases such parasitic effects. However, the range of passively renderable stiffnesses is decreased for both lead and lag compensators, compared to using proportional controllers. Therefore, the trade-off between the passivity bounds and rendering performance improvement should be considered while utilizing lag compensation in the force control loop.

Finally, we study the effects of filtering in shaping of the reference impedance models, consisting of linear combinations of ideal mass-spring-damper elements, to ensure their causality and trackability by the closed-loop system with a finite

bandwidth. Our results indicate that introducing a properly chosen high-frequency roll-off to the reference stiffness model improves spring rendering performance without negatively affecting the passivity bounds. Similarly, the addition of high-frequency roll-offs to reference viscous damping and mass models not only ensures causality of these reference impedances but also enables passive rendering of virtual damping and passive compensation of virtual masses, significantly extending what is possible without such filters.

The passivity conditions for viscous damping and mass rendering indicate that there exist tight upper and lower bounds on such passively renderable impedances. While utilizing a reference impedance model of an ideal mass, the passively renderable minimum mass is bounded by the mass of the plant. However, it becomes possible to further decrease this limit by adding positive damping to the reference model. While utilizing a reference impedance model consisting of a parallel mass-damper, a negative damping term can be used in the reference model to compensate for the system damping, while enabling higher maximum passively renderable mass levels. Similarly, a negative mass term can be used in the reference model to compensate for the system mass, enabling reference models with higher viscous damping, increasing the limit for maximum passively renderable damping levels. Furthermore, while rendering viscous damping or mass-damper models, a decrease in the cut-off frequency of the reference model relaxes the passivity conditions; however, this also causes a decrease in the haptic rendering performance.

In general, our results indicate that utilizing filters has a significant effect on the stability robustness-rendering performance trade-off of SEA. It is recommended to use low-pass filtering in the inner motion controller together with a force controller introducing sufficient lag characteristics to minimize parasitic damping while rendering virtual stiffness, at the cost of introducing a lower bound to the passively renderable stiffness levels. Shaping the reference impedance model to feature a high-frequency roll-off is not only recommended but also is often necessary, to ensure passivity, for instance, during pure mass or viscous damping rendering. While the range of passively renderable damping and mass levels increase with more aggressive cut-off frequencies of the reference shaping filter, the cut-off frequency should be also carefully selected to properly balance the trade-off between the conservativeness of the passivity bounds and the haptic rendering performance.

All our theoretical results are validated through systematic experimental verifications of coupled stability and characterizations of kinesthetic haptic rendering performance. We further demonstrate the effects of filtering on the kinesthetic haptic rendering performance of humans through a psychophysics experiment.

Overall, this study helps achieve a comprehensive understanding of the effects of filtering on the stability robustness-rendering performance trade-off of haptic rendering with SEA. Our results may guide researchers in pHRI to make more informed decisions about the use of filters in haptic rendering applications; to attenuate noise, to enhance system performance, and/or to roll-off high-frequency content of the reference signals.

Özgür Taylan Kenanoğlu

Mekatronik Mühendisliği, Yüksek Lisans Tezi, 2023

Tez Danışmanı: Prof. Dr. Volkan Patoğlu

Anahtar kelimeler: Fiziksel insan-robot etkileşimi, seri elastik eyleme, hız kaynaklı empedans kontrolü, dokunsal algı yaratma, pasiflik, alçak geçiş filtrelemesi, fiziksel gerçekleştirme.

Özet

Robotik sistemlerin yüksek üretkenliği ile insanların yüksek adaptasyona sahip karar verme yeteneklerini sinerji ile birleştiren fiziksel insan-robot etkileşimi (fİRE) ameliyat, rehabilitasyon ve hizmet robotik sistemlerinin yapı taşlarından birisi haline gelmiş ve üretim, tarım ve eğlence sektörlerininde de yer edinmiştir. fİRE sistemleri hem yüksek etkileşim performansına sahip olmalı hem de etkileşim sürecinde insanın güvenliğini sağlamalıdır. Ancak, fİRE sistemlerinin gürbüz kararlılığı ile dokunsal algı yaratma performansı arasında temel ödenleşimler mevcuttur.

Fiziksel etkileşimler sırasında kararlılık koşullarını gevşetmek için yaygın olarak kullanılan bir yöntem, eyleyici ile etkileşim noktası arasına kasıtlı olarak esnek bir eleman eklemektir. Seri elastik eyleme (SEE) olarak adlandırılan etkileşim kontrolü yaklaşımı, bu tür bir esnek eleman üzerindeki kuvvetin ölçülmesine ve esnekliğin modelini kullanan geri-beslemeli bir kuvvet kontrolcüsüne dayanır. Hız kaynaklı empedans kontrolörü (HKEK) adı verilen çok kademeli bir denetleyici SEE'nin kuvvet geri-beslemeli kontrolünde doğal etkileşimler elde etmek için yaygın olarak kullanılır. HKEK, çok çeşitli sanal dinamikler (SD) için güçlü performans sağlayabilmesi ve kontrolcü kazançlarının kolay belirlenebilmesi nedeniyle tercih edilmektedir.

Bu tezde, filtre kullanımının HKEK altındaki SEE'nin gürbüz kararlılığı ve dokunsal algı yaratma performansı üzerindeki etkilerini inceliyor ve doğrusal SD modellerinin uygulanmasındaki temel ödünleşimleri araştırıyoruz. HKEK altındaki SEE'nin kapalı-döngü pasif fiziksel gerçekleştirmelerini türeterek, dokunsal algı yaratma performanslarını incelerken, sistemin pasifliği için gerekli ve yeterli koşul-

ları hesaplayarak, kararlılığın gürbüzlüğünü analiz ediyoruz. HKEK altındaki SEE'nin filtreli ve filtresiz koşullardaki pasiflik sınırlarının ve pasif fiziksel gerçekleştirmelerinin titiz karşılaştırmalarıyla temel ödünleşimleri belirliyoruz.

HKEK altındaki SEE ile SD'nin dokunsal algısının yaratılması sırasında filtrelerin üç farklı kullanımının etkilerini araştırıyoruz; (i) yüksek frekanslı sensör gürültüsünü azaltma, (ii) sistemin faz tepkisini iyileştirmek için bir kontrolcü olarak kullanma ve (iii) izlenebilirliği ve nedenselliği sağlamak için referans modelin yüksek frekans dinamiklerini şekillendirme.

İlk olarak SEE ile doğrusal sanal yay algısı yaratmak için, HKEK'in iç hareket kontrol geri-besleme sinyalindeki sensör gürültüsünü azaltmak bir alçak geçiş filtresi ekleyerek sistemi inceliyoruz. Alçak geçiş filtresi, motor hızının analog bir sensörle ölçüldüğü durumda sensör gürültüsünü, motor konumunun dijital bir sensörle ölçüldüğü durumda sayısal türev işlemi nedeniyle oluşan nicemleme gürültüsünü azaltır. Fitre, aynı zamanda sayısal türev işleminin nedenselliğini de sağlar. Çalışmamız sonucunda filtrenin sistemin pasifliğini olumsuz etkilemediğini ve sistemdeki parazitik sönümleme etkilerini azalttığı için dokunsal algı yaratma performansını artırdığını gösteriyoruz. Ayrıca, iç hareket kontrol geri-beslemesinde alçak geçişli filtre kullanıldığı durumda, kuvvet kontrolcüsünün de gürültü azaltma özelliğine sahip bir filtre içermesi gerektiğini gösteriyoruz.

İkinci olarak, HKEK kontrolcüye sahip SEE ile sanal yay geri-beslemesi sırasında kuvvet kontrolcüsünde faz gecikmeli veya faz ileretici denetleyicilerin kullanımını analiz ediyoruz. Pasif fiziksel gerçekleştirmelerin karşılaştırılması yoluyla, faz gecikmeli denetleyicinin parazitik sönümleme etkilerini azaltarak yay geri-besleme performansını artırabildiğini, faz ileretici denetleyicinin ise bu tür parazitik etkileri arttırdığını gösteriyoruz. Bununla birlikte, pasif olarak geri-beslenebilen sanal sertlik aralığının, bu tür bir denetleyici içermeyen duruma kıyasla, hem faz ileretici hem de faz gecikmeli denetleyiciler için azaldığını gösterdik. Sonuç olarak, kuvvet kontrocüsünde faz gecikmeli denetleyici kullanılması durumunda pasiflik sınırları ile performans arasında temel bir ödünleşim olduğunu gösterdik.

Son olarak, ideal kütle-yay-sönümleyici elemanların kombinasyonlarından oluşan referans empedans modellerinin şekillendirilmesinde filtrelemenin etkilerini inceliyoruz. Burada filtreleme hem nedensellik ilkesini hem de sınırlı bant genişliğine sahip kapalı döngü sisteminin takip edilebilirliğini sağlamak açılarından gereklidir. Sonuçlarımız, referans sertlik modeline uygun şekilde seçilmiş fitre bant

genişliğinin, pasiflik sınırlarını olumsuz etkilemeden sanal yay geri-besleme performansını iyileştirdiğini göstermektedir. Benzer şekilde, referans sönümleme ve kütle modellerinin filtrelenmesi, hem bu referans empedansların nedenselliğini sağlar, hem de pasiflik sınırları içerisinde sanal sönümlemenin arttırılmasına ve sanal kütlelerin telafisine olanak sağlar.

Sanal sönümleme ve kütle modelleri için türetilen pasiflik koşulları, pasif olarak geri-beslenebilecek SD'lerin üst ve alt sınırlarının bulunduğunu göstermektedir. Referans empedans modeli sadece kütle içeriyorsa, pasif olarak geri-beslenebilen minimum kütle, modelin kütlesi ile sınırlıdır. Ancak referans modele sönümleme etkilerinin eklenmesi ile bu sınırın düşürülmesi mümkün hale gelir. Referans empedans modeli paralel bir kütle ve sönümleyiciden oluşuyorsa, sistem sönümlemesini telafi etmek için negatif bir sönümleme terimi kullanılabilir ve pasifliği bozmadan daha yüksek kütleler geri-beslenebilir. Benzer şekilde, sistem kütlesini telafi etmek için referans modelde negatif bir kütle terimi kullanılabilir ve böylece pasifliği bozmadan daha yüksek sönümlemeli referans modellerinin geri-beslemesine olanak sağlanabilir. Ayrıca sönümleme veya paralel kütle ve sönümleme modelleri oluşturulurken referans modelin bant genişliğinin sınırlandırılması pasiflik koşullarını gevşetir; ancak bu durum aynı zamanda dokunsal algı yaratma performansının da düşmesine neden olur.

Genel olarak sonuçlarımız, filtre kullanımının SEE'nin gürbüz kararlılığı ve dokunsal algı yaratma performansı üzerinde önemli bir etkiye sahip olduğunu göstermektedir. Pasif olarak geri-beslenebilen sanal sertlik seviyelerine bir alt sınır getirme pahasına, sanal sertliği oluştururken istenmeyen sönümlemeyi en aza indirmek için filtrelenmiş bir kuvvet kontrolcüsüyle birlikte filtreli bir iç hareket kontrolcüsü kullanılması tavsiye edilir. Referans empedans modelinin alçak geçirgen filtre ile modellenmesi genel olarak tavsiye edilir; aynı zamanda, örneğin kütle veya sönümleme geri-beslemesi sırasında pasifliği sağlamak için zorunludur. Referans bant aralığını sınırlayan filtrelerin kullanımı durumunda, daha alçak geçiş frekanslarının kullanımı pasif olarak geri-beslenebilen sönümleme ve kütle seviyelerini arttırır. Ancak, alçak geçiş frekansından kaynaklanan pasiflik sınırları ile dokunsal algı yaratma performansı arasındaki ödünleşime dikkat edilmelidir.

Tüm teorik sonuçlarımız, kararlılık ve kinestetik dokunsal performans karakterizasyon deneyleri ile doğrulanmıştır. Ayrıca bir psikofizik deneyle, filtrelemenin kinestetik dokunsal algı oluşturma performansı üzerindeki etkileri doğrulanmıştır.

Genel olarak, bu çalışma, filtrelemenin SEE ile SD'lerin geri-beslemesi sırasında gürbüz kararlılığı ve dokunsal algı yaratma performansı üzerindeki ödünleşimlerinin kapsamlı bir şekilde anlaşılması açısından faydalıdır. Sonuçlarımız, fİRE araştırmacılarının, dokunsal algı yaratma uygulamalarında filtrelerin kullanımı hakkında daha bilinçli kararlar vermeleri konusunda yol gösterebilir.

Acknowledgments

First and Foremost, I would like to extend my deepest gratitude to my supervisor, Prof. Dr. Volkan Patoğlu. His exceptional skill, patience, support, and genuine passion for research have not only fueled my enthusiasm for scientific research but have also significantly enhanced my daily life in a positive manner. He will remain a strong role model which I will try to honor through my career.

I would like to thank to the jury members of this thesis: Prof. Dr. Çağatay Başdoğan and Asst. Prof. Dr. Melih Türkseven for their time, effort and valuable feedback.

I would like to thank to members of our lab, not only for their help and collegiality but also for their understanding, support and friendship: Ali Yaşar, Çağatay Irmak, Cansu Öztürk, Uğur Mengilli, Deniz Ece Susuz, Melike Cezayirlioğlu, Selim Ahmet İz, Bilal Çatkın, Alperen Kenan, İlhami Osman Karakurt, Harun Tolasa and Ömer Burak Aladağ. Eventhough our shared time have been very limited, they have made this journey very enjoyable whether our activities consisted of grabbing a cup of coffee or trying to make some hardware work while spending our entire night. I would especially want to thank to Bilal Çatkın, Alperen Kenan, İlhami Osman Karakurt, Harun Tolasa and Ömer Burak Aladağ for being my companions through applying to PhD programs and valuable discussions about life. Lastly I would like to thank to Celal Umut Kenanoğlu. Your presence in both Sabancı University and my life have made my days much more enjoyable. To you and rest of our lab mates, I wish the best of joys and fulfillment of all your aspirations.

I am profoundly grateful to my father İlhan Kenanoğlu and my mother Sezen Kenanoğlu, for their boundless support and love. Your encouragement has been my guiding light, helping me through challenges. I feel incredibly fortunate to have such an exceptional family. Thank you for being the driving force behind all my current and future achievements. I want to thank to Elanur Kenanoğlu, her presence in my life is a constant source of strength and joy. Thank you for being my light, closest friend and the heartbeat of my life. I am truly blessed to have you by my side.

This study was partially supported by TÜBİTAK Grant 22AG003.

To my beloved family...

Contents

List of Figures

List of Tables

Chapter 1

Introduction

Physical human-robot interaction (pHRI) aims to combine the adaptable decision-making capabilities of humans with the high productivity and precision of robots. High fidelity control and safety of pHRI are required for kinesthetic haptic rendering applications in order to enhance user experiences and enable new possibilities of human-robot collaboration.

pHRI must ensure coupled stability for the safety of the interacting agent while maintaining high haptic rendering performance for the fidelity of the interaction. However, the non-collocation of sensors and actuators induces bounds on the controller gains to ensure stability robustness [1, 2], limiting the haptic rendering performance. This results in haptic rendering performance stability robustness trade-off for closed-loop force control. One method to tackle the fundamental trade-off between the stability robustness and haptic rendering performance is to introduce intentional physical compliance between the actuator and the interaction port and utilize the model of the compliance in the control architecture, to result in the force control paradigm called series elastic actuation (SEA). For haptic rendering applications, SEA can relax the bounds on the control gains, enabling coupled stability for safe human-robot interaction. Furthermore, in combination with position sensing encoders and large deflections, SEA can produce precise force sensing while reducing the cost of traditional force control methods that rely on expensive force sensors.

The haptic rendering of SEA has been extensively studied under different control architectures [3, 4, 5]. One of the most commonly employed controllers for the haptic rendering of SEA is called velocity-sourced impedance control (VSIC) [6, 7], which consists of an inner motion loop that effectively eliminates parasitic forces, an outer torque loop that enhances the haptic rendering performance, and an impedance reference that determines the dynamic response of the interaction port. VSIC is preferred as the controller gains the inner motion loop and the outer force loop can be tuned empirically.

SEA under VSIC can render a wide range of safe and high-fidelity virtual environments. The safety of haptic rendering of SEA under VSIC has commonly been studied through the passivity analysis framework [8]. Even though passivity analysis is considered to be conservative, the insight from rigorously derived closed-form analytical conditions provides indispensable intuition on how system parameters and controller gains affect the stability robustness of the rendered virtual environments.

The rendering fidelity of SEA can be studied through a number of methods, including effective impedance analysis and network synthesis. Effective impedance analysis provides a basic intuition of the system response by mapping the imaginary part of the impedance transfer function at the interaction port to effective stiffness and effective mass components while mapping the real part of the impedance transfer function to effective damping [9, 10, 11]. Network synthesis provides further details about the system response by enabling the formation of passive physical equivalents that describe physically realizable behaviors using a topological connection of primitive passive elements. Passive physical equivalents provide valuable insights into the effects of plant parameters and controller gains on haptic rendering performance [12, 13].

In this thesis, the effects of the use of filters on the stability robustness, and kinesthetic haptic rendering performance of SEA under VSIC are studied. We investigate the underlying trade-offs while rendering linear virtual environments by deriving the necessary and sufficient conditions for the passivity, forming the passive physical equivalents, and conducting effective impedance analysis on closed-loop SEA under VSIC during haptic rendering. We study the utilization of filtering and its effects on three distinct use cases for filters:

- (i) to attenuate high-frequency sensor noise,

- (ii) to serve as a compensator to improve the phase response of the system, and
- (iii) to shape the dynamics of the reference impedance model to ensure its trackability and causality.

To compare the effects of filtering on stability robustness and haptic rendering performance trade-offs, we study the utilization of filters to attenuate high-frequency sensor noise by introducing a low-pass filter to the actuator velocity feedback of the inner motion loop of VSIC while rendering linear springs with SEA. Filtering of the actuator velocity feedback is required regardless of the velocity measurement/estimation method; if the actuator velocity is measured through analog sensing, filtering attenuates the sensor noise; on the other hand, if the position is measured by a digital encoder, then the low pass filter not only attenuates the quantization noise amplified due to numerical differentiation but also ensures the causality of numerical differentiation.

Next, we study the utilization of filters as phase-shaping compensators of the force control loop of VSIC during linear spring rendering with SEA. The addition of a negative phase, by utilization of lag compensators, to SEA under VSIC is expected to enhance haptic rendering performance; however, the effects of phase shaping on stability robustness must also be rigorously compared to the case where no phase is added or subtracted, via lead/lag compensation, from the system.

Finally, we study the effects of filtering on shaping the reference impedance model that consists of linear combinations of ideal mass-spring-damper elements. The filtering not only ensures the trackability of the reference by the closed-loop system with a finite bandwidth but also ensures the causality of the model. Shaping the impedance reference by limiting the haptic rendering bandwidth by the addition of a high-frequency roll-off to the reference virtual environment and further refraining from the negative effects of dictating the reference impedance characteristics at high interaction frequencies that are outside the interaction frequency range of the haptic rendering application, is expected to extend either stability robustness or haptic rendering performance limits. Therefore our main interest mainly lies within the stability robustness and haptic rendering trade-offs induced by the bandwidth limitations specified through filtering characteristics.

1.1 Related Work

1.1.1 Filtering for Noise Attenuation During Interaction Control

The effect of filtering on interaction control for noise attenuation has been studied under various contexts. Volpe and Khosla demonstrated that the closed-loop performance of explicit force control can be increased with the addition of a low-pass filter to the velocity feedback, as the behavior of velocity feedback with a low-pass filter closely matches that of using an integral controller gain [14]. They have recommended that the pole of the low-pass filter of the force sensor should be selected to be significantly larger than the system's natural frequency under explicit force control [15]. Eppinger and Seering show that if a low-pass filter is introduced to the force controller to attenuate noise, the system becomes unstable faster when compared to unfiltered case [1].

In the case of natural admittance control, Dohring and Newman conducted a numerical analysis and showed that if there is a low-pass filter on the velocity feedback, another low-pass filter must also be employed on force feedback to maintain passivity [16]. They have demonstrated non-passive behavior of the driving point admittance when a cut-off frequency mismatch, either from inherent sensor dynamics or deliberate filtering, between the velocity and force filter occurs. They have numerically shown that in order to maximize interaction performance, the filter on the velocity feedback and force feedback should be matched as closely as possible. Vallery *et al.* [17] derived a set of sufficient conditions for the passivity of SEA under VSIC when actuator velocity feedback is low-pass filtered.

In this thesis, we study the effects of noise attenuation on the actuator velocity feedback of the SEA under VSIC on stability robustness and haptic rendering performance. We expand upon the work carried out in [17] and we derive the necessary and sufficient conditions for the passivity of linear spring rendering of the SEA under VSIC when the actuator velocity feedback is filtered. We derive passive physical equivalents of the linear spring rendering of the SEA under VSIC when the actuator velocity feedback is filtered to provide an intuitive understanding of how plant parameters and controller gains affect the stability robustness and haptic rendering performance. We show that; even

though filtering of the actuator velocity feedback does not result in more conservative passivity conditions while increasing haptic rendering performance it also results in noise amplification. As Dohring and Newman [16] have shown through numerical analysis, we demonstrate that if the actuator velocity feedback is filtered then the force controller is also required to feature filtering to avoid noise amplification. We rigorously compare the haptic rendering performances and passivity bounds when the actuator velocity is and is not filtered. As Volpe and Khosla [14] have shown that filtering enhances explicit force control performance, we also show that when the force controller is filtered, haptic rendering performance improves by decreasing the parasitic damping effects, even though it also introduces more strict bounds on the range of passively renderable stiffness levels. We conclude that the upper bound on the range of passively renderable stiffness improves as the cut-off frequency of the low-pass filter increases while the lower bound improves as the time constant of the controller approaches the mechanical time constant of the system. We experimentally verify the range of passively renderable stiffness and the performance enhancements due to filtering with systematic coupled stability and performance characterization experiments.

1.1.2 Filters as Phase Shaping Compensators During Interaction Control

For explicit force control, Volpe and Khosla [18] showed that an integral gain improves the force tracking performance by attenuating noise and reducing steady-state errors; however, the controller gains need to be carefully selected to ensure coupled stability. Eppinger and Seering [1] studied filtering for phase addition to the explicit force controller, utilizing a lead/lag compensator as the force controller, and demonstrated that lead compensators can increase the closed-loop bandwidth. They noted that higher-order compensators may increase bandwidth even further; however, they are likely to be more susceptible to modeling errors.

In the context of SEA, Pratt and Williamson presented a set of sufficient for the passivity of SEA under PID force controller with a filtered-integral gain. They have shown the need for an integral roll-off to ensure passivity [4]. Through a set of sufficient conditions for the passivity of SEA under VSIC, Vallery *et al.* [17] concluded that when actuator

velocity feedback is low-pass filtered, the utilization of integrators in both torque and motion controllers is not feasible if the derivative tern in the force controller is not low-pass filtered.

Fabrizio and O'Malley [19] studied spring rendering with SEA where the force controller consists of a lead/lag compensator. Through numerical analyses, they showed that an acceptable compromise between stability and performance is provided only by a lead compensator.

Tosun and Patoglu [20] provided a set of necessary and sufficient conditions for the passivity of SEA under VSIC when both the torque and motion controllers consist of PI compensators. They proved that when the torque controller contains an integral gain, the inner motion loop must also include an integral gain in the motion controller to preserve passivity. The addition of the integral gain that adds a negative phase, corresponding to a lag compensator, is important to further study since an integral gain on the force controller requires the inclusion of an additional integral gain on the motion controller for passivity, resulting in over-complications in the implementation process.

In this thesis, we study the effects of phase shaping of linear spring rendering SEA under VSIC on stability robustness and haptic rendering performance. We analyze the addition of the positive phase by featuring a lead compensator and the addition of the negative phase by featuring a lag compensator, in the force controller of the VSIC. We derive necessary and sufficient conditions for the passivity of linear spring rendering of SEA under VSIC and show that utilization of either a lead or lag compensator results in more conservative passivity bounds, limiting the range of passively renderable stiffness levels when compared to the case where a zero phase inducing proportional gain is used. We show that there is a limit to the maximum passively removable phase from the system, meaning there exists an upper bound on the compensation factor of the lag compensator, that must roll off the force controller to maintain passivity, a similar result to the work carried out by Pratt and Williamson [4]. We derive passive physical equivalents of linear spring rendering of SEA under VSIC where the force controller consists of either a lead or lag compensator. Unlike the compromise between the stability and performance relationship found through numerical analysis by Fabrizio and O'Malley [19], through passive physical equivalents, we show that utilization of lag compensator improves haptic rendering performance by reducing the parasitic damping while utilization

of lead compensator results in an increase in parasitic damping, reducing the haptic rendering performance. Tosun and Patoglu [20] had also previously shown that utilization of an integral gain, the addition of negative phase, improves haptic rendering performance while resulting in more conservative passivity conditions. We perform systematic simulations to show the effects of the utilization of filters as phase-adding agents. We experimentally validate our theoretical results through systematic coupled stability and performance characterization experiments. We conduct a psycho-physics experiment to showcase how phase addition through filtering increases the performance of perception of haptic interaction.

1.1.3 Filters as Reference Model Shaping Agents During Interaction Control

Qian and Schutter studied reference shaping in the context of explicit force control, utilizing low-pass filters on the feed-forward loop [21]. They have found that the addition of low-pass filters to the feed-forward compensation copes with instability caused by the flexible dynamics of the arm/joint system of the robot, and a choice of sufficiently low cut-off frequency can always guarantee stability.

Newman studied natural admittance control, under the context of low-frequency admittance shaping [22] that utilizes a desired admittance model containing a desired stiffness and desired damping that asymptotically converges to the natural end-point admittance, the open-loop response of the plant. He emphasized it is important to model or measure the system's admittance parameters and use the high-frequency behavior of the natural endpoint admittance, the inertial constraint of the plant, under the specifications of the target dynamics which contains desired stiffness, desired damping, and the high-frequency behavior of the open-loop response of the plant.

Multiple control methodologies have drawn attention in the literature to satisfy the system constraint [23]. Reference governors are add-on control units, that decouple low-level control law from the high level-guidance system by acting as an intermediary layer. The reference governor's auxiliary control unit generates a reference signal that ensures the constraints are satisfied while a closed-loop response enables high tracking performance and stabilizes the underlying system. Reference governors are simple to interpret and

systematic to use, enabling the use of existing control solutions where systems are subjected to constraints. Even though the reference governor control scheme was initially introduced for generic nonlinear systems [24, 25], recently a new scheme called explicit reference governor (ERG) was introduced for LTI systems [26]. The explicit reference governor enables high-fidelity reference generation for closed-loop control systems and consists of a navigation field and a dynamic safety margin that is utilized for realizing the safety of human-robot interaction by introducing appropriate safety margins to satisfy constraints [27]. For the case of a feed-forward reference governor, governor schemes which do not rely on the plant state but are used to avoid high-frequency responses by filtering the reference signals have also been studied [23]. For the safety of haptic rendering of SEA constraints are not necessarily physical elements that are to be evaded but also high-frequency responses of reference virtual environments that might destabilize the system if not rolled-off. In other words, shaping the reference input to roll-off high frequency constraints that are undesirable might increase stability robustness and haptic rendering performance.

Previously Griffiths *et al.* [28] had shown through gain-phase integral relationship, compensation of certain hardware dynamics to match desired passive dynamics could be only achieved by the violation of passivity and passivity can be only achieved by reduction of performance bandwidth while the virtual environment consists of a virtual mass and the infinite frequency dynamics of the plant consists of end-effector inertia. The rolling-off of the reference input studied in this thesis aims to limit the performance bandwidth to study the stability robustness and haptic rendering trade-offs. In fact, shaping the reference impedance model has not drawn any attention in the context of SEA. The stability robustness and haptic rendering performance trade-off due to impedance reference shaping and rolling-off of the high-frequency component of the reference input is an important concept to study. Under the assumption that the end-effector inertia of the SEA is negligible, the open-loop response of the SEA at high frequencies consists of the physical stiffness that is used to realize the SEA and reference shaping of the impedance reference such that rolling of the impedance references that do not show the same characteristics as the open-loop response of the SEA at high frequencies might lead to more favorable haptic rendering performance or a wider range of passively realizable virtual environments.

In this thesis, we study impedance reference shaping by utilizing an impedance model that contains a filtered stiffness reference, and a linear parallel mass-spring-damper reference model where the reference mass and damper are filtered. In the case where the virtual environment consists of a linear spring and the reference stiffness is filtered to ensure trackability and rolling off the high-frequency content of the reference input, through rigorously derived necessary and sufficient conditions and derived passive physical equivalent, it is observed that filtering the reference impedance model improves the haptic rendering performance by decreasing the parasitic damping and there exists a precise cut-off frequency for all passive linear spring virtual environments (that are lower than the stiffness of the SEA) resulting in zero parasitic damping. Even though filtering results in more conservative passivity bounds, less conservative cut-off frequencies enable passive rendering of all stiffness values smaller than the physical stiffness of the SEA with zero parasitic damping. Therefore it is observed that shaping impedance reference such that the high frequency content is rolled-off results in a stability robustness and haptic rendering performance trade-off. For the case where the reference impedance consists of a linear parallel mass-spring-damper model where reference mass and damper are filtered such that the high-frequency content of the reference impedance converges to a spring, the open-loop response of the SEA, as argued in [22], through rigorously derived necessary and sufficient conditions we show that setting an upper bandwidth limit to the reference damper and mass models and a decreasing of the cut-off frequency, increases the maximum passively renderable virtual mass and damping levels, extending the safe region for human-robot interaction as argued in [21]. However, through passive physical equivalents, we show that as the cut-off frequency increases the haptic rendering performance increases as well resulting in a stability robustness, haptic rendering performance trade-off. We further show that by rolling off or limiting the bandwidth of the reference mass and damper models, otherwise passively not possible rendering of damping and compensation of system mass becomes feasible. We conduct numerical simulations and experimentally validate our theoretical results with systematic coupled stability and performance characterization experiments.

1.1.4 Haptic Rendering of Ideal Mass, Viscous Damping and Springs Models

Ideal linear mass, spring, and damping elements constitute the basic building blocks of most virtual environments. The haptic rendering fidelity and coupled stability of interactions of SEA under VSIC while rendering null impedance and linear springs have been extensively studied in the literature [13, 20, 29, 30, 31, 32], as the null impedance is commonly utilized to achieve active backdrivability of the system, while ideal springs are used to implement virtual constraints. It has also been established that Voigt models cannot be passively rendered with SEA [30, 31]; however, physical dissipation can be added in parallel to the compliant element to enable passive Voigt model rendering [32, 33].

Rendering ideal mass with SEA has not received any attention. While it has been well-established in the literature that the endpoint mass of a system with non-collocation between its actuator and interaction port cannot be passively compensated by any casual controller [22, 34, 35], this result does not imply that virtual masses higher than that of the endpoint mass cannot be rendered. Given that the end-effector mass of SEA is typically designed to be quite low, it may be feasible to passively render a wide range of virtual mass levels with SEA.

Mass rendering has commonly been studied with admittance-type devices, due to their favorable causality for this task [36]. Newman [22] proved that attempting to imitate a driving-point admittance equivalent to a mass lighter than the actual endpoint mass results in instability. Mass rendering with an admittance-type device is passive, as long as compensation of the natural device inertia (located after the non-collocation) is not attempted [22, 34, 35]. Studies focusing on inertia compensation are based on coupled stability analyses that utilize a model of the environment with excess passivity (damping).

Gil *et al.*[37] studied the inertia compensation of an impedance-type haptic device with feed-forward compensation and derived conditions for the stability with discrete analysis. They experimentally observed the stability of the haptic device depends strongly on how the user grasps the device. Keemink *et al.*[36] showed that mass compensation is feasible when non-causal feed-forward compensation is employed for admittance control.

Aguirre *et al.* [38] studied mass compensation of a lower extremity exoskeleton with low-pass filtering of the acceleration of the patient and found that stability of the interaction relies on the damping between the human and the exoskeleton. Desai *et al.*uses a model matching framework based on numerical robust stability analysis to render virtual mass with an impedance-type device [39]. Colonnese *et al.*has studied mass rendering with impedance-type haptic interfaces and numerically characterized the range of passively renderable virtual masses, called the M-width [9].

In this thesis, we analyze the feasibility of rendering linear parallel mass-spring-damper virtual environments. We rigorously derive necessary and sufficient conditions of parallel mass-spring-damper rendering of SEA under VSIC and further analyze this system where either reference stiffness or reference mass or both are equivalent to zero, to provide better insight. We derive passive physical equivalents of combinations of linear parallel mass-spring-damper rendering of SEA under VSIC and show continuation of these passive physical equivalents such that the realization of parallel mass-spring-damper virtual environment becomes equal to the passive physical equivalent of Voight model virtual environment when the reference mass is equal to zero. Similar to Colonnese *et al.* [9], we show that mass rendering of SEA has both a lower and an upper bound, and a decrease in the cut-off frequency results in less conservative passivity bounds. We further show that the minimum passively renderable mass is equal to plant mass when the effective damping value is equal to zero however reducing the passively renderable mass is possible by introducing damping to the impedance reference. Unlike previous results stating that passive Voigt model rendering is not possible with SEA [30, 31], we show that both Voigt model rendering and damping compensation of the Voigt model are passively feasible with SEA. We further show both passive damping rendering and passive damping compensation are possible with SEA. For the case where both the reference mass and damper are substituted with zeros, we recover the necessary and sufficient conditions for the passivity of spring rendering of SEA under VSIC and the passive physical equivalent of spring rendering of SEA under VSIC given in [13].

1.2 Contributions

In this thesis, we analyze the haptic rendering with series elastic actuation (SEA) under velocity-sourced impedance control (VSIC) when filters are introduced to different locations in the control loop, to attenuate noise, to shape the phase response of the closed-loop system as a compensator, or to limit the bandwidth of the reference impedance model to ensure trackability of the reference.

On the one hand, we study the coupled stability of interactions through passivity analysis and investigate the effects of plant parameters and controller gains on stability robustness. On the other hand, we derive passive physical equivalents to establish the effects of plant and controller parameters on haptic rendering performance. Finally, we study the closed-loop systems with and without filters to determine the underlying trade-offs affecting stability robustness and haptic rendering fidelity.

We demonstrate the validity of our findings through systematic coupled stability experiments with the most destabilizing environments, while we experimentally characterize haptic rendering fidelity via closed-loop system identification techniques. We further demonstrate the effects of filtering on the kinesthetic rendering performance through a psychophysical experiment.

The contributions of the thesis may be listed as follows:

- We rigorously study the passivity of SEA under VSIC to establish analytical closed-form expressions for necessary and sufficient conditions of haptic rendering while rendering virtual environments consisting of combinations of parallel mass-spring-damper elements. We compare the necessary and sufficient conditions of closed-loop systems with and without filters to determine the effects of filtering on stability robustness.

- We derive passive physical equivalents of closed-loop SEA while rendering virtual environments consisting of combinations of parallel mass-spring-damper. Through passive physical equivalents, we provide a clear understanding of how the plant parameters and controller gains affect the haptic rendering performance. We compare passive physical equivalents of closed-loop systems with and without filters to determine the effects of filtering on the fidelity of haptic rendering.

- For linear spring rendering, we show that the utilization of filters to attenuate sensor noise on the actuator velocity feedback does not negatively impact the passivity bounds while filtering enhances haptic rendering performance. However, filtering also results in noise amplification, necessitating the force controller also feature a compensator with noise attenuation properties.

- We show that the utilization of either a lag compensator or a lead compensator in the torque controller results in more conservative passivity bounds and the range of passively renderable impedances are maximized when the torque controller consists of a proportional gain.

- We show that the utilization of a lag compensator in the force control loop of the VSIC can increase the spring rendering performance by decreasing the parasitic damping effects, while the utilization of lead compensators increases such parasitic effects.

- We show that utilizing a filter to roll off the high-frequency content of the reference virtual stiffness model improves the spring rendering performance by reducing the parasitic damping, at the cost of more strict passivity bounds. We also prove that there exists a critical cut-off frequency that maximizes both the passively renderable impedance range and performance of virtual spring rendering.

- We show that utilizing a filter to roll off the high-frequency content of the reference virtual mass and damper models not only ensures the causality of real-time implementations but also enables passive renderings of higher virtual damping levels and compensation of virtual masses that are not possible without such filters.

- We prove that filtering of the reference virtual mass and damper model significantly extends the passively renderable mass and damping levels by relaxing the passivity bounds, at the expense of decreased performance bandwidth during haptic rendering.

- We demonstrate that while rendering virtual parallel mass-damper environments, compensation of mass increases the bound on the maximum passively renderable damping, and compensation of the damping increases the bound of the maximum passively renderable mass.

- We conclude that utilizing filters has a significant effect on the stability robustness-rendering performance trade-off of SEA. It is recommended to use low-pass filtering in the inner motion controller together with a force controller introducing sufficient lag characteristics to minimize parasitic damping while rendering virtual stiffness, at the cost of introducing a lower bound to the passively renderable stiffness levels.

- Shaping the reference impedance model to feature a high-frequency roll-off is not only recommended, but also is often necessary, to ensure passivity, for instance, during pure mass or viscous damping rendering. While the range of passively renderable damping and mass levels increase with more aggressive cut-off frequencies of the reference shaping filter, this frequency should be also carefully selected to properly balance the trade-off between the conservativeness of the passivity bounds and the haptic rendering performance.

- We present results of systematic simulations to showcase the underlying stability robustness and rendering fidelity trade-offs induced by filtering. Furthermore, we experimentally validate our passivity bounds and rendering performance through real-time experiments utilizing a single-axis SEA. We also present results from a human subject experiment to show how filtering can increase the perceived performance of haptic rendering.

1.3 Outline

The rest of the thesis is organized as follows:

Chapter 2 presents an overview of the concepts regarding SEA, introduces passivity theorems used for derivations of necessary and sufficient conditions for the passivity, defines the causality constraint for real-time implementations, introduces passive physical equivalents, and provides spring rendering with SEA under VSIC while both torque and motion controllers consist of proportional gains as an example to demonstrate the passivity analysis and derivation of passive physical equivalents.

Chapter 3 presents the necessary and sufficient conditions for the passivity of spring rendering of SEA under VSIC, when the actuator velocity feedback is filtered for noise attenuation. This chapter also provides passive physical equivalents of the filtered cases and compares the case of the filtered actuator velocity feedback with its unfiltered counterpart. Chapter 3 further presents numerical evaluations to show the stability robustness and haptic rendering performance trade-offs that are induced by the noise attenuating filter and experimental evaluations for validations of theoretical results on stability robustness and haptic rendering performance trade-offs.

Chapter 4 presents the necessary and sufficient conditions for the passivity of spring rendering of SEA under VSIC when filters are used as phase shaping compensators to add lead or lag to the force control loop of VSIC and provides passive physical equivalents of two cases where either a lead or a lag compensator is utilized. The effects of lead/lag compensators on the robustness-performance trade-offs are compared with the case with no phase shaping through the rigorously derived necessary and sufficient conditions for the passivity and passive physical equivalents. The theoretical results are experimentally validated with systematic coupled stability and haptic rendering performance characterization experiments. The effects of phase-shaping compensators on haptic rendering performance are further studied through human-subject haptic perception studies where participants are asked to evaluate the perceived properties of phase-shaping compensators.

Chapter 5 presents the necessary and sufficient conditions for the passivity of SEA under VSIC when the rendered virtual environment consists of parallel combinations of linear mass-spring-damper elements. In this chapter, filters are employed to shape the reference

impedance to ensure tractability and causality by introducing high-frequency roll-off characteristics. The effects of filter cut-off frequency, plant parameters, and controller gains are studied through comparisons of the necessary and sufficient conditions for the passivity with the unfiltered case.

Chapter 6 presents the passive physical equivalents of the SEA under VSIC where the rendered virtual environment consists of parallel combinations of linear mass-spring-damper elements while filters are utilized for reference shaping. Haptic rendering performance is studied through comparisons of the passive physical equivalents with the unfiltered case.

Chapter 7 presents the numerical evaluations of the passivity bounds and haptic rendering performance of SEA under VSIC where the rendered virtual environment consists of parallel combinations of linear mass-spring-damper elements while filters are utilized for reference shaping.

Chapter 8 presents the experimental verification of the theoretical results for haptic rendering of SEA under VSIC where the rendered virtual environment consists of parallel combinations of linear mass-spring-damper elements while filters are utilized for reference shaping.

Chapter 9 concludes the thesis with a comprehensive summary and discusses future work.

Chapter 2

Preliminaries

In this chapter, we provide a brief overview of the technical background required to follow the analysis presented in this thesis.

2.1 Series Elastic Actuation

Figure 2.1 depicts a schematic of SEA model. The compliant element, K represents the SEA stiffness. J_m represents the reflected inertia of the actuator while B_m represents the reflected damping of the actuator. The symbols θ_end represents the end effector position while θ_m represents the actuator position of the SEA system. The torque supplied by the actuator is represented with the symbol τ_m. Human applied torques are divided into unintentionally applied passive component, τ_h and intentionally applied active components, τ_h^*, that are not applied with the consideration of system states.[8]

We assume that the end effector inertia of the SEA is negligible and the torque on the compliant element is equal to the human applied torque such that $\tau_{SEA}=\tau_h+\tau_h^*$. The impedance at the interaction port can be defined as $Z_{end}=-\frac{\tau_{SEA}}{\omega_{end}}$, where the SEA torque is considered as positive when the SEA is in a compression state.

Figure 2.2 depicts the block diagram of SEA under VSIC. C_t and C_m are the torque and motion controllers respectively. Inner motion loop of the cascaded controller, increases the robustness and eliminates parasitic forces while the outer force loop increases rendering performance of virtual environments. τ_{SEA} is the physical torque acting on the

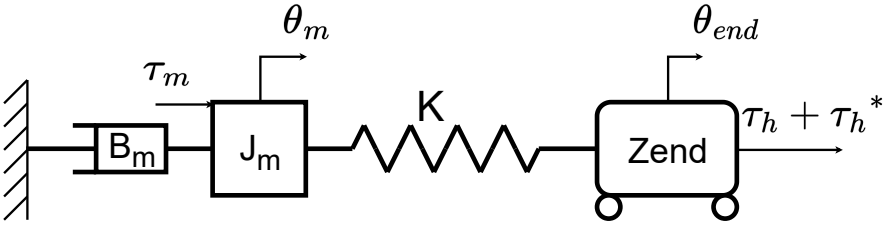

FIGURE 2.1: Schematic of SEA Model

compliant element of the SEA. τ_{SEA} can be computed with the Hooke's law with the assumption that the compliant element of the SEA is linear. Thick lines denote physical forces acting on the SEA. θ_{end} is the measured end effector position.

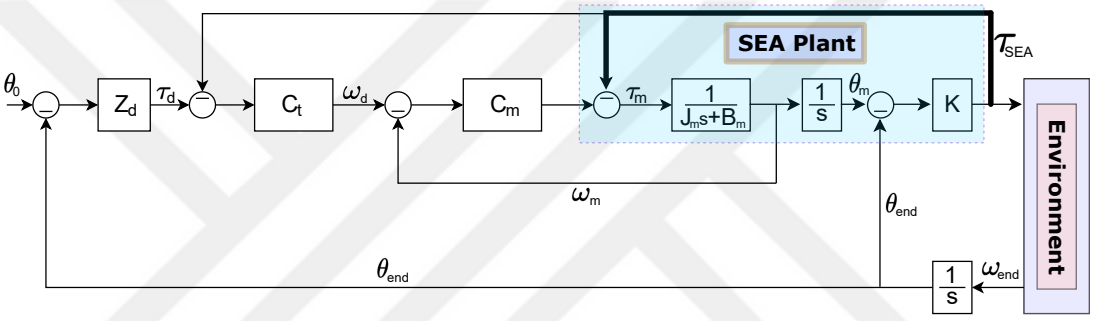

FIGURE 2.2: Block Diagram of SEA under VSIC

The following assumptions are considered for the analysis:

1. Without loss of generality, motion reference, θ_0 is assumed to be zero.
2. SEA model is considered to be linear time-invariant (LTI), negating the nonlinear effects such as backlash, stiction and actuator saturation.
3. Deflection of the compliant element of the SEA is considered to be measured with negligible time delay.
4. Physical plant parameters and controller gains are assumed to be positive while desired impedance is allowed to be negative.

2.2 Passivity Theorems

Positive realness of an impedance transfer function $Z(s)$ equates to passivity of an LTI system. Positive realness of an LTI system's transfer function, $Z(s)$, can be shown with the following Theorem.

Theorem 2.1 ([40]). *An LTI system's impedance transfer function Z(s) is said to be passive if and only if*
(i) $Z(s)$ has all of its poles in the open left half plane,
(ii) Poles on the imaginary axis are allowed as long as they are simple with positive real residues, and
(iii) $Re\{Z(j\omega)\} \geq 0$ in which $\omega \in (-\infty, \infty)$.

Following lemmas have been established in the literature and are used for determining the necessary and sufficient conditions for the passivity of LTI systems.

Lemma 2.2. *Given an rational impedance transfer function $Z(s) = \frac{N(jw)}{D(jw)}$, $Re[Z(jw)] \geq 0$ if and only if $H(w) = Re[N(jw)D(-jw)] = \sum_{i=0}^{n} f_i w^i \geq 0$ for $w \in [-\infty \ \ \infty]$, where f_i represent the coefficients of w^i.*

Lemma 2.3. *Given second degree polynomial $P(s) = x_1 s^2 + x_2 s + x_3$, $P(s) \geq 0$, for $x \in [0 \ \ \infty]$ if and only if $x_1 \geq 0, x_3 \geq 0$ and $x_2 \geq -2\sqrt{x_1 x_3}$.*

2.3 Passive Physical Equivalents

Passive physical equivalents have been largely studied in the field of network synthesis, aiming to provide an intuitive physical understanding with basic natural analogs. Colgate and Hogan [12] have studied contact instability of interaction control through passive physical equivalents and have shown a fundamental limitation of passive inertia compensation for force-feedback systems with sensor-actuator non-collocation. Kenanoglu and Patoglu [13] have provided passive physical equivalents of Voigt model, linear spring and null impedance rendering of SDEA under VSIC with the usage of force-current analogy.

Force-current analogy ties together mechanical and electrical domains. In the force-current analogy, Forces and velocities are considered to be analogous to currents and voltages, respectively. Inerter is an ideal energy storage element, completing the force-current analogy [41]. In force-current analogy, an inerter in the mechanical domain is analogous to an un-grounded capacitor in the electrical domain.

Thanks to the force-current analogy, all classical results of network synthesis such as Foster's reactance theorem [42] and Brune's construction method [43] for the minimal realization of positive-real functions consisting of inductors, capacitors, resistors, and transformers, can be employed in the formation of passive physical equivalents of transfer functions of the mechanical system. A sample passive physical equivalent and its derivation method is also provided in Subsection 2.5.1.

2.4 Causality of Real-Time Systems

In real-time robotic systems, meaning physical systems that have a constant data stream between various sensors and actuators, causality restricts methods that are not realizable. Causality constrains ideal filtering or ideal differentiation as well as cancellation of a system's relative degree.

Definition 2.4. A system is said to be causal if the response of the system at any time t is not influenced by the input at times greater than t.

Accordingly to Definition 2.4, differentiation of a system parameter, such as joint position, can not be computed in real time. Real-time estimation of the joint velocity must be conducted with other methods that induce time delay to the system for the sake of causality.

2.5 Spring Rendering with SEA under VSIC

In this section, we provide passive physical equivalent and, necessary and sufficient conditions for the passivity of SEA under VSIC during spring rendering, when both controllers consist of proportional gains. This section is used for comparisons between

the studied systems in this thesis and the system provided in this subsection. The necessary and sufficient conditions have been studied extensively in the literature.[13]

Given the measured end effector position θ_{end} and assuming SEA under VSIC when force and motion controllers consist of proportional gains, P_t and P_m respectively, the impedance at the interaction port during spring rendering, Z_d=K, is equal to

$$Z_S^{P-P}(s) = \frac{J_m\,K\,s^2 + K\,\beta\,s + K\,K_{\text{ref}}\,\alpha}{J_m\,s^3 + \beta\,s^2 + K\,(\alpha+1)\,s} \tag{2.1}$$

where α=$P_m P_t$ and β=$B_m + P_m$. The following expressions constitute the necessary and sufficient conditions for the passivity of $Z_S^{P-P}(s)$.

$$K \geq K_{ref}\,\frac{\alpha}{\alpha+1} \tag{2.2}$$

$$K_{ref}\frac{\alpha}{\alpha+1} \geq 0 \tag{2.3}$$

2.5.1 Derivation of the passive physical equivalent of spring rendering of SEA under VSIC

This subsection provides an example of how to derive the passive physical equivalent of SEA under VSIC during spring rendering while both torque and motion controllers consist of proportional gains. The impedance transfer function at the interaction port is denoted as the following:

$$Z_S^{P-P}(s) = \frac{J_m\,K\,s^2 + K\,\beta\,s + K\,K_{\text{ref}}\,\alpha}{J_m\,s^3 + \beta\,s^2 + K\,(\alpha+1)\,s} \tag{2.4}$$

The rendered stiffness at low frequencies of the given impedance transfer function in Eqn. (2.4), K_{vir}, is marked with a different tone than the rest of the impedance transfer function. The denominator of the marked part has a relative order of one compared to the numerator, representing a spring. Therefore, K_{vir} is equal to;

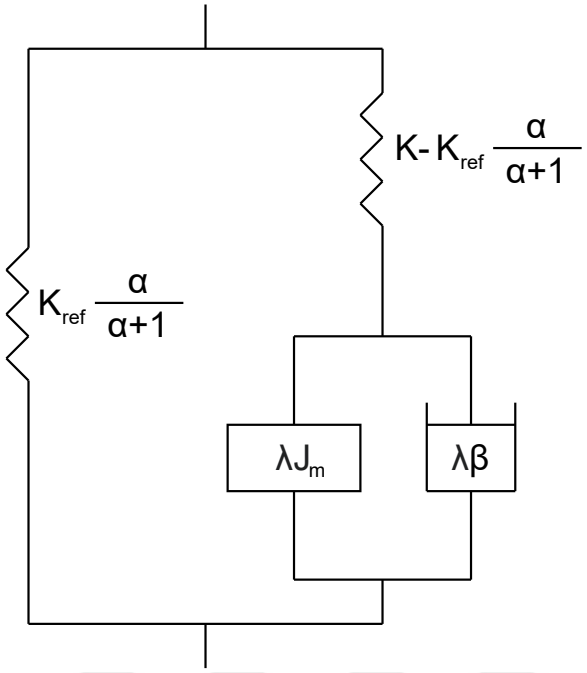

FIGURE 2.3: Passive physical equivalent of spring rendering of SEA under VSIC

$$K1_S^{P-P} = \frac{K_{\text{ref}}\,\alpha}{\alpha+1} \tag{2.5}$$

The dynamics of the rendered stiffness must be separated from the dynamics of the impedance transfer function.

$$Z2_S^{P-P}(s) = \left(Z_S^{P-P}(s) - \frac{K_{\text{ref}}\,\alpha}{\alpha+1}\right) \tag{2.6}$$

$$= \frac{J_m\,(K\,(\alpha+1) - K_{ref}\,\alpha)s\, + \beta\,(K(\alpha+1) - K_{ref}\,\alpha)}{J_m(\alpha+1)s^2\, + \beta\,(\alpha+1)\,s + K\,(\alpha+1)^2} \tag{2.7}$$

Next, the high frequency dynamics must be separated from the impedance transfer function given in Eqn. (2.7). The high-frequency part is toned differently from the rest of the impedance transfer function.

$$K2_S^{P-P} = \frac{J_m\,(K\,(\alpha+1) - K_{ref}\,\alpha)}{J_m(\alpha+1)} \tag{2.8}$$

Separating the high frequency term from the impedance transfer function given in Eqn. (2.7) in series:

$$Z3_S^{P-P}(s) = \left(Z2_S^{P-P}(s)^{-1} - \left(\frac{J_m \left(K \left(\alpha + 1 \right) - K_{ref}\, \alpha \right)}{J_m(\alpha + 1)} \right)^{-1} \right)^{-1} \tag{2.9}$$

$$= J_m \frac{K(\alpha + 1) - K_{ref}\alpha}{K \left(\alpha + 1 \right)^2} s + \beta \frac{K(\alpha + 1) - K_{ref}\alpha}{K \left(\alpha + 1 \right)^2} \tag{2.10}$$

The last two remaining terms of the Eqn. (2.10) can be separated as parallel inerter and damper;

$$B1_S^{P-P}(s) = J_m \frac{K(\alpha + 1) - K_{ref}\alpha}{K \left(\alpha + 1 \right)^2} \tag{2.11}$$

$$C1_S^{P-P}(s) = \beta \frac{K(\alpha + 1) - K_{ref}\alpha}{K \left(\alpha + 1 \right)^2} \tag{2.12}$$

where $B1_S^{P-P}(s)$ denotes the parasitic inerter and $C1_S^{P-P}(s)$ denotes the parasitic damper.

Overall the inerter element $B1_S^{P-P}(s)$ and the damper element $C1_S^{P-P}(s)$ are in parallel to each other while both of them are in series to the spring $Z2_S^{P-P}$. Finally the rendered stiffness at low frequencies, K_{vir} is equal to $K1_S^{P-P} = \frac{K_{\text{ref}}\, \alpha}{\alpha+1}$ and is parallel to all remaining elements. The dominant elements at high interaction frequencies is the combination of two spring elements:

$$Z_{S_{inf}}^{P-P}(s) = \frac{K_{\text{ref}}\, \alpha}{\alpha + 1} + \frac{J_m \left(K \left(\alpha + 1 \right) - K_{ref}\, \alpha \right)}{J_m(\alpha + 1)} \tag{2.13}$$

$$= \frac{J_m \left(K \left(\alpha + 1 \right) \right)}{J_m(\alpha + 1)} \tag{2.14}$$

$$= K \tag{2.15}$$

where K represents the SEA stiffness.

Figure 2.3 depicts the passive physical equivalent of SEA under VSIC when both controllers are proportional gains during spring rendering, where λ=$\frac{1}{\alpha+1}$-$\frac{\alpha}{(\alpha+1)^2}\frac{K_{ref}}{K}$. Through the passive physical equivalent, it is observed that the rendered stiffness at low frequencies, K_{vir}, is equal to $K_{ref}\frac{\alpha}{\alpha+1}$. The serial spring, K-$K_{ref}\frac{\alpha}{\alpha+1}$, is feasible if and only if the condition given in Eqn. (2.2) is fulfilled while the parallel spring, $K_{ref}\frac{\alpha}{\alpha+1}$ is feasible if and only if the condition given in Eqn. (2.3) is fulfilled. It can be observed that as

α increases the parasitic damping decreases, resulting in an increase in haptic rendering performance.

Chapter 3

Effects of Noise Attenuation on Haptic Rendering with SEA

In this chapter, we study the utilization of filters for noise attenuation as in Figure 3.1. We present necessary and sufficient conditions for the passivity of SEA under VSIC with filtered velocity actuator feedback. The actuator and end-effector velocities are denoted by ω_m and ω_{end}, respectively. While it may be possible to directly measure ω_m using the Hall effect at the motor winding, in this study, a low-pass filter with a cut-off frequency ω_c is introduced to VSIC, to attenuate the measurement noise or to capture the effects of causal differentiation used to estimate ω_m from the motor encoder measurements. The measurement of the end-effector position θ_{end} is sufficient for spring and the null impedance rendering; hence, velocity estimates/measurements for the end-effector are not necessary.

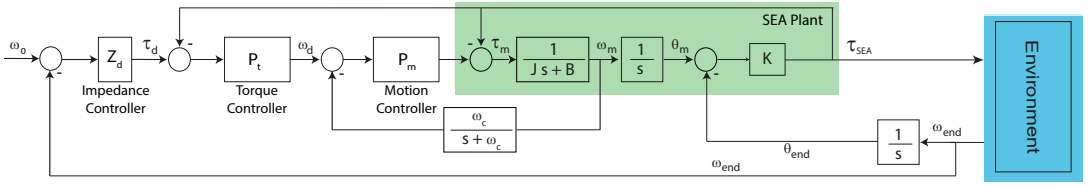

FIGURE 3.1: Block diagram of SEA under VSIC with filtered actuator velocity feedback

3.1 Passivity and Passive Physical Equivalents of SEA under VSIC with Filtered Actuator Velocity Feedback

We limit our analysis to rendering linear springs (used to realize virtual constraints with penalty-based methods) by setting $Z_d = K_d/s$ and null impedance rendering (used to implement free space) by setting $Z_d = 0$, where K_d represents the desired stiffness. We only present the passivity bounds and physical equivalents for spring rendering, since the results for the null impedance rendering can be recovered from the spring rendering case when the virtual stiffness is set to zero, thanks to the continuity of solutions.

The controllers studied are selected to be as simple as possible while capturing the main effects of interest, such that the passivity analyses result in closed-form analytic expressions and their physical realization can be presented in a human-understandable form.

3.1.1 Passivity of P-P Control with Filtered Velocity Feedback

Given the low-pass filtered velocity feedback $\frac{\omega_c}{s+\omega_c}\omega_m$, we first study VSIC with proportional torque P_t and motion P_m controllers. The rendered stiffness is defined as K_{vir}. The impedance at the interaction port $Z_{Spring_F}^{SEA^{P-P}}(s)$ of SEA under VSIC while rendering a linear spring can be derived as

$$\frac{J\,K\,s^3 + K\,(B + J\,\omega_c)\,s^2 + K\,(K_d\,\zeta + \sigma\,\omega_c)\,s + K\,K_d\,\zeta\,\omega_c}{J\,s^4 + (B + J\,\omega_c)\,s^3 + (\sigma\,\omega_c + K\,(\zeta + 1))\,s^2 + K\,\omega_c\,(\zeta + 1)\,s} \tag{3.1}$$

where $\zeta = P_m\,P_t$ and $\sigma = B + P_m$. The necessary and sufficient condition for the passivity of $Z_{Spring_F}^{SEA^{P-P}}(s)$ is derived as:

Proposition 3.1. *Consider SEA under VSIC as in Figure 3.1 with proportional torque P_t and motion P_m controllers and low-pass filtered velocity feedback $\frac{\omega_c}{s+\omega_c}\omega_m$ such that the driving port impedance at the interaction port is characterized by Eqn. (3.1).*

Let the controller parameters be positive. Then, the necessary and sufficient condition for the passivity of $Z_{Spring_F}^{SEA^{P-P}}(s)$ *is* $K_{vir} \leq K$*, where* $K_{vir} = \frac{\zeta}{\zeta+1} K_d$*.*

Proof. (i) Since all plant parameters are positive and the controller parameters are assumed to be positive, $Z_{Spring_F}^{SEA^{P-P}}(s)$ has all of its roots in the closed LHP.

(ii) $Z_{Spring_F}^{SEA^{P-P}}(s)$ has a single pole at $s = 0$ on the imaginary axis. The residue is K_{vir}, which is positive and real.

(iii) The sign of $\mathrm{Re}\{Z_{Spring_F}^{SEA^{P-P}}(j\omega)\}$ can be checked as

$$f_4\,\omega^4 + f_2\,\omega^2 \geq 0 \quad \omega \in (-\infty, \infty) \tag{3.2}$$

$$\text{where} \quad f_2 = \sigma\,{\omega_c}^2\,K\,(K + \zeta\,(K - K_d))$$
$$f_4 = B\,K\,(K + \zeta\,(K - K_d))$$

Eqn. (3.2) is satisfied iff $K_{vir} \leq K$, ensuring that $f_4 \geq 0 \wedge f_2 \geq 0$. □

Note that the upper bound of $Z_{Spring_F}^{SEA^{P-P}}(s)$ remains unchanged compared to the P-P VSIC controller with no velocity filtering, as presented in [13].

3.1.2 Realization of P-P Control with Filtered Velocity Feedback

A passive physical equivalent of Eqn. (3.1) is presented in Figure 3.2, where $\psi = \frac{1}{\zeta+1} - \frac{\zeta}{(\zeta+1)^2}\frac{K_d}{K}$. Feasibility conditions of a passive physical equivalent, imposing non-negativeness to each fundamental mechanical element used to realize the driving-point impedance, also provide sufficient conditions for its passivity. In particular, the non-negativeness of the coupling spring in Figure 3.2 dictates the (necessary and) sufficient condition in Proposition 1 as $K_{vir} \leq K$. Therefore, the realization is valid as long as the system is passive.

Passive physical equivalents present a topological connection of fundamental elements providing an intuitive understanding of the effective impedance. In Figure 3.2, the rendered dynamics of the realization approaches to the virtual stiffness K_{vir} at low frequencies, as K_{vir} is parallel to all other elements. At high frequencies, the rendered dynamics converge to the parallel connection of the springs K_{vir} and $(K - K_{vir})$, which is equal to the stiffness K of the series elastic element. The remaining elements in Figure 3.2 capture the effects of parasitic dynamics on the haptic rendering performance, which can be reduced with the selection of high controller gains.

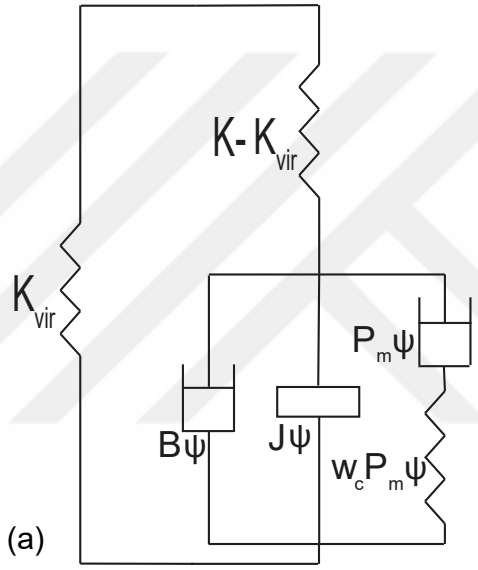

FIGURE 3.2: Passive physical equivalents of SEA under VSIC while rendering linear springs with filtered velocity feedback when both controllers are P.

A comparison of the passive physical equivalent of SEA during spring rendering under VSIC with P-P control and filtered velocity feedback in Figure 3.2 with the passive physical equivalent of SEA under VSIC with P-P control and no filtering presented in [13] indicates that they have a similar topology, except the extra serial damping-spring term in the case with filtered velocity feedback. Both realizations have identical inerter elements, while the low-pass filtering of the velocity feedback decouples the parasitic damping effects due to B and P_m into two distinct branches: The parasitic damping due to B is captured by a damper that is in parallel to a serial spring-damper term that captures the damping of P_m, as depicted in Figure 3.2. The serial spring-damper term displays frequency-dependent

dynamics that converge to $P_m\,\psi$ at low frequencies and approaches to $\omega_c\,P_m\,\psi$ at high frequencies. The decoupling due to low-pass filtering allows for the parasitic effect of P_m be reduced by more aggressive filtering, corresponding to a more compliant spring in the realization. The decoupling also enables higher P_m gains to be utilized, as the parasitic damping due to P_m can be counterbalanced by a lower ω_c.

Unfortunately, SEA under VSIC with P-P control and filtered velocity feedback does not result in good interaction control performance due to its noise amplification characteristics. It can be shown through a rearrangement of the LTI block diagram in Figure 3.1 that P-P control with filtered velocity feedback is equivalent to a PD-I_R controller with unity feedback, where $I_R = P_m\frac{\omega_c}{s+\omega_c}$ represents an integrator with a low-frequency roll-off and $D = \frac{Gt}{\omega_c}\,s$ denotes an ideal differentiation. Note that the derivative effect significantly amplifies the noise in both the force and end-effector motion measurements, resulting in chatter, especially for high torque controller gains.

3.1.3 Passivity of I_R-P Control with Filtered Velocity Feedback

When low-pass filtered velocity feedback is used, another low-pass filter needs to be introduced to the force controller of SEA under VSIC with P-P control to avoid noise amplification problems. In this section, we consider an integral controller with a low-frequency roll-off (also called first-order lag or filtered gain) $I_R = I_t\,\frac{\omega_c}{s+\omega_c}$ for the torque controller, while the motion controller is taken as a proportional gain P_m. The rendered stiffness is defined as $K_{vir}^{I_R-P} = K_d\frac{I_t\,P_m}{I_t\,P_m+1}$. The impedance at the interaction port $Z_{Spring_F}^{SEA^{I_R-P}}(s)$ of SEA under VSIC while rendering linear springs can be derived as

$$\frac{J\,K\,s^3 + (B + J\,\omega_c)\,K\,s^2 + K\,\beta\,\omega_c\,s + K\,K_d\,\alpha\,\omega_c}{J\,s^4 + (B + J\,\omega_c)\,s^3 + (K + \beta\,\omega_c)\,s^2 + (1+\alpha)\,K\,\omega_c\,s} \tag{3.3}$$

where $\alpha = P_m\,I_t$ and $\beta = B + P_m$. The necessary and sufficient conditions for the passivity of $Z_{Spring_F}^{SEA^{I_R-P}}(s)$ derived according to Theorem 2.1 are as follows.

Proposition 3.2. *Consider SEA under VSIC as in Figure 3.1 with integral with roll-off torque* $\frac{\omega_c}{s+\omega_c} I_t$ *and proportional* P_m *motion controllers and low-pass filtered velocity feedback* $\frac{\omega_c}{s+\omega_c}\omega_m$ *such that the driving port impedance at the interaction port is characterized by Eqn. (3.3). Let the controller parameters be positive. Then, the necessary and sufficient conditions for the passivity of* $Z_{Spring_F}^{SEA^{I_R-P}}(s)$ *are*

(a) $I_t \leq \frac{B}{J\,\omega_c\,P_m} + \frac{\beta\,(B+J\,\omega_c)}{P_m\,J\,K}$, *and*

(b) $\left(\frac{\alpha}{\alpha+1} - \frac{B}{J\,\omega_c\,(\alpha+1)}\right) K \leq K_{vir} \leq \left(\frac{1}{K} + \frac{1}{\beta\,\omega_c}\right)^{-1}$.

Proof. (i) According to the Routh-Hurwitz stability criterion, $Z_{Spring_F}^{SEA^{I_R-P}}(s)$ is stable iff

$$(B + J\,\omega_c)\,(K + \beta\,\omega_c) - J\,(K\,\omega_c(1+\alpha)) \geq 0 \tag{3.4}$$

$$(1+\alpha)\,\omega_c\,K \geq 0 \tag{3.5}$$

If Eqn. (3.4) is satisfied, then $Z_{Spring_F}^{SEA^{I_R-P}}(s)$ has all of its roots in the closed LHP.

(ii) $Z_{Spring_F}^{SEA^{I_R-P}}(s)$ has a single pole at $s = 0$ on the imaginary axis. The residue is $\frac{\alpha}{(1+\alpha)}\,K_d$, which is positive and real. When Eqn. (3.4) is equal to zero, the residue of the simple pole on the imaginary axis can be shown to be positive, if the upper bound of Condition (b) in Proposition 3.2 is satisfied.

(iii) The sign of $\mathrm{Re}\{Z_{Spring_F}^{SEA^{I_R-P}}(j\omega)\}$ can be checked as follows:

$$f_4\,\omega^4 + f_2\,\omega^2 \geq 0 \quad \omega \in (-\infty, \infty) \tag{3.6}$$

$$\text{where} \quad f_2 = K(K\,\beta\,{\omega_c}^2\,(\alpha+1) - K_d\,\alpha\,\omega_c\,(K + \beta\,\omega_c))$$
$$f_4 = K(B\,K - J\,\alpha\,\omega_c\,(K - K_d))$$

Eqn. (3.6) is satisfied iff Condition (b) of Proposition 3.2 is satisfied, ensuring that $f_4 \geq 0 \wedge f_2 \geq 0$. □

The upper bound on the virtual stiffness in Condition (b) of Proposition 3.2 can be interpreted as a serial connection of two linear springs with the stiffness values of K and $\beta\,\omega_c$. This upper bound converges to the physical stiffness of the series elastic actuator as $\beta\,\omega_c \to \infty$, indicating that $\beta\,\omega_c$ should be maximized to passively render stiff virtual springs. Hence, if aggressive low-pass filtering is used, then the sum of actuator damping and motion controller gain ($P_m + B$) must be set high to improve the upper bound on passive spring rendering.

The integral with roll-off under the filtered velocity feedback introduces a lower bound for the passively renderable stiffness, as in Condition (b) of Proposition 3.2. In [20], a similar bound for the passively renderable stiffness has been derived for SEA under VSIC with PI-PI control and no filtering, due to an integral term introduced to the motion controller.

To maximize the range of passively renderable stiffness levels, the lower bound in Proposition 3.2 can be set to zero by setting $J\,\alpha\,\omega_c - B = 0$. This equality dictates a relationship among the mechanical time constant of SEA, the cut-off frequency of the low-pass filter, and the I_R-P controller gains: the best performance is achieved when the time constant $1/(\alpha\,\omega_c)$ of the controller with filtered velocity feedback is equal to the mechanical time constant (J/B) of SEA.

3.1.4 Realization of I_R-P Control with Filtered Velocity Feedback

A passive physical equivalent of Eqn. (3.3) is presented in Figure 3.3, where $b_1 = \frac{J\,(K+\alpha(\,K-K_d))^2}{K^2\,(\alpha+1)^2}$, $c_1 = \frac{(K+\alpha(K-K_d))^2\,(B\,K+\alpha\,J\omega_c(K_d-K))}{K^3\,(\alpha+1)^2}$, while the rest of the terms are presented as a Matlab script[1]. The feasibility condition for c_1 imposes the lower bound in Condition (b) of Proposition 3.2. The feasibility of c_2 is ensured when Eqn. (3.4) and the upper bound of Condition (b) in Proposition 3.2 are satisfied.

In Figure 3.3, the rendered dynamics of the passive physical equivalent approaches to the virtual stiffness K_{vir} at low frequencies, as K_{vir} is parallel to all other

[1]The Matlab script including the parameters of the realization in Figure 3.3 is available at `https://hmi.sabanciuniv.edu/RealizationIRPVf.m`.

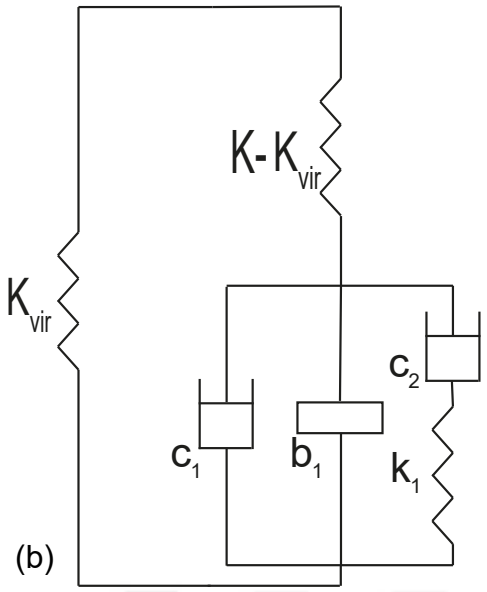

FIGURE 3.3: Passive physical equivalents of SEA under VSIC while rendering linear springs with filtered velocity feedback when the force controller is I_R and the motion controller is P.

elements. At high frequencies, the rendered dynamics converge to the parallel connection of the springs K_{vir} and $(K - K_{vir})$, which is equal to the stiffness K of the series elastic element. However, it is important to note that the range of K_{vir} is limited as dictated by Condition (b). If this condition is not satisfied, then the realization becomes infeasible and cannot be used for analysis. The remaining elements of the realization capture the effects of parasitic dynamics on the haptic rendering performance. Systematic numerical analyses indicate that the low-pass filter cut-off frequency affects the system in a similar manner as in the P-P case: a lower selection of ω_c reduces the effect of frequency-dependent parasitic damping c_2, due to the reduction of the stiffness k_1. Furthermore, the choice of higher force and motion controller gains reduces both b_1 and c_1.

A comparison of inertial effects in the realizations of P-P and I_R-P controller architectures indicates that the inerter term of the I_R-P controller is always higher than the inerter term of the P-P controller for feasible realizations. In addition, the ratios of serial spring-dampers in Figures 3.2 and 3.3 are equal to ω_c and $(G_m I_t + 1)(1 - K_{vir}/K)\ \omega_c$, respectively.

A comparison of the passive physical equivalent of SEA under I_R-P controller

with filtered velocity feedback in Figure 3.3 with the passive physical equivalent of SEA under I_R-P controller with no filter (not presented due to space limitations) during spring rendering indicates that they both have the same topology as in Figure 3.3. The parasitic damping element of the realization with no velocity filtering is always greater than c_1 in Figure 3.3, while their parasitic inerter terms are identical. Consequently, filtering the velocity results in a reduction of the parasitic damping effects, leading to a better performance.

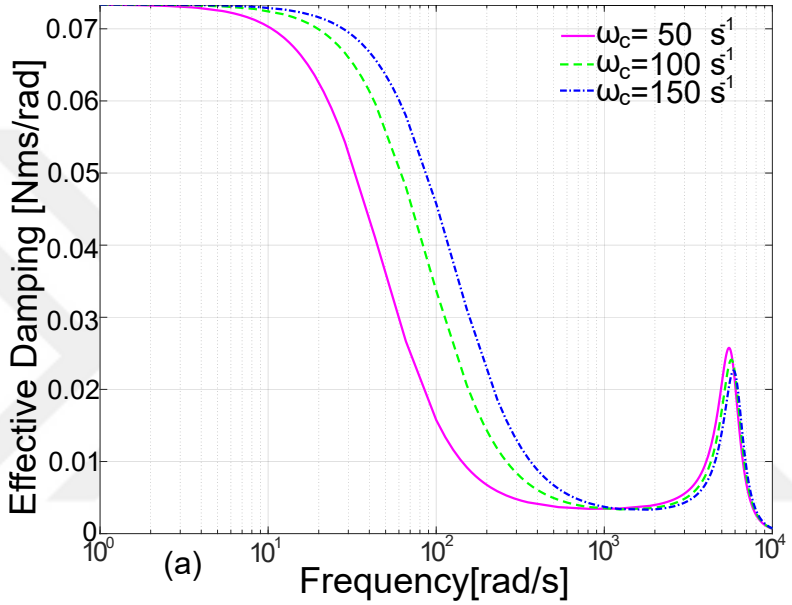

FIGURE 3.4: Effective damping of $Z^{SEA^{P-P}}_{Spring_F}(s)$.

3.2 Numerical Evaluations of Effective Impedance

We demonstrate the effects of system parameters on the rendering performance through numerical evaluations of effective impedance in the frequency domain. Table 7.1 presents the system parameters used in the simulations for rendering K_d=200 Nm/rad. During the simulations, the transmission ratio is taken as one.

The effect of the low-pass filter cut-off frequency ω_c on $Z^{SEA^{P-P}}_{Spring_F}(s)$ is demonstrated in Figure 3.4. It can be observed that as ω_c decreases, the effective damping of the system also decreases in Figure 3.4 due to the reduced parasitic damping, as

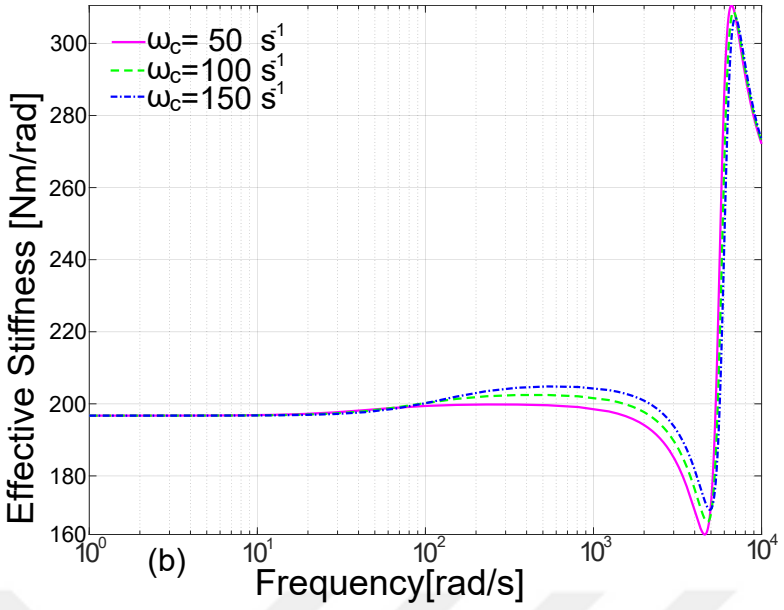

FIGURE 3.5: Effective stiffness of $Z_{Spring_F}^{SEA^{P-P}}(s)$.

TABLE 3.1: System parameters used for the numerical simulations for noise attenuation

Parameter	J	B	K
Value	0.0005 kg-m^2	1 Nm s/rad	250 Nm/rad
Parameter	P_t or I_t	P_m	K_d
Value	3 rad/(s Nm)	20 Nm s/rad	200 Nm/rad

predicted by the passive physical equivalent in Figure 3.2. Similarly, a lower ω_c also enhances the frequency range in which the effective stiffness of the system tracks the desired stiffness, as shown in Figure 3.5. The effective stiffness of $Z_{Spring_F}^{SEA^{I_R-P}}(s)$ (not presented due to space limitations) displays a similar characteristic, with the frequency range of high fidelity spring rendering increasing for lower ω_c.

Figure 3.6 demonstrates the effect of the low-pass filter cut-off frequency ω_c on effective damping of $Z_{Spring_F}^{SEA^{I_R-P}}(s)$. It can be observed that, as ω_c decreases, the effective damping of the system also decreases in Figure 3.6, due to reduced parasitic damping as predicted. Our numerical simulations also verify that linear spring and null impedance rendering performance increase for $Z_{Spring_F}^{SEA^{P-P}}(s)$ and $Z_{Spring_F}^{SEA^{I_R-P}}(s)$ with higher P_m.

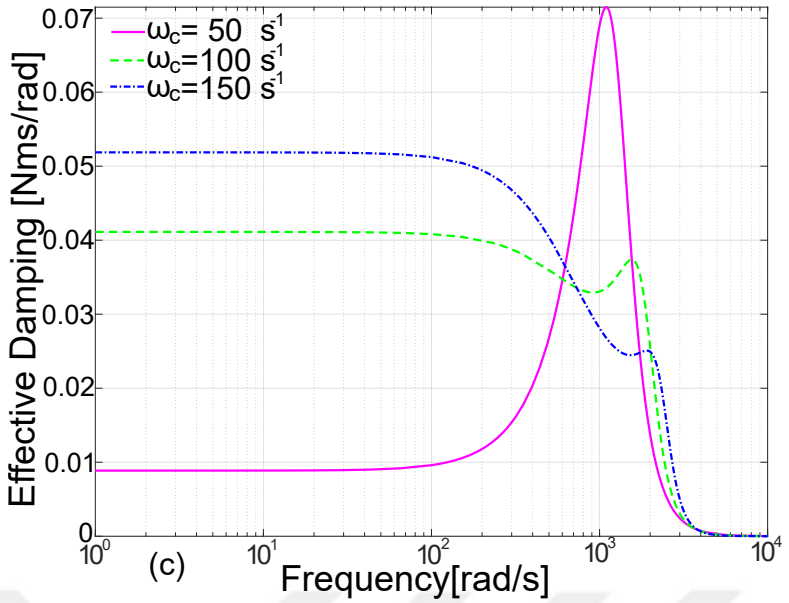

FIGURE 3.6: Effective damping of $Z_{Spring_F}^{SEA^{I_R-P}}(s)$.

3.3 Experimental Validations of Passivity Limits and Rendering Performance

The theoretical results are validated through the SEA brake pedal developed in [44]. The system parameters are experimentally determined via closed-loop system identification of the LTI system under the inner velocity control loop with $P_m = 0.0576$ Nms/rad to determine $J = 0.52$ gm^2 and $B = 0.011$ Nms/rad with $R^2 = 0.95$. The stiffness of the compliant element is characterized independently as $K = 252$ Nm/rad with $R^2 = 0.99$, by measuring deflections of the spring in response to pre-determined forces. Since the transmission ratio of the brake pedal is $n = 38.1$, the following mappings are applied to utilize the theoretical results: $J_{eq} = n^2\, J$, $B_{eq} = n^2\, B$, $P_{m_{eq}} = n^2\, P_m$, and $P_{t_{eq}} = 1/n\, P_t$.

The difficulty of accurately measuring the phase of a system makes using Bode plots to test a system's passivity unreliable. Instead, passivity can be determined by examining the coupled stability of interactions with the most destabilizing environments, defined as ideal springs or inertias with arbitrary magnitudes [34]. For SEA, inertial environments result in the worst case. The coupled stability

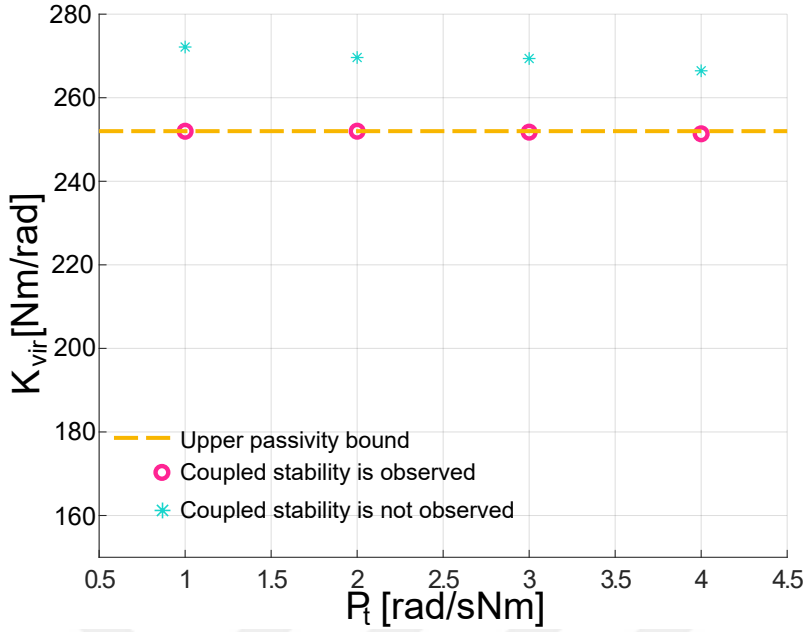

FIGURE 3.7: Verification of the passivity bounds of SEA while rendering virtual stiffness under VSIC with P-P control and velocity filtering.

of SEA during spring rendering when VSIC controllers are P-P and I_R-P with filtered velocity feedback are studied in Figures 3.7 and 3.8.

Figure 3.7 presents the experimental validation of the passivity bounds for $Z_{Spring_F}^{SEA^{P-P}}(s)$, where passive and active K_{vir} values are verified for four distinct P_t gains. The experimental results closely agree with the theoretical predictions for $Z_{Spring_F}^{SEA^{P-P}}(s)$, with experiments being about 6% more conservative than the theoretical bounds due to unmodeled dissipation effects. Note that P_t gain cannot be selected high for this controller, due to the noise amplification effects resulting in chatter, as predicted in Subsection 3.1.3. In particular, P_t can be increased five folds during the coupled stability experiments when there is no velocity filtering.

Figure 3.8 presents the experimental validation of the passivity bounds determined according to Proposition 3.2 for $Z_{Spring_F}^{SEA^{I_R-P}}(s)$. The experimental results are in good agreement with the theoretical predictions for $Z_{Spring_F}^{SEA^{I_R-P}}(s)$, with experimental data being about 4% more conservative. In this controller, the torque controller gain can be selected higher, unlike in the P-P case. However, as the integral with roll-off gain I_t increases, the range of the passively renderable stiffness

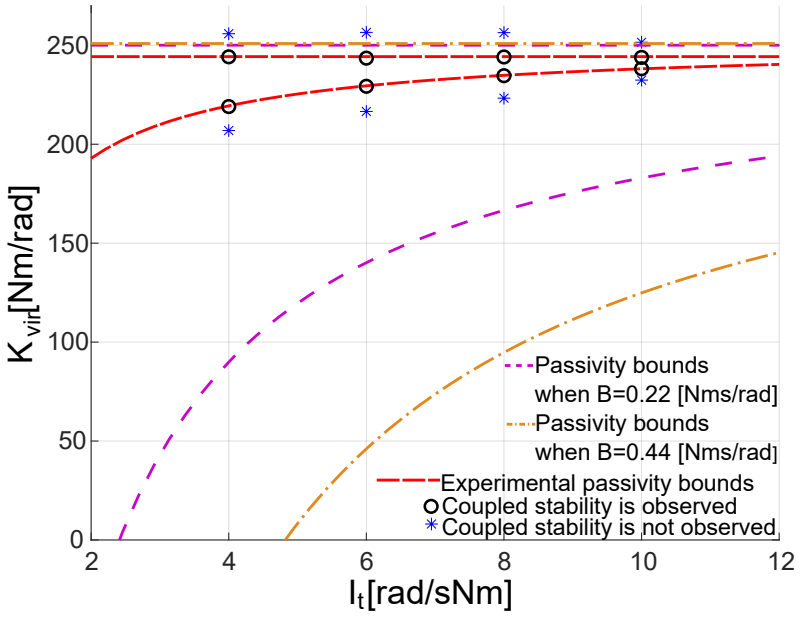

FIGURE 3.8: Verification of the passivity bounds of SEA while rendering virtual stiffness under VSIC with I_R-P control and velocity filtering.

levels gets narrower, inducing more strict lower bounds on K_{vir}. As emphasized in Subsection 3.1.3, to maximize the range of passively renderable stiffness levels, the time constant $1/(\alpha\,\omega_c)$ of the controller can be selected to be equal to the mechanical time constant (J/B) of the SEA. One method to achieve this equality without influencing the control parameters is to add extra mechanical/electrical damping to the plant [45]. Figure 3.8 also presents the passivity bounds of $Z_{Spring_F}^{SEA^{I_R}\text{-}P}(s)$ when $B = 0.22$ Nms/rad and $B = 0.44$ Nms/rad.

Figure 3.9 presents the null impedance rendering performance of SEA under VSIC with P-P control and velocity filtering. To quantify performance, the end-effector of the SEA brake pedal is rigidly connected to an ideal velocity source that excites the system with sine waves at 11 different frequencies, ranging from 0.3 rad/s to 6.28 rad/s, while the system is rendering the null impedance. The resulting interaction forces are recorded and presented as magnitude Bode plots in Figure 3.9 for two distinct motion controller gains. From these figures, it can be observed that the null rendering performance of SEA under P-P controller with velocity filtering increases as motion controller gain P_m increases from 0.005 Nms/rad to 0.01 Nms/rad. The increase in motion controller gain results in 9.5%

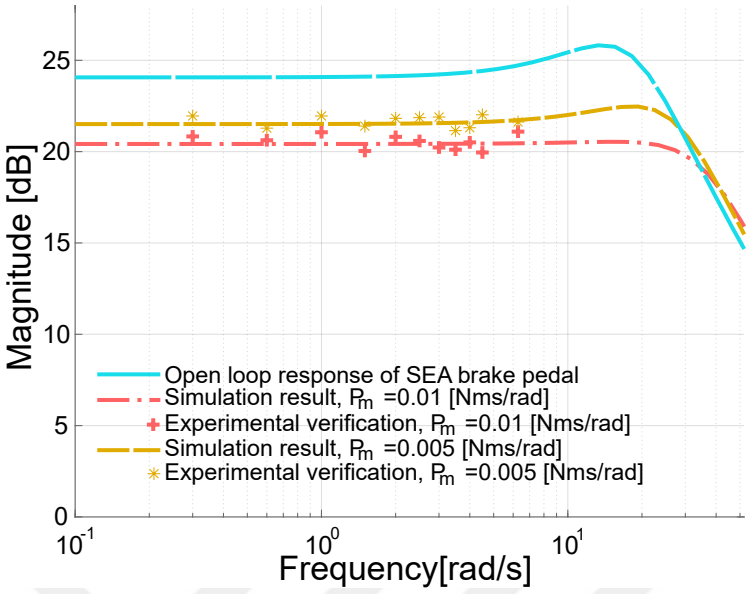

FIGURE 3.9: The null impedance rendering performance of SEA under VSIC with $P_t = 5$ rad/sNm and various motion controller gains..

decrease in the reflected impedance at the interaction port. The average errors between the experimental data and theoretical predictions are computed as 4.4% for $P_m = 0.01$ Nms/rad and 3.7% for $P_m = 0.005$ Nms/rad.

Similarly, the spring rendering performance of SEA under VSIC with I_R-P control and velocity filtering is experimentally characterized by observing the system's ability to produce the proper virtual spring forces when the end-effector is systematically excited with an ideal velocity source. For the low-pass filter cut-off frequencies of $\omega_c = 100$ s^{-1} and $\omega_c = 400$ s^{-1}, the end-effector of the SEA brake pedal is excited by an ideal velocity source inducing sine waves with frequencies ranging from 1 rad/s and 3 rad/s, while rendering a virtual stiffness of 220 Nm/rad. When the excitation frequency is set to 1 rad/s, the normalized root mean squared errors (NRMSEs) between the reference and measured torque values are calculated as 1.22% and 1.46% for $\omega_c = 100$ s^{-1} and $\omega_c = 400$ s^{-1}, respectively. Likewise, when the excitation frequency is set to 3 rad/s, NRMSEs are calculated as 1.35% and 1.51%, respectively. The performance increases with more aggressive filtering as predicted in Subsection 3.1.4.

3.4 Conclusion

In conclusion, while the inclusion of filtering to the velocity feedback improves the rendering performance, filtering comes with a cost for both controllers: VSIC with P-P controller amplifies noise at the torque controller, while I_R-P controller significantly limits the range of passively renderable springs, by introducing a lower limit on K_{vir}. Therefore it is observed that utilization of filtering on actuator velocity feedback for noise attenuation results in two distinct trade-offs; if the torque controller is not filtered as well, the filtering on actuator velocity feedback puts a limit on maximum selectable controller gains to avoid noise amplification. If the torque controller is filtered as well, then the maximum passivele renderable stiffness range decreases however the haptic rendering performance increases, resulting in a stability robustness haptic rendering performance trade-off.

Chapter 4

Effects of Phase Shaping Compensators on Passivity and Rendering Performance of SEA

In this chapter, we study the effects of filtering on stability robustness and haptic rendering performance trade-offs of haptic rendering with SEA under VSIC when filters are utilized as phase-shaping compensators.

We study passivity and haptic rendering fidelity of linear spring rendering of SEA under VSIC as given in Figure 2.2 by setting $Z_d = K_{ref}$, where K_{ref} represents the reference stiffness. The lead/lag compensator introduced as the torque controller is modeled as

$$C_t = P_t \frac{s + \eta\, w_a}{s + w_a} \tag{4.1}$$

where

$\eta < 1$ denotes lead compensator

$\eta > 1$ denotes lag compensator

The force controller is therefore denoted as a transfer function with a single pole at $-w_a$ and single zero at $-\eta\ w_a$ with a proportional gain P_t. In the special case where η is equal to one, the force controller reduces to proportional gain P_t. On the case η is equal to zero, the torque controller reduces to causal P-D controller where P denotes a proportional gain and D denotes a derivative gain and for $eta \rightarrow \infty$ the torque controller converges to P-I controller where P denotes a proportional gain and I denotes an integral gain.

4.1 Passivity of Spring Rendering with SEA

We first study passivity of SEA under VSIC when the torque controller consists of either a lead/lag compensator while motion controller consists of a proportional gain. Impedance from the interaction port, $Z_{Spring}^{SEA^{L_c-P}}(s)$ of SEA under VSIC while the torque controller consists of either a lead/lag compensator while motion controller consists of a proportional gain can be derived as

$$\frac{J_m\,K\,s^3 + K\,(\beta + J_m\,w_a)\,s^2 + K\,(K_{\text{ref}}\,\alpha + \beta\,w_a)\,s + K\,K_{\text{ref}}\,\alpha\,\eta\,w_a}{J_m\,s^4 + (\beta + J_m\,w_a)\,s^3 + (\beta\,w_a + K\,(\alpha+1))\,s^2 + K\,w_a\,(\alpha\,\eta + 1)\,s} \tag{4.2}$$

where $\alpha = P_m\,P_t$ and $\beta = B_m + P_m$. The rendered stiffness at low frequencies, K_{vir}, is equal to $K_{ref}\,\frac{\alpha\eta}{\alpha\eta+1}$. Necessary and sufficient conditions for the passivity of $Z_{Spring}^{SEA^{L_c-P}}(s)$ is derived as:

Proposition 4.1. *Consider SEA under VSIC as in Figure 3.1 where the torque consists of a lead/lag compensator, $P_t\,\frac{s+\eta\,w_a}{s+w_a}$, and the motion controller consists of proportional gain, P_m. Let the controller gains and the desired impedance be positive. Impedance seen from the interaction port is derived as Eqn. (4.2). The following conditions make up the necessary and sufficient condition for the passivity of $Z_{Spring}^{SEA^{L_c-P}}(s)$:*

$$\textbf{1.1}\ \eta < 1 + \beta \frac{(w_a(J_m w_a + \beta) + K(\alpha + 1))}{J_m K \alpha w_a} \tag{4.3}$$

$$\textbf{2.1}\ \eta \leq 1 + \frac{\beta (K(\alpha + 1) - K_{\text{ref}} \alpha)}{J_m \alpha w_a (K - K_{\text{ref}})} \tag{4.4}$$

$$\textbf{3.1}\ K_{\text{ref}} \leq \frac{K \beta w_a (\alpha \eta + 1)}{\alpha (K(\eta - 1) + \beta \eta w_a)} \tag{4.5}$$

Proof. (i) Stability of $Z_{Spring}^{SEA^{Lc-P}}(s)$ is checked with Routh-Hurwitz stability criterion. $Z_{Spring}^{SEA^{Lc-P}}(s)$ has no right hand poles if and only if

$$\beta w_a (\beta + J_m w_a) + K \beta (\alpha + 1) - J_m K \alpha w_a (\eta - 1) \geq 0 \tag{4.6}$$

$$K w_a (1 + \alpha \eta) \geq 0 \tag{4.7}$$

The condition given in Eqn. (4.3) ensures the condition given in Eqn. (4.6) being fulfilled. Eqn. (4.7) is always ensured to be fulfilled due to positiveness of plant and controller parameters.

(ii) $Z_{Spring}^{SEA^{Lc-P}}(s)$ has a single pole at $s = 0$ on the imaginary axis. The residue is K_{vir}, which is positive and real. In the case the right-hand side of Eqn. (4.6) becomes equal to the left hand-side, the positiveness of plant parameters results in negative residues, therefore the resultant poles on the imaginary axis are omitted and the left and right hand side of Eqn. (4.3) are not allowed to be equal.

(iii) The sign of $\text{Re}\{Z_{Spring}^{SEA^{Lc-P}}(s)\}$ can be checked as

$$d_4 \omega^4 + d_2 \omega^2 \geq 0 \quad \omega \in (-\infty, \infty) \tag{4.8}$$

$$d_4 = J_m \alpha \eta w_a (K_{ref} - K) + K \beta + (\alpha \beta + J_m \alpha w_a)(K - K_{\text{ref}})$$
$$d_2 = K_{\text{ref}} (K \alpha - \eta (K \alpha w_a + \alpha \beta w_a)) + K \beta (w_a + \alpha \eta w_a)$$

Eqn. (4.8) is satisfied if and only if $d_4 \geq 0 \wedge d_2 \geq 0$. If $K \geq K_{ref}$, the condition $d_4 \geq 0$ is satisfied iff the condition given in Eqn. (4.9) is fulfilled. If $K_{ref} \geq K$,

then $d_4 \geq 0$ is satisfied iff the condition given in Eqn. (4.10) is fulfilled. Likewise if $\eta \geq \frac{K}{K+\beta\, w_a}$, the condition $d_2 \geq 0$ is satisfied iff the condition given in Eqn. (4.11) is fulfilled. If $\eta < \frac{K}{K+\beta\, w_a}$, the condition given in Eqn. (4.12) must be fulfilled to satisfy $d_2 \geq 0$. □

4.1.1 Discussions on Passivity Bounds

To avoid inequality sign flip un-sureness the explicit forms of the necessary and sufficient conditions are given below. The inequality sign of the Eqn. (4.4) can be better understood with Eqns. (4.9,4.10), where the inequaltity sign is dictated by the relative magnitudes of the SEA stiffness, K, and reference stiffness K_{ref}. Likewise the direction of the inequality sign given in Eqn. (4.5) is explicitly given in Eqns. (4.11,4.12), with the pre-condition of if η is greater or equal to $\frac{K}{K+\beta\, w_a}$, or not.

$$\text{if } K \geq K_{ref}$$

$$\textbf{2.1}\ \eta \leq 1 + \frac{\beta\,(K\,(\alpha+1) - K_{\text{ref}}\,\alpha)}{J_m\,\alpha\,w_a\,(K - K_{\text{ref}})} \tag{4.9}$$

$$\text{if } K < K_{ref}$$

$$\textbf{2.2}\ \eta > 1 - \frac{\beta\,(K\,(\alpha+1) - K_{\text{ref}}\,\alpha)}{J_m\,\alpha\,w_a\,(K_{ref} - K)} \tag{4.10}$$

$$\text{if } \eta \geq \frac{K}{K+\beta\, w_a}$$

$$\textbf{3.1}\ K_{\text{ref}} \leq \frac{K\,\beta\,w_a\,(\alpha\,\eta+1)}{\alpha\,(K\,(\eta-1)+\beta\,\eta\,w_a)} \tag{4.11}$$

$$\text{if } \eta < \frac{K}{K+\beta\, w_a}$$

$$\textbf{3.2}\ K_{\text{ref}} > \frac{K\,\beta\,w_a\,(\alpha\,\eta+1)}{\alpha\,(K\,(\eta-1)+\beta\,\eta\,w_a)} \tag{4.12}$$

The stability condition given in Eqn. (4.3) is always fulfilled if the torque controller is set as a proportional gain by setting η to one. Setting η to one, consequently results in the discovery of necessary and sufficient condition of spring rendering when both torque and motion controllers consists of proportional gains studied in [13], $K \geq K_{ref}\frac{\alpha}{\alpha+1}$, from the conditions given in Eqns. (4.9,4.10,4.11). It is

observed that when $\eta \to \infty$ the stability condition given in Eqn. (4.3) can not be fulfilled. Therefore it shown that SEA under VSIC when the torque controller consists of proportional and integral gains while the motion controller consists of proportional gain can not passively render stiffnesses [20]. When the controller gains are high, meaning $\alpha \to \infty$, the stability condition reduces to

$$\eta < 1 + \frac{\beta}{J_m\, w_a} \tag{4.13}$$

The equation can be arranged to be equivalent to $\frac{1}{(\eta-1)\, w_a} > \frac{J_m}{\beta}$ where J_m is the plant mass and β is the system damping and $\frac{J_m}{\beta}$ is the mechanical time constant of the SEA plant. The inequality is ensured to be fulfilled when $\eta < 1$, meaning the torque controller is a lead compensator (PD). However if the torque controller is a lag compensator, $\eta > 1$, the time constant of the lag compensator (PI), $\frac{1}{(\eta-1)\, w_a}$ must be greater than the mechanical time constant of the plant.

The validity of the necessary and sufficient condition between Eqn. (4.9) and Eqn. (4.10) depends on whether if the SEA stiffness, K, is higher than the desired stiffness, K_{ref} or not. It is observed that a lead compensator $\eta < 1$, always fulfills the condition given in Eqn. (4.9) while a lag compensator, $\eta > 1$, always ensures Eqn. (4.10) being fulfilled. For reasonably tuned controller gains, the condition $K_{ref} \geq K$ results in rendered stiffness K_{vir} being close to SEA stiffness itself, therefore the case where $K \geq K_{ref}$ is a much more common occurrence. Through Eqns. (4.9,4.10) it is observed that as system damping, β, increase, the maximum passively selectable η increase for $K \geq K_{ref}$ and minimum passively selectable η decrease for $K_{ref} > K$. Likewise as the compensator frequency w_a and plant inertia J_m decrease, maximum passively selectable η increase for $K \geq K_{ref}$ and minimum passively selectable η decrease for $K_{ref} > K$.

The ruling condition among Eqns. (4.11) and Eqns. (4.12) depends on the condition of $\eta \geq \frac{K}{K+\beta\, w_a}$. The validity of the condition given in Eqn. (4.11) is more likely for real time implementations since the multiplication of system damping β and the compensator frequency w_a dominates over the SEA stiffness resulting in

a very narrow range where $\eta < \frac{K}{K+\beta\, w_a}$ is feasible. Rewritting Eqn. (4.11) as a bound on maximum passively renderable stiffness, K_{vir} results as the following

$$K_{vir} \leq K \frac{\beta\, \eta\, w_a}{K\,(\eta - 1) + \beta\, \eta\, w_a} \tag{4.14}$$

From the inequality given in Eqn. (4.14) it can be observed that the condition reduces to $K \geq K_{vir}$ when the compensator factor, η, is equal to one. It is further observed that for both lag compensator and lead compensator, $\eta > 1$ and $\eta < 1$ respectively, maximum passively renderable stiffness decreases as η increases.

Remark 4.2. Necessary and sufficient conditions for passivity of null impedance rendering of SEA under VSIC where the torque controller consists of a lead/lag compensator, and the motion controller consists of a proportional gain can be recovered from Proposition 4.1 by setting K_{ref}=0. Accordingly, Eqn. (4.3), Eqn. (4.9) make up the necessary and sufficient conditions. Eqn. (4.12) is dropped since multiplication of $(\alpha\,(K\,(\eta - 1) + \beta\, \eta\, w_a))$ with K_{ref}=0 yields a zero and no inequality sign change is required. Eqn. (4.11) is always fulfilled since $0 \leq K\beta w_a(\alpha\eta + 1)$ is guranteed to be fulfilled due to positive plant and controller parameters.

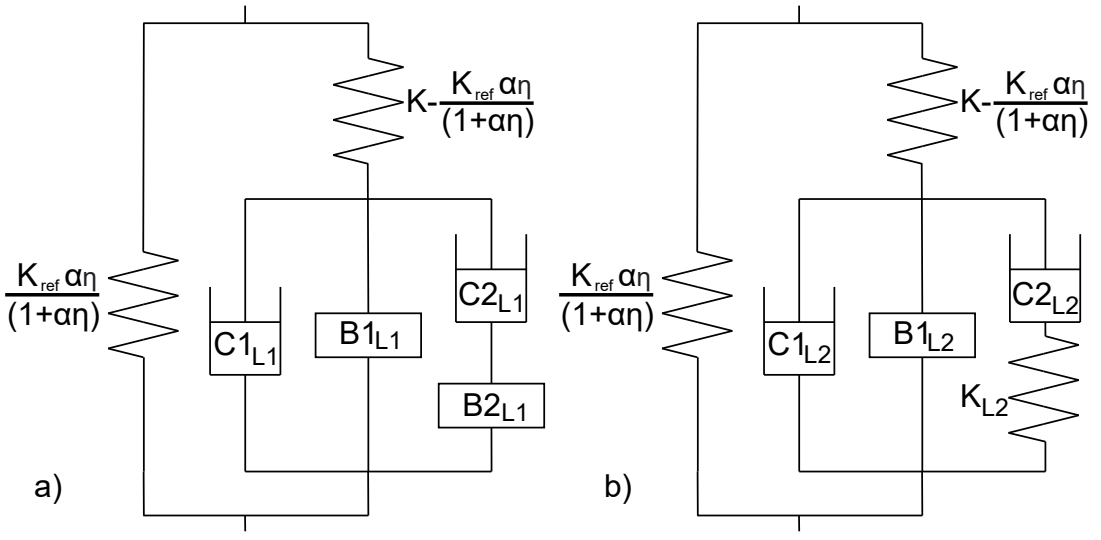

FIGURE 4.1: Passive physical equivalents of spring rendering with SEA under VSIC, with lead/lag torque and proportional motion controllers

4.2 Passive Physical Equivalents of Spring Rendering with SEA under VSIC

Figures 4.1a and 4.1b depict a passive physical equivalent of spring rendering of SEA under VSIC when the torque controller consists of a lead/lag compensator while motion controller is a proportional gain. Figures 4.1a and 4.1b terms are presented as a Matlab script[1]. The feasibility condition of $C1_{L1}$ of Figure 4.1a imposes the Eqns. (4.11) and (4.12) and the feasibility condition of $C1_{L2}$ of Figure 4.1b imposes the Eqns. (4.9) and (4.10). Serial inerter-damper system of Figure 4.1a and serial spring-damper system of Figure 4.1b are complicated to derive rigorous sufficient conditions of Proposition 4.1, but numerical studies show that their feasibility range completes each other. In addition, numerical studies show that Figure 4.1a feasibility range is wider than Figure 4.1b feasibility range for lag compensator ($\eta < 1$), while Figure 4.1b feasibility range is wider than Figure 4.1a feasibility range for lead compensator ($\eta > 1$). Please note that Figures 4.1a and 4.1b reduce to the SEA under VSIC for P-P controller which is presented in [13].

Figures 4.1a and 4.1b approach K_{vir} at low frequencies, and K_{vir} is parallel to all other elements. $K - K_{vir}$ and K_{vir} are coupled at high frequencies, thus Figures 4.1a and 4.1b go to physical stiffness. The rest of the terms can be called parasitic terms which negatively affect haptic rendering performance. Parasitic inerter terms $B1_{L1}$ and $B1_{L2}$ are identical for Figures 4.1a and 4.1b, and as P_t increases, $B1_{L1}$ and $B1_{L2}$ decrease. Systematic numerical analyses indicate that as η and P_t increase, $C1_{L1}$ and $C1_{L2}$ decrease. In addition, numerical analyses shows that selection of lower ω_a relaxes the upper bound of η as argued in Subsection 4.1 and selection of higher η decreases the parasitic damping of the system. The biggest difference between Figures 4.1a and 4.1b include serial damper-inerter and serial damper-spring terms, respectively. Figure 4.1a introduces frequency-dependent damping term where $C2_{L1}$ is added to $C1_{L1}$ as frequency increases because of

[1]The Matlab script including the parameters of the realizations in Figures 4.1a and 4.1b are available at `https://hmi.sabanciuniv.edu/SEA_VSIC_Spring_lead_lag`.

existence of $B2_{L1}$. Figure 4.1b introduces frequency-dependent damping, and numerical analyses show that lower ω_a reduces the effect of damping term $C2_{L2}$ due to a decrease of K_{L2}.

4.3 Interpretation of Compensators as Low-Pass Filters

Previously it was shown that a low pass filter on the velocity actuator feedback, through rearrangement of the block diagram, is a derivative-proportional gain on the torque controller, and an additional low-pass filter is required in the torque controller to avoid noise amplification. The lead/lag compensator in this study can be represented as seperate filters on the torque controller and actuator velocity feedback. A lag compensator, $\eta \geq 1$, denotes a system where the filter cut-off frequency of the actuator velocity feedback is higher than of the torque controller and a lead compensator, $\eta \leq 1$, denotes a system where the filter cut-off frequency of the actuator velocity feedback is lower than of the torque controller. Therefore it can be concluded that for better performance the inner motion loop must have a higher cut-off frequnecy than of the torque controller or in other words the inner motion loop must be admissible to run in higher frequencies than of the torque controller for better performance.

4.4 Numerical Evaluations of Effective Impedance

We study the effects of controller gains on rendering performance through numerical evaluations. Bode plots and effective impedance approaches are used for numerical evaluation. Effective impedance definitions partition the frequency-dependent impedance function into its basic components, where the real positive part is assigned to effective damping, while the imaginary part is mapped to effective spring and effective inertia based on their phase response [46].

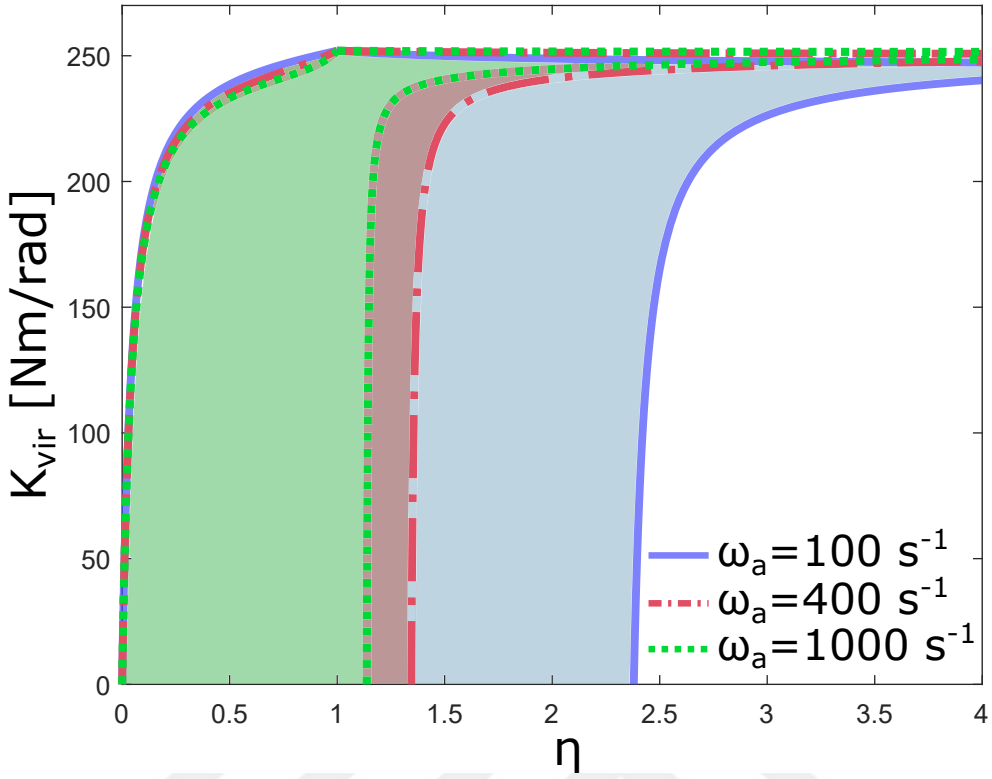

FIGURE 4.2: Passivity bounds of K_{vir} and η at different cut-off frequencies, w_a, when P_t=10 $rad/(s\,Nm)$.

For faithful numerical evaluations, plant and controller parameters must be chosen within a sensible range of plausible real-time hardware specifications. In this light, plant and control parameters used in this section are chosen as the parameters of the real-time SEA break pedal system, presented in Section 4.5.

Figure 4.2 presents presents maximum amount amount of renderable stiffness, K_{vir}, with respect to different η values with distinct cut-off frequencies, w_a. The shaded area in between the lines depicts the passivity region. It is observed that the maximum amount of renderable stiffness increase in between $0 \leq \eta \leq 1$, and reaches a maximum value that is equal to SEA stiffness, K, when η is equal to one. When $\eta \geq 1$, the maximum amount of renderable stiffness decrease and an upper bound to η is introduced. The upper bound on K_{vir} and the upper bound on η intersect with each other when the condition given in Eqn. (4.3) is violated. As mentioned in Subsection 4.1 an increase in the cut-off frequency, w_a, results in a decrease in maximum passively selectable η value.

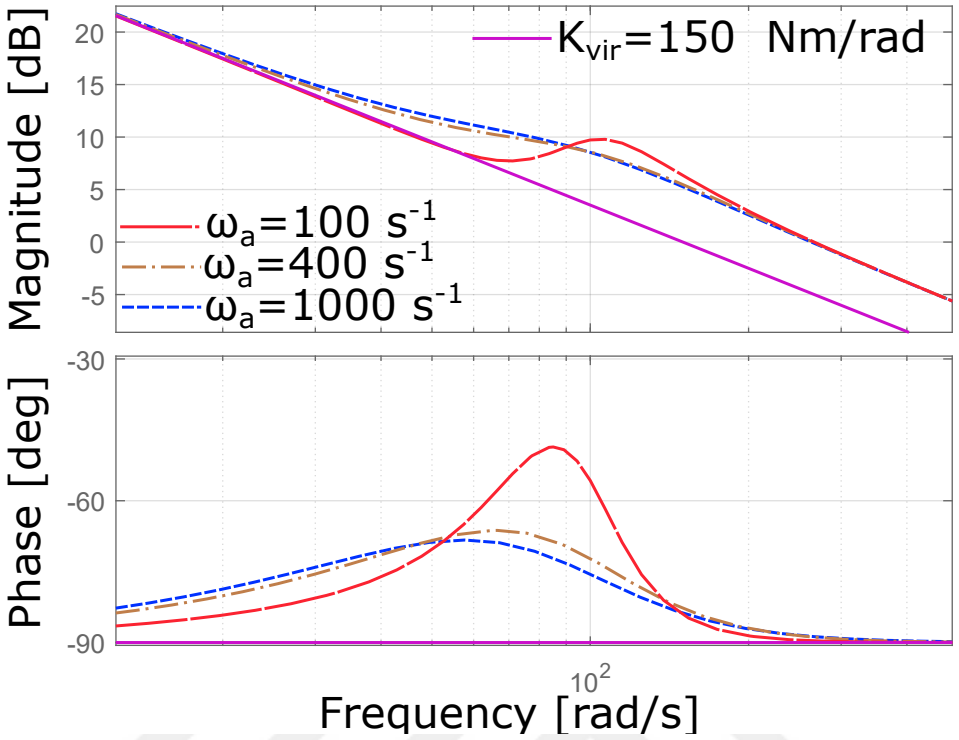

FIGURE 4.3: Bode plots of rendering a stiffness of K_{vir}=150 Nm/rad with P_t=10 $rad/(s\,Nm)$ with maximum passively selectable η at different cut-off frequencies, w_a.

Figure 4.3 presents Bode plots of spring rendering of SEA under VSIC while the torque controller consists of a lag compensator with the maximum passively selectable η value. From Figure 4.2, it is observed that as the cut-off frequency w_a decrease maximum passively selectable η increase. It is observed that the spring rendering performance increases as the cut-off frequency, w_a, decreases and η increases.

Figure 4.4 and Figure 4.5 depict effective stiffness and damping of SEA under VSIC during spring rendering, respectively, while the torque controller consists of a lead compensator (η=0.8), Proportional gain (η=1) and lag compensator (η=1.2). It is observed that the lag compensator increases spring rendering performance by reducing the effective damping in the system and prolonging the spring rendering bandwidth. It is also noted that eventhough the lead compensator does not positively effect the spring rendering performance, it can be utilized for increasing the effective damping in the system.

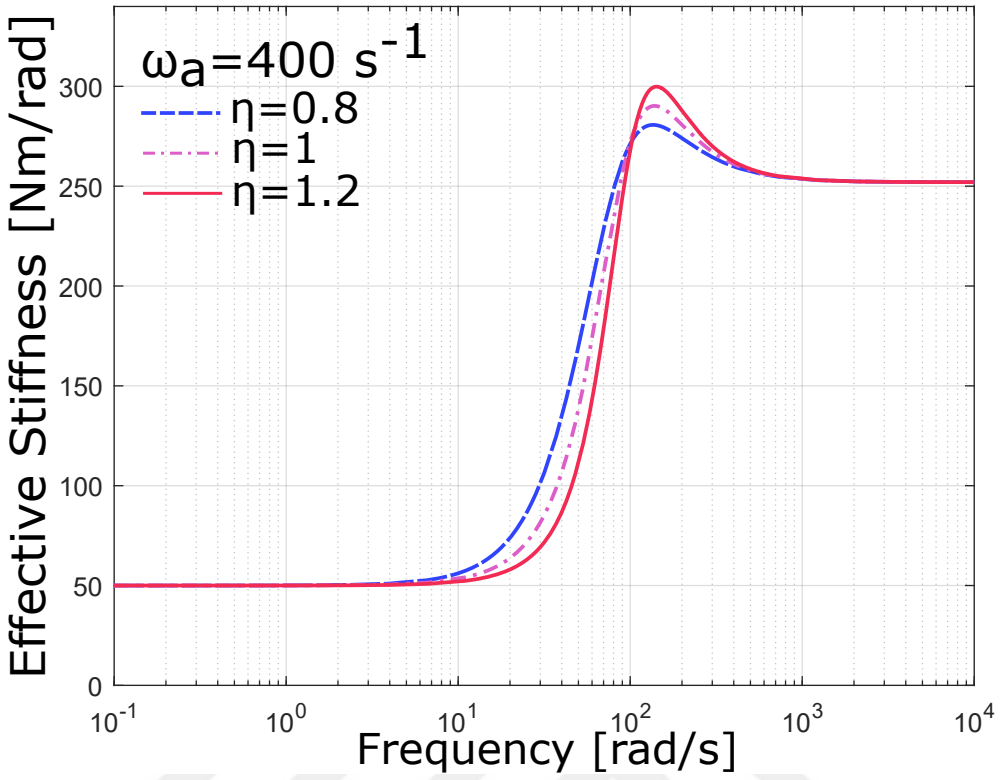

FIGURE 4.4: Effective stiffness when the torque controller consists of; a lead compensator, P gain and lag compensator.

4.5 Experimental Validations of Passivity Limits and Rendering Performance

In this section, we present experimental validations of theoretical passivity bounds through the use of the most destabilizing environments and systematic haptic rendering fidelity experiments through magnitude bode plots. The custom SEA break pedal hardware used in this study is previously presented in [44]. The SEA break pedal utilizes a DC motor with a cross-flexure element in between the interaction port and the motor side. The torques generated by the motor are amplified through a total transmission ratio of 1:38.1. The deflections of the cross-flexure joint are measured with an optical encoder. All controllers are implemented through an industrial PC with an EtherCAT bus network.

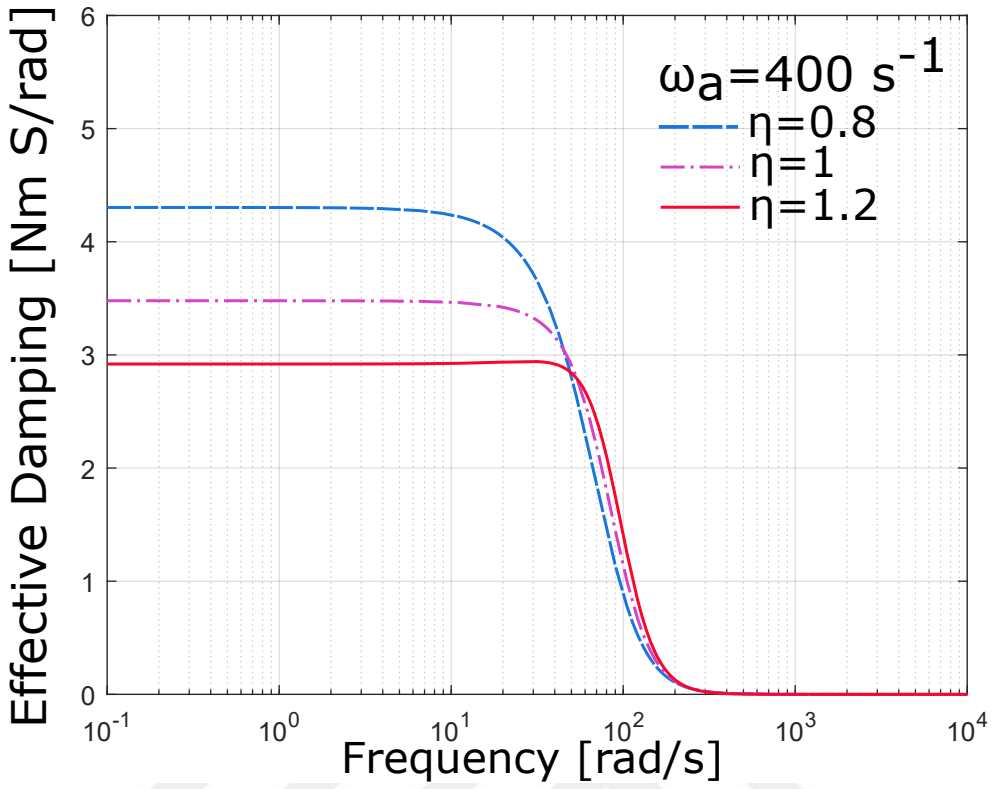

FIGURE 4.5: Effective damping when the torque controller consists of a lead compensator, P gain and lag compensator.

4.5.1 System Identification

Precise identification of plant parameters are important for accurate comparisons between the experimental and theoretical results. The SEA stiffness of the cross-flexure is identified through measurements of deflections of predetermined torques on the interaction port. The SEA stiffness is characterized as $K = 252\,Nm/rad$ with $R^2 = 0.99$. Plant damping and inertia are determined by closed-loop system identification. The system identification is conducted with a motion controller gain of $P_m = 0.0576\,Nm\,s/rad$ and the plant inertia, J_m and damping, B_m are found as $0.52\,gm^2$ and $0.011\,Nm\,s/rad$ respectively, with $R^2 = 0.95$.

4.5.2 Verification of Passivity Bounds

We employ coupled stability experiments while the interaction port is coupled to most destabilizing environments [8]. Figure 4.6 present the K_{vir}-η plot, maximum

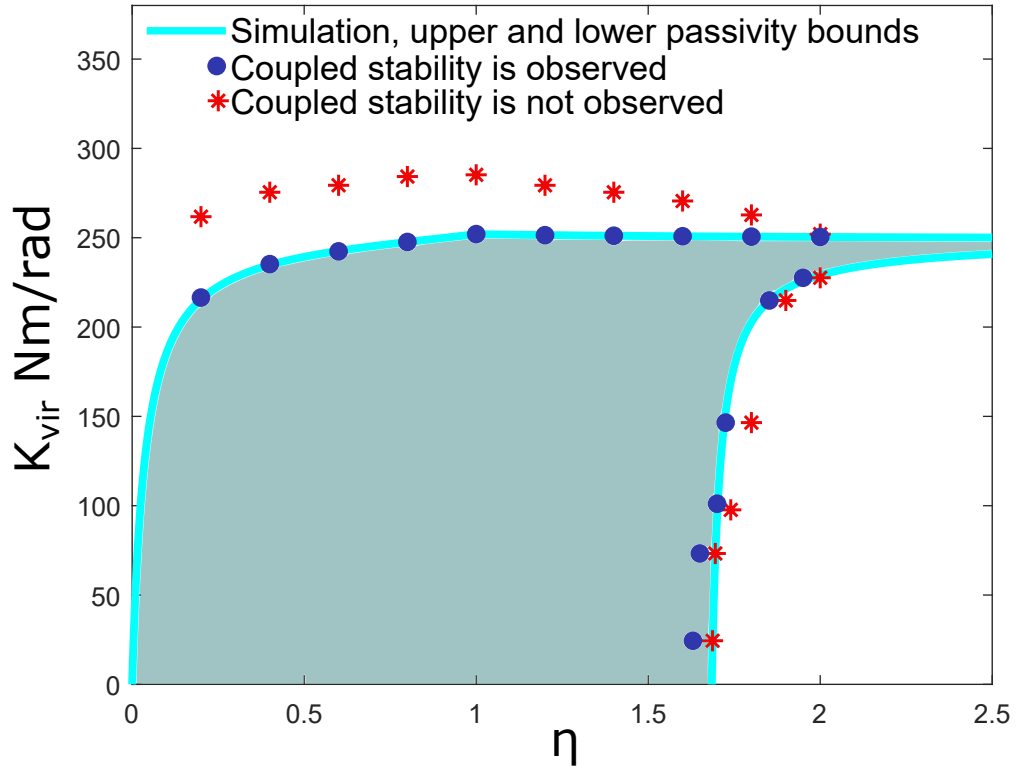

FIGURE 4.6: Experimental verification of passivity bounds with P_t=12 $rad/(s\,Nm)$, w_a=200 s^{-1}.

and minimum amount of renderable stiffness at each η value. The figure depicts experimental points where coupled stability is observed and is not observed. The errors for upper bound on K_{vir} and upper bound on η are calculated separately. The average error for the upper bound of K_{vir} is calculated as 10.8 % while the average error for the upper bound of η is calculated as 2.96 %. The experimental points where coupled stability is observed, are found to be less conservative than the simulation results for the upper passivity bound on K_{vir}. On the other hand experimental points where coupled stability is observed, are found to be less conservative for the upper passivity bound on η for high K_{vir} values and simulation results become less conservative than experimental points once K_{vir} value decrease below 75 Nm/rad.

In this section, we present experimental validation of haptic rendering fidelity of SEA through systematic coupled excitation experiments. The interaction port of

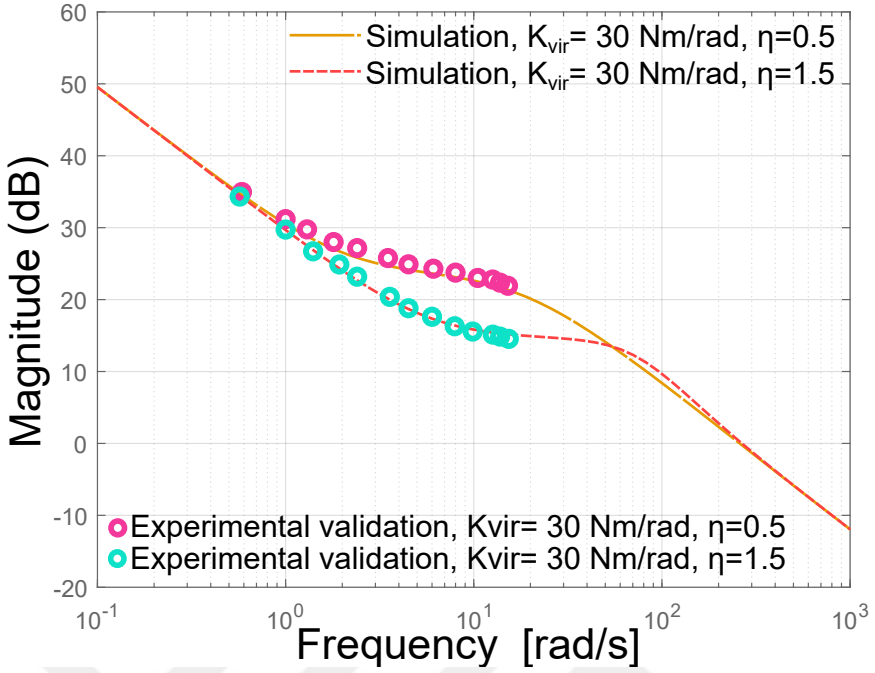

FIGURE 4.7: Experimental verification of haptic rendering fidelity with P_t=5 $rad/(s\,Nm)$, w_a=250 s^{-1}.

the SEA break pedal is rigidly coupled to an ideal motion source and the system is excited with a chirp signal sweeping through 0.1 rad/s to 15.5 rad/s. At distinct frequency intervals, the measured torque on the SEA, τ_{SEA}, and the end effector positions are saved. The end-effector position is fitted to a sine wave in each frequency interval to calculate end effector velocity, ω_{end}, in post-processing. Interaction port impedance is experimentally derived as $\frac{\tau_{sea}}{\omega_{end}}$. The resultant interaction port impedance at each frequency interval are presented in magnitude bode plots. Then simulation results and experimental data are compared to determine haptic rendering fidelity.

Figure 4.7 presents magnitude bode plots while rendering a stiffness of K_{vir}=30 Nm/rad with a lead compensator, $\eta = 0.5$ and a lag compensator $\eta = 1.5$. As presented in Subsection 4.2, an increase in η increases the spring rendering performance by reducing the effective damping in the system and increasing spring rendering bandwidth. The errors for this set of experiments are founds as 8.1% for η=0.5 and 3.7% for η=1.5.

A tracking test is conducted via a chirp excitation from the ideal motion source in which the desired torque from the desired impedance, τ_d and the estimated torque from the SEA, τ_{SEA} are collected. The chirp signal traces in between 0.1 to 12.57 rad/s while a spring of 30 Nm/rad is rendered with $P_t = 12$ rad/(s Nm) with $w_a = 200\, s^{-1}$. The normalized RMS error for the tracking test is computed as 3.79% for the lead compensator(η=0.5) and 1.63% for the lag compensator(η=1.5). Therefore it is observed that employment of a lag compensator enhances force tracking performance.

4.6 Psychophysical Experiments

A psychophysical experiment is designed to study the human perception of the haptic rendering fidelity when lead and lag compensators are utilized. Eight human subjects, all having ample experience with the device but not expertise, are asked to do position-tracking tasks.

4.6.1 Method

A visual reference and the end effector position of the haptic device are displayed through a monitor and participants are asked to track the reference signal while interacting with the haptic device. Before the experiments, the participants are trained to track the visual reference with minimal error. The experiment consists of 4 stages in which the participants are asked to compare:

1) Lead and lag compensators at a low frequency (0.5 rad/s),
2) Lead and lag compensators at a high frequency (4 rad/s),
3) Lag compensator at a low frequency (0.5 rad/s), and a high frequency (4 rad/s),
4) Lead compensator at a low frequency (0.5 rad/s), and a high frequency (4 rad/s).

Each stage consists of a total of five sets where each set contains two interaction sequences (lead and lag compensators for stages one and two or a low frequency (0.5 rad/s), and a high frequency (4 rad/s) for stages three and four) at random order. The comparison is made through binary answers for each set where the participants mark down their results on the basis of:

1) If the interaction task feels like a linear spring or a viscous damper, and
2) Which task conducts a higher peak torque value through the interaction in each set, where if two interaction torques are similar participants are asked to leave blank.

4.6.1.1 System parameters and Tracking Task

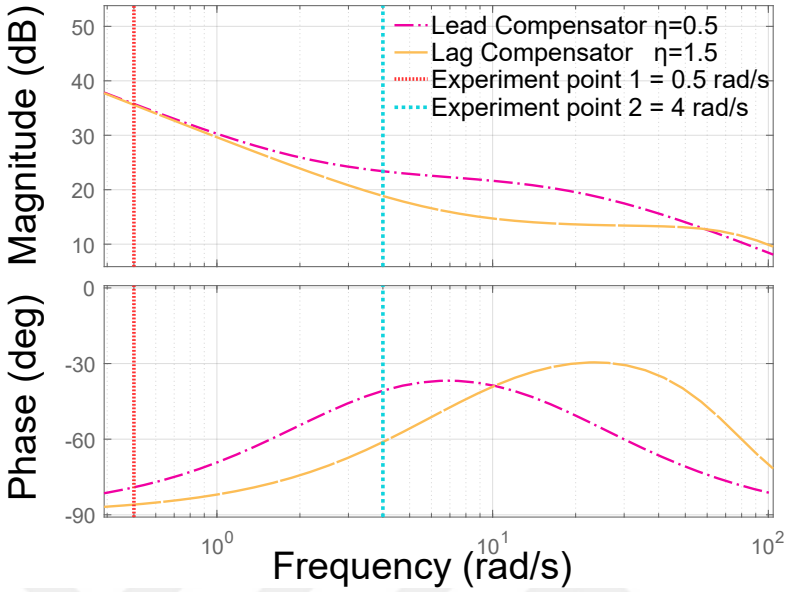

FIGURE 4.8: Bode plots of the end point impedance of the experimented controller architectures and experimental frequency points.

Figure 4.8 presents the bode plots of spring rendering of lead and lag compensators while rendering a linear spring of 30 Nm/rad with $P_t = 6\,rad/(s\,Nm)$, P_m=0.0576 Nms/rad and w_a=200 s^{-1}. The interaction frequencies, 0.5 rad/s and 4 rad/s are marked down and it is shown that for 0.5 rad/s both systems consisting of either lead or lag compensator have a magnitude response with an error of less than 1% and for 4 rad/s, the lead compensator has a magnitude of 23.36 dB and the lag compensator has a magnitude of 18.81 dB, corresponding to a decrease of impedance magnitude of 38.3%. For test stages one and two, the visual reference signal is set as 0.1 rad amplitude sine wave and for test stages three and four, the amplitude of the sine wave is set as 0.05 rad for 4 rad/s and 0.4 rad for 0.5 rad/s to maintain the same peak interaction velocity between frequency comparisons.

TABLE 4.1: Participant results where either a linear spring or viscous damper is decided to be the interaction environment and the more torque applying environment is designated by the participant.

Stage 1 (0.5 rad/s)	Spring	Damper	Exerts More Force
Lead Comp.	31	9	13
Lag Comp.	38	2	9

Stage 2 (4 rad/s)	Spring	Damper	Exerts More Force
Lead Comp.	2	38	33
Lag Comp.	32	8	3

Stage 3 (Lag Comp.)	Spring	Damper	Exerts More Force
0.5 rad/s	39	1	40
4 rad/s	28	12	0

Stage 4 (Lead Comp.)	Spring	Damper	Exerts More Force
0.5 rad/s	35	5	38
4 rad/s	11	29	0

4.6.2 Results

Table 4.1 presents the results of the human subject experiment with the saved answers in each set where each participant filled in a binary answer sheet, containing a total of forty answers at each stage of the experiment. At stage one of the experiment, where the participants interact with SEA either with a lag or lead compensator torque controller with a reference sine wave of a frequency of $0.5\,rad/s$, 77.5 % of the participant answers were saved as a linear spring and 22.5 % of the participant answers were saved as a viscous damper for SEA where the lead compensator is employed as the torque controller while 95 % of participants answers were saved as linear spring and 5 % of participant answers were saved as viscous damper for SEA where the lag compensator is employed as the torque controller. Therefore the theoretical results and the results of the first stage of the the human subject experiment are in a good correlation. A majority, 45 %, of the participant answers stated that both systems exert the same amount of torque when compared to each other while 32.5 % of participant answers state that SEA where the lead compensator is employed as the torque controller exerts more torque while 22.5 % of the participant answers state that SEA where the lag

compensator is employed as the torque controller exerts more torque. Figure 4.8 shows that SEA where the torque controller consists of a lead compensator has a higher force magnitude gain at higher frequencies than the lag compensator. It is thought that the non-perfect tracking performance of the human user results in application of high frequency interactions in between the tracking task, resulting in sudden spikes of torque on the interaction port. The results therefore highlight the importance of high fidelity haptic rendering performance even when the aimed interaction frequency is relatively low.

The second stage of the experiment requires participants to interact with SEA either with a lag or lead compensator torque controller with a reference sine wave of a frequency of $4\,rad/s$. 5 % of the participant answers and 95 % of the participant answers were saved as a linear spring and as a viscous damper respectively, for SEA where the lead compensator is employed as the torque controller while 80 % of participants answers were saved as linear spring and 20 % of participant answers were saved as viscous damper for SEA where the lag compensator is employed as the torque controller. That is the expected theoratical outcome as the haptic system employing the lead compensator converges to a viscous damping around $2\,rad/s$ interaction frequency as the bode magnitude response stays the same for higher frequencies in the given limited range whereas the lag compensator is still expected to act as a linear spring where the bode magnitude response decreases as the interaction frequency increases. However, it is still important to note that a lower percentage of answers were saved as a linear spring when compared to stage one for the SEA employing a lag compensator, due to interaction frequency getting closer to the convergence point where viscous damping is rendered. Still, through the experiment, it is shown that employment of the lag compensator increases the haptic rendering performance and a high majority of the participant saved SEA where the torque controller consists of lead compensator as the more torque exerting haptic environment with 82.5 % of total answers while SEA, where the torque controller consists of lag compensator, scored 7.5 % as the more torque exerting environment and 10 % of the participant answers were saved as two system exerting the same amount of torque.

At the third stage of the experiment the participants were asked to compare two interaction frequencies, $0.5\,rad/s$ and $4\,rad/s$ for linear spring rendering of SEA where the torque controller consists of a lag compensator. While the interaction frequency is $0.5\,rad/s$, 97.5 % of the participant answers were saved as a linear spring, while 2.5 % of the participant answers were saved as a viscous damper. When the interaction frequency is set as $4\,rad/s$ participant answers for linear spring dropped to 70 % and participant answers for viscous damper increased to 30 %. All participant answers, 100 %, stated that the lower interaction frequency, $0.5\,rad/s$ results is a higher maximum peak torque through the interaction. Again the results of the human subject experiment are in good agreement with the theoretical results as a lower interaction frequency exerts more amount of torque on the interacting subject and as the interaction frequency increases the damping content of the haptic environment increases as well.

Fourth stage of the experiment the participants were asked to compare two interaction frequencies, $0.5\,rad/s$ and $4\,rad/s$ for linear spring rendering of SEA where the torque controller consists of a lead compensator.At the designated low interaction frequency, $0.5\,rad/s$, 87.5 % of participant answers were saved as a linear spring while 12.5 % of participant answers were saved as a viscous damping while for high interaction frequency, $4\,rad/s$, 27.5 % of participant answers were saved as a linear spring and 72.5 % of participant answers were saved as a viscous damping. 95 % of the participant answers saved the lower interaction frequency, $0.5\,rad/s$ as the more torque exerting interaction frequency while 5 % of the participant answers saved two interaction frequencies as exerting the same amount of torque. Therefore the majority of the participant answers state that at low frequencies the spring rendering of SEA where the torque controller consists of a lead compensator exert more torque through the interaction eventhough the high frequency interactions with the system feels like an interaction with a viscous damping. Again our theoratical results and human subject experiment results are in good correlation as the increase in torque magnitude as the interaction frequency decrease is expected eventhough at $4\,rad/s$ the SEA system where the torque controller consists of a lead compensator is expected to act as a viscous damper.

TABLE 4.2: Tests of within-subjects effects for the human perception of the linear spring rendering of SEA where the torque controller consists of either a lead or lag compensator and subjects interact with the system with two distinct frequencies.

Source	Type III Sum of Squares	df	Mean Square	F	Sig.	Partial Eta Squared
Controller Type(CT)						
Sphericity Assumed	120,125	1	120,125	192,2	<,001	,965
Greenhouse-Geisser	120,125	1	120,125	192,2	<,001	,965
Huynh-Feldt	120,125	1	120,125	192,2	<,001	,965
Lower-bound	120,125	1	120,125	192,2	<,001	,965
Error-Controller Type						
Sphericity Assumed	4,375	7	,625			
Greenhouse-Geisser	4,375	7	,625			
Huynh-Feldt	4,375	7	,625			
Lower-bound	4,375	7	,625			
Interaction Frequency(IF)						
Sphericity Assumed	136,125	1	136,125	49,181	<,001	,875
Greenhouse-Geisser	136,125	1	136,125	49,181	<,001	,875
Huynh-Feldt	136,125	1	136,125	49,181	<,001	,875
Lower-bound	136,125	1	136,125	49,181	<,001	,875
Error-Interaction Frequency						
Sphericity Assumed	19,375	7	2,768			
Greenhouse-Geisser	19,375	7	2,768			
Huynh-Feldt	19,375	7	2,768			
Lower-bound	19,375	7	2,768			
(CT)*(IF)						
Sphericity Assumed	78,125	1	78,125	397,727	<,001	,983
Greenhouse-Geisser	78,125	1	78,125	397,727	<,001	,983
Huynh-Feldt	78,125	1	78,125	397,727	<,001	,983
Lower-bound	78,125	1	78,125	397,727	<,001	,983
Error-(CT)*(IF)						
Sphericity Assumed	1,375	7	,196			
Greenhouse-Geisser	1,375	7	,196			
Huynh-Feldt	1,375	7	,196			
Lower-bound	1,375	7	,196			

4.6.3 Analysis

Two-way repeated measures ANOVA was performed to evaluate the significant difference in the utilization of lead and lag compensators on human perception of the haptic system based on whether the interaction task feels like a spring or a damper. The answer sets of all stages are combined into a two-by-two matrix based on the number of times the participants have selected "Spring Virtual Environment" depending on the:

- controller consisting of either a lead or a lag compensator,
- interaction frequency pre-determined by the visual reference.

Table 4.2 presents the results of two-way repeated measures ANOVA. ANOVA indicates a statistical significance for the controller type when the torque controller

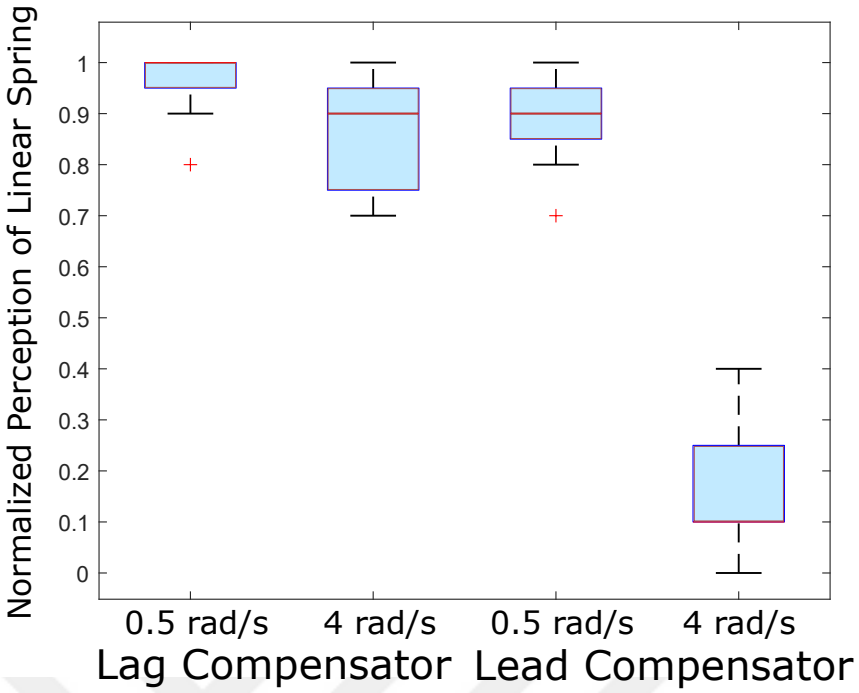

FIGURE 4.9: Box plot of human perception of linear spring rendering of SEA under VSIC where the torque controller consists of either a lag compensator or a lead compensator and interaction consists of either a low frequency (0.5 rad/s) or a high frequency (4 rad/s).

consists of either a lead compensator or a lag compensator ($F(1,7) = 192,2$ and $p < 0,001$). It is further observed that the interaction frequency and the interaction of controller type and interaction frequency have a statistical significance for human perception of spring rendering as well with $F(1,7)$=$(49,181)$, $p < 0,001$ and $F(1,7)$=$(397,727)$, $p < 0,001$ respectively.

Figure 4.9 presents the box plot of human perception of linear spring rendering of SEA. It is observed that for the interaction frequency of $0.5\,rad/s$ in both systems that either feature a lead or lag compensator, the answers of the participants mainly agree that the system feels more like a spring rather than a damper even though the answer set of the system featuring lag compensator is more concentrated and the median lies in the certainty region (Normalized perception=1). For the interaction frequency of $4\,rad/s$ it is observed that the answer set for lag compensator is concentrated in between the normalized region of $0.75 - 0.95$ while the answer set of the lead compensator is concentrated in between the normalized region of $0.1 - 0.25$, indicating that the haptic perception of humans differ

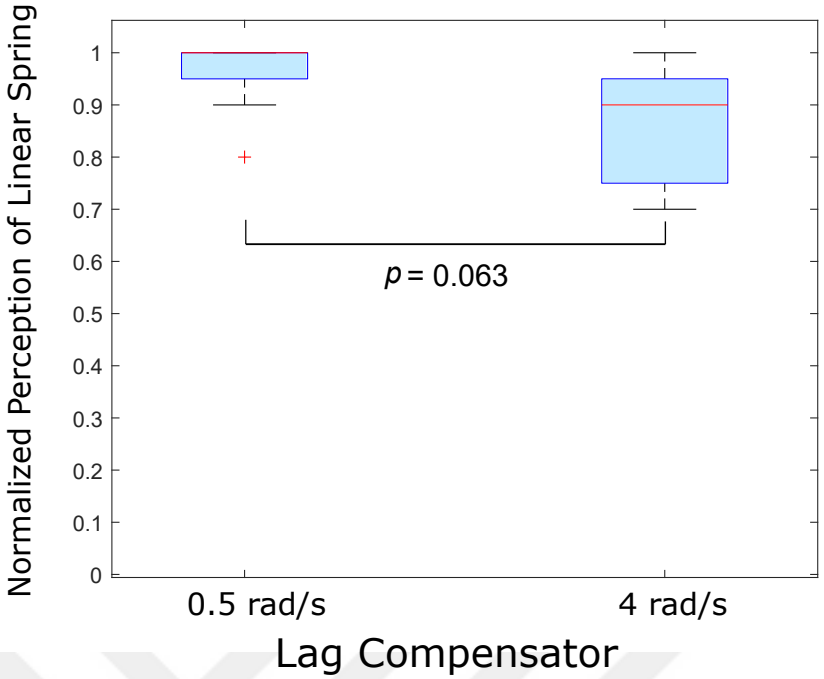

FIGURE 4.10: Box plot of human perception of linear spring rendering of SEA under VSIC where the torque controller consists of a lag compensator and the p-value between interaction frequencies.

with a change in interaction frequency when negative phase is introduced via lag compensation and when positive phase is introduced via lead compensation.

Figure 4.10 presents the box plot of human perception of linear spring rendering of SEA when lag compensation is utilized. The p-value obtained is through one-way repeated measures ANOVA ($F(1,14)$=$4,073$, p=$0,063$). Since p-value is greater than $0,05$ the null hypothesis is accepted, and it is concluded that the increase in the interaction frequency between the given range does not significantly affect the perceived kinesthetic haptic feedback. Figure 4.11 presents the box plot of human perception of linear spring rendering of SEA when lead compensation is utilized. The null hypothesis is rejected by the conduction of one-way repeated measures ANOVA ($F(1,14)$=$156,987$, $p < 0,001$). It is observed that the increase in the interaction frequency has a statistically significant effect on the perceived kinesthetic haptic feedback.

Next, we consider the human perception of torque exertion when the torque controller features either a lag or a lead compensator and the interaction frequency is

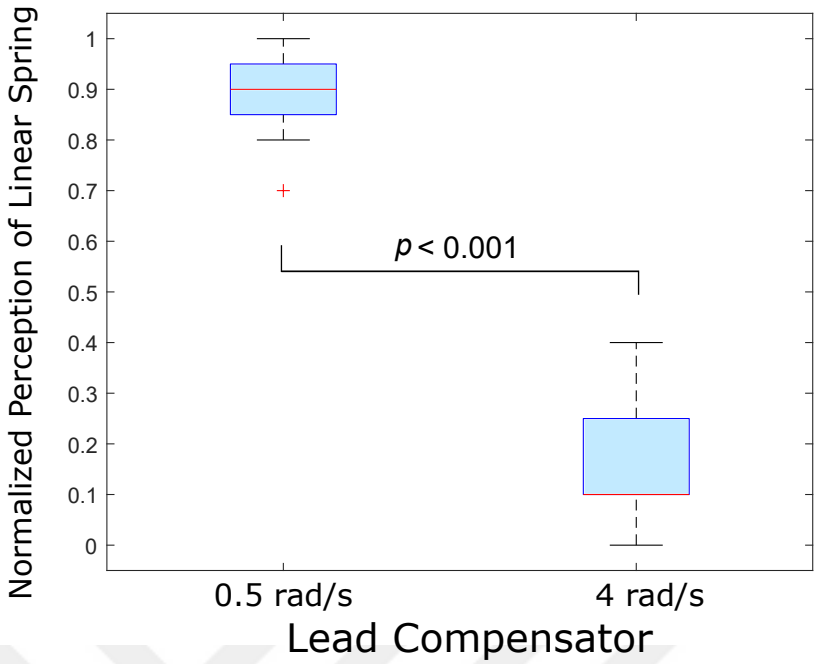

FIGURE 4.11: Box plot of human perception of linear spring rendering of SEA under VSIC where the torque controller consists of a lead compensator and the p-value between interaction frequencies.

either $4\,rad/s$ or $0.5\,rad/s$. Stages 1 and 2, and stages 3 and 4 are separated into two groups since human subjects compare lead and lag compensators at stages 1 and 2 and interaction frequencies at stages 3 and 4.

Figure 4.12 presents the box plot of torque exertion comparison between lead and lag compensators at low frequency (0.5 rad/s). One-way repeated measures ANOVA shows that the difference between the torque exertion of lead and lag compensators at low frequencies is not statistically significant ($F(1,14)=1.1$, $p=0.3125$). Therefore null hypothesis is accepted and it is concluded that the perception of torque exertion does not depend on the compensator choice.

Figure 4.13 presents the box plot of torque exertion comparison between lead and lag compensators at high frequency (4 rad/s). One-way repeated measures ANOVA shows that the difference between the torque exertion of lead and lag compensators at high frequencies is statistically significant ($F(1,14)=47.01$, $p<0.001$). Therefore null hypothesis is rejected and it is concluded that the choice of the compensator and the choice of addition of positive or negative phase affects the human

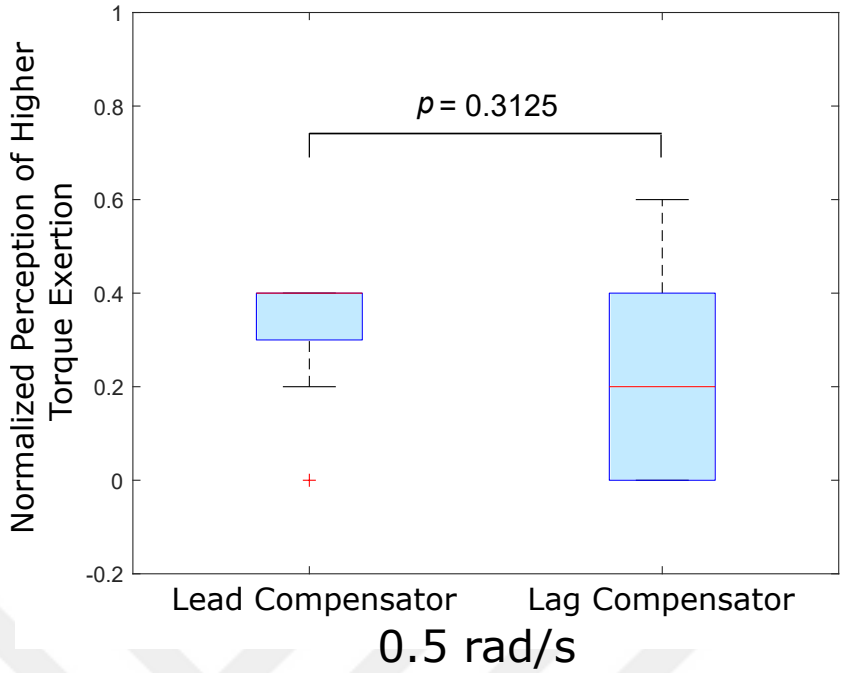

FIGURE 4.12: Box plot of human perception of higher torque exertion of SEA under VSIC where the torque controller consists of either a lag compensator or a lead compensator and interaction consists of a low frequency (0.5 rad/s).

perception of torque exertion and the compensator design must be made with the effects on haptic rendering performance in mind.

For stages 3 and 4, where low and high-frequency responses of compensators are compared, the resultant choice of higher frequency exerting more force on the human subject is null, meaning no human subject has chosen high frequency as the more torque exerting system. However, due to human subjects selecting the low frequency as 100% of the answers, it is concluded that the low-frequency behavior of both compensators exerts more force compared to high-frequency behavior.

4.7 Conclusion

We have presented the passivity analysis and provided necessary and sufficient conditions for the passivity of SEA under VSIC while rendering linear springs and null impedance while the torque controller consists of a transfer function with a single pole and a single zero with a proportional gain, which is generalized to a

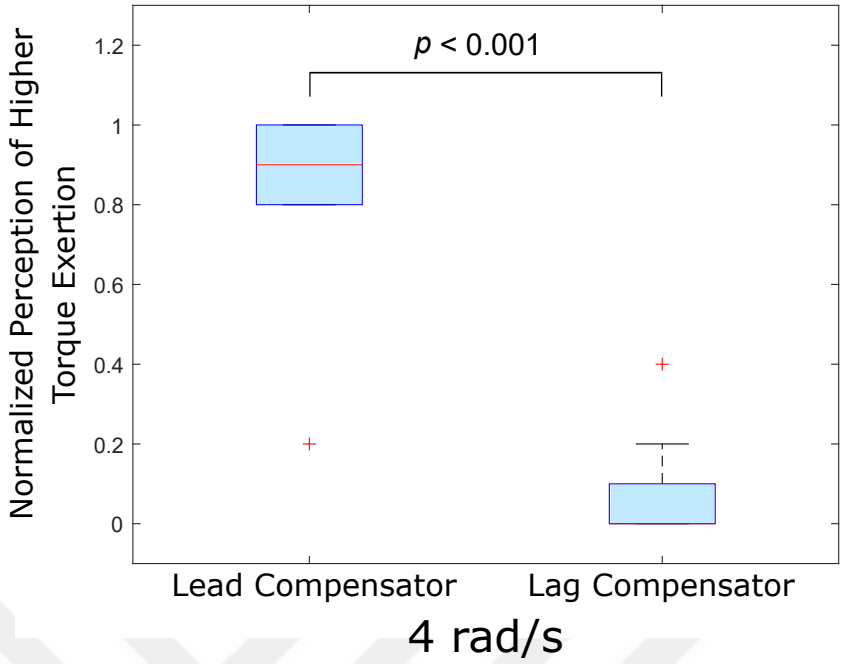

FIGURE 4.13: Box plot of human perception of higher torque exertion of SEA under VSIC where the torque controller consists of either a lag compensator or a lead compensator and interaction consists of a high frequency (4 rad/s).

single proportional gain, a lead/lag compensator, causal derivative action or to proportional-integral action with a low frequency roll-off. We have shown that a pure integral gain on the controller results in a non-passive system however employment of a lag compensator heavily increases the haptic rendering performance while allowing for a wide range of passively renderable stiffness. We have experimentally validated our results with coupled stability and systematic performance experiments.

Overall it has been observed that addition of negative phase by utilization of a lag compensator as the torque controller increases the haptic rendering performance while resulting in more conservative maximum passively renderable stiffness range.

Chapter 5

Effects of Shaping the Reference Virtual Environment during Mass-Spring-Damper Rendering with SEA

In this chapter, we study the effects of bandwidth limiting and reference shaping of the reference virtual environment model to ensure its reference trackability and to ensure causality by introducing high-frequency roll-off characteristics.

5.1 Passivity of SEA under VSIC during Linear Spring Rendering with Impedance Reference Roll-off

We start our study by considering linear spring rendering of SEA under VSIC while the impedance reference model is filtered to introduce a high-frequency roll-off. Our main aim in this section is to observe the stability-robustness and performance

trade-off of the bandwidth limitation the filter enacts on the haptic rendering performance of SEA.

Given the measured end effector position θ_{end}, when both controllers are taken as proportional gains, P_m and P_t, and if the reference impedance is set to Z_d= $K_{ref}\frac{\omega_a}{s+\omega_a}$, the impedance transfer function at the interaction port of the SEA is derived as the following:

$$\frac{(J_m\,K)\,s^3+(K\,(\beta+J_m\,\omega_a))\,s^2+(K\,\beta\,\omega_a)\,s+K\,K_{\mathrm{ref}}\,\alpha\,\omega_a}{J_m\,s^4+(\beta+J_m\,\omega_a)\,s^3+(\beta\,\omega_a+K\,(\alpha+1))\,s^2+(K\,\omega_a\,(\alpha+1))\,s} \tag{5.1}$$

where, β=P_m+B_m and α=P_tP_m.

The passivity of SEA under VSIC while spring rendering with impedance reference roll-off is established with the following theorem.

Theorem 5.1. *Consider linear spring rendering with impedance roll-off of SEA under VSIC as in Figure 2.2 where* Z_d=$K_{ref}\frac{\omega_a}{s+\omega_a}$*, and the torque and motion controllers consist of proportional gains* P_t *and* P_m*. The following expression constructs necessary and sufficient conditions for the passivity of* $Z_{S_{BW}}^{SEA^{P-P}}(s)$*:*

$$K_{ref} \leq \frac{K(\alpha+1)}{\alpha}\frac{\beta\omega_a}{K(\alpha+1)+\beta\omega_a} \tag{5.2}$$

Proof.

• Routh-Hurwitz stability criterion dictates that the system is stable iff:

$$\beta\,(K\,(\alpha+1)+\omega_a\,(J_m+\beta))\geq 0$$
$$K\omega_a\,(\alpha+1)\geq 0$$

The positiveness of controller gains and plant parameters ensures the stability of $Z_{S_{BW}}^{SEA^{P-P}}(s)$.

• The system has one single pole at $s=\ 0$ on the imaginary axis, where residue is $\frac{K_{\mathrm{ref}}\,\alpha}{\alpha+1}$, which is positive and real. Through Routh-Hurwitz stability criterion and

the positiveness of all plant parameters and controller gains, it is shown that there are no additional poles on the imaginary axis.

• The sign of $\mathrm{Re}\{Z_{FS}^{SEA^{P-P}}(s)\}$ can be checked as follows:

$$J_2\,\omega^2 + J_0 \;\geq 0 \quad \omega \in (-\infty, \infty) \tag{5.3}$$

where

$$J_0 = K\,\beta\,\omega_a\,(\alpha+1) - K_{\mathrm{ref}}\,\alpha\,(\beta\,\omega_a + K\,(\alpha+1))$$
$$J_2 = \beta\,(\alpha+1)\,K^2 + J_m\,K_{\mathrm{ref}}\,\alpha\,\omega_a\,K$$

Eqn. (5.3) holds if and only if $J_2 \geq 0 \wedge J_0 \geq 0$, which is fulfilled by Eqn. (5.2). □

Remark 5.2. Kenanoglu and Patoglu [13] had previously shown the necessary and sufficient conditions for linear spring rendering of SEA under VSIC where torque and motion controllers consist of proportional gains without filtering of the impedance reference. The necessary and sufficient condition that ensures the passivity of SEA under VSIC while spring rendering is provided in the Subsection 2.5.

If the filter cut-off frequency is high such that; $\omega_a \to \infty$, Eqn. (5.2) recovers the case where no bandwidth limit is enacted and the reference model is unfiltered, given in Section 2.5. The filtering of the reference impedance does not change the rendered stiffness, K_{vir}, and is found as $K_{ref}\frac{\alpha}{\alpha+1}$, which is equal to the K_{vir} of the unfiltered case. The extra term added to the upper bound in Eqn. (5.2), that arises due to bandwidth limitation of the filtering of the reference impedance, $\frac{\beta\omega_a}{K(\alpha+1)+\beta\omega_a}$, can be thought as series connections of two springs of values; 1 and $\beta\omega_a/K(\alpha+1)$. Accordingly the maximum value this series connection can take is equal to 1, if $\beta\omega_a/K(\alpha+1)$ is infinite. Therefore as the total damping of the plant and the motion loop, β, cut-off frequency ω_a, SEA stiffness K and product of controller gains, α, increase the upper bound on maximum renderable stiffness K_{vir} increase.

Therefore the cut-off frequency selection of the reference impedance filter must be chosen accordingly to the desired stiffness that is to be rendered and there exists a minimum value for the cut-off frequency for all passive virtual stiffness levels up to the SEA stiffness K.

5.2 Passivity of SEA under VSIC during Parallel Mass-Spring-Damper Rendering with Impedance Reference Roll-off

We continue our study by setting bandwidth limits to impedance reference, by filtering the reference damping and reference mass. We present necessary and sufficient conditions for the passivity of haptic rendering while the reference virtual environment consists of combinations of linear parallel mass, spring, and damper. Even though we are mainly interested in the stability robustness and haptic rendering performance trade-offs that are caused by the rolling-off of the mass and damper reference that filters enact on the reference impedance model, haptic rendering of a virtual environment that contains dampers or masses is not feasible without filtering, since without the filtering estimation of the end effector velocity or acceleration can not be causally carried out from the end effector position. Therefore haptic rendering without filtering is not implementable in real-time systems due to the causality of real-time differentiation. Likewise, if analog sensing is used to estimate the velocity or acceleration of the end effector, filtering is still required in real-time applications in order to attenuate sensor noise.

Given the end effector position θ_{end}, consider SEA under VSIC as in Figure 2.2. The reference virtual environment without filtering can be expressed as; $Z_d = M_{ref}s^2+B_{ref}s+K_{ref}$, in which M_{ref} is the reference mass, B_{ref} is the reference damping, K_{ref} is the reference stiffness. The s^n is the n^{th} order ideal differentiation in which ideal differentiation is not implementable due to the causal nature

of the real-time systems. However filtering the reference model, in order to estimate velocity or acceleration results in real-time implementable systems as well as removing the high frequency content of the reference input, shaping a reference impedance model that does not interfere with the high-frequency plant dynamics, and asymptotically converging to dynamics of the open-loop response of the plant as argued in [22]. To enable real-time implementation and to limit the bandwidth of the reference impedance input to low frequencies, the reference impedance is set as the following:

$$Z_d = K_{\text{ref}} + B_{\text{ref}}\frac{s\,\omega_a}{s+\omega_a} + M_{\text{ref}}\frac{s^2\,{\omega_a}^2}{\left(s+\omega_a\right)^2} \tag{5.4}$$

where $\frac{\omega_a}{s+\omega_a}$ is a first-order linear filter with a cut-off frequency of ω_a.

This section presents the necessary and sufficient conditions for the passivity of SEA under VSIC when both torque and motion controllers consist of proportional gains while rendering a virtual environment consisting of a parallel mass, spring, and damper. When torque and motion controllers are set as proportional gains and when the reference impedance is set as Eqn. (5.4), impedance transfer function of SEA under VSIC is $Z_{MSD}^{SEA^{P-P}}(s)$=W_1/W_2, where

$$\begin{aligned} W_1 =&(J_m\,K)\,s^4 + (K\,(\beta + 2\,J_m\,\omega_a))\,s^3 \\ &+ \left(K\left((J_m + M_{\text{ref}}\,\alpha)\,{\omega_a}^2 + (2\,\beta + B_{\text{ref}}\,\alpha)\,\omega_a + K_{\text{ref}}\,\alpha\right)\right)s^2 \\ &+ (K\,\omega_a\,(2\,K_{\text{ref}}\,\alpha + \omega_a\,(\beta + B_{\text{ref}}\,\alpha)))\,s + K\,K_{\text{ref}}\,\alpha\,{\omega_a}^2 \end{aligned} \tag{5.5}$$

$$\begin{aligned} W_2 =&J_m\,s^5 + (\beta + 2\,J_m\,\omega_a)\,s^4 + (\omega_a\,(2\,\beta + J_m\,\omega_a) + K\,(\alpha+1))\,s^3 \\ &+ (\omega_a\,(\beta\,\omega_a + 2\,K\,(\alpha+1)))\,s^2 + \left(K\,{\omega_a}^2\,(\alpha+1)\right)s \end{aligned} \tag{5.6}$$

with $\alpha = P_m P_t$ and $\beta = B_m + P_m$. The passivity of parallel mass, spring, and damper rendering with impedance reference roll-off of SEA under VSIC can be ensured with the following theorem.

Theorem 5.3. *Consider SEA under VSIC as in Figure 2.2 with* $Z_d = K_{ref} + B_{ref}\frac{s\,\omega_a}{s+\omega_a} + M_{ref}\frac{s^2\,{\omega_a}^2}{(s+\omega_a)^2}$*, where the torque and velocity controllers consist of proportional gains* P_t *and* P_m*. The following expression constitutes the necessary and sufficient conditions for the passivity of* $Z^{SEA^{P-P}}_{MSD_{BW}}(s)$*:*

$$K_{ref} \leq \frac{K\,(\alpha+1)}{\alpha} - \frac{\omega_a\,(B_{ref}\,(\beta + J_m\,\omega_a) + M_{ref}\omega_a\,(\beta + 2\,J_m\,\omega_a))}{\beta} \tag{5.7}$$

$$B_{ref} \geq \beta\left(\frac{K_{ref}}{K\,(\alpha+1)} - \left(\frac{1}{\alpha}\right)\right) \tag{5.8}$$

$$\begin{aligned} M_{ref} \geq & -\frac{2\,\beta\,(K_{ref}\,\alpha + K\,(\alpha+1)) - B_{ref}\,\alpha\,(K\,(\alpha+1) - \omega_a\,(\beta + J_m\,\omega_a))}{\alpha\omega_a\,(\beta\omega_a + 2\,K\;(\alpha+1))} \\ & - 2\sqrt{\zeta}/(\alpha\omega_a\,(\beta\omega_a + 2\,K\;(\alpha+1))) \end{aligned} \tag{5.9}$$

where

$$\begin{aligned} \zeta = & -K^3\,{\omega_a}^4\,(\alpha+1)\,(\beta + B_{ref}\,\alpha) \\ & \left(\alpha\,\beta\left(M_{ref}{\omega_a}^2 + B_{ref}\omega_a + K_{ref}\right) - K\,\beta\,(\alpha+1) + J_m\,\alpha\,{\omega_a}^2\,(B_{ref} + 2\,M_{ref}\omega_a)\right) \end{aligned}$$

Proof.

• Routh-Hurwitz stability criterion dictates that the system is stable iff:

$$(2\,J_m)\,{\omega_a}^3 + (4\,J_m\,\beta)\,{\omega_a}^2 + \left(2\,\beta^2\right)\omega_a + K\,\beta\,(\alpha+1) \geq 0 \tag{5.10}$$

$$2\,\beta\,\omega_a\,(K\,(\alpha+1) + \omega_a\,(\beta + J_m\,\omega_a))^2 \geq 0 \tag{5.11}$$

The positive control gains and plant parameters ensures the stability of $Z^{SEA^{P-P}}_{MSD}(s)$.

• The system has one single pole at $s = 0$ on the imaginary axis, where residue is $\frac{K_{\mathrm{ref}}\,\alpha}{\alpha+1}$, which is positive and real. Through Routh-Hurwitz stability criterion and positiveness of all plant parameters and controller gains, it is shown that there are no additional poles on the imaginary axis.

• The sign of $Re\{Z^{SEA^{P-P}}_{MSD_C}(s)\}$ can be checked as follows:

$$F_4\,\omega^4 + F_2\,\omega^2 + F_0 \;\geq 0 \quad \omega \in (-\infty, \infty) \tag{5.12}$$

where

$$\begin{aligned}
F_0 =& -K(K\,\beta\,(\alpha+1) - K_{\text{ref}}\,\alpha\,\beta \\
&- \alpha\,\omega_a\,(B_{\text{ref}}\,(\beta + J_m\,\omega_a) + M_{\text{ref}}\,\omega_a\,(\beta + 2\,J_m\,\omega_a))) \\
F_2 =& B_{\text{ref}}\,\alpha\,(K\,(\alpha+1) - \omega_a\,(\beta + J_m\,\omega_a)) - 2\,\beta\,(K_{\text{ref}}\,\alpha + K\,(\alpha+1)) \\
&+ M_{\text{ref}}\,\omega_a\,(\beta + 2\,K\,\alpha\,(\alpha+1)) \\
F_4 =& K\,{\omega_a}^4\,(K\,(\alpha+1)\,(\beta + B_{\text{ref}}\,\alpha) - K_{\text{ref}}\,\alpha\,\beta)
\end{aligned}$$

Accordingly to lemma 2.3 it can be shown that Eqn. (5.12) holds if and only if $F_4 \geq 0 \wedge F_0 \geq 0 \wedge F_2 \geq -2\sqrt{F_4 F_0}$. Positiveness of F_4 and F_0 guarantees the positiveness of the resulting square root term. Accordingly Eqn. (5.7) ensures positiveness of F_4, Eqn. (5.8) ensures positiveness of F_0 and Eqn. (5.9) ensures the condition $F_2 \geq -2\sqrt{F_4 F_0}$. □

Due to the complexity of the passivity bounds, the effects of the system parameters are argued for the sufficient conditions of ζ=0. For the case of linear spring rendering, setting B_{ref} and M_{ref} to 0 results in Eqn. (5.7) recovering the necessary and sufficient conditions for passivity as studied in [13] and given in Section 2.5. Eqn. (5.7) shows that as ω_a increases both maximum passively selectable B_{ref} and M_{ref} values decrease. Eqn. (5.7) further shows that a selection of negative B_{ref}, increases the maximum passively selectable M_{ref} value and a selection of negative M_{ref}, increases the maximum passively selectable B_{ref} value. It is further observed that when ω_a is set to infinity, for positive values of B_{ref} and M_{ref}, K_{ref} bound in Eqn. (5.7) reduces to a negative value violating the passivity conditions, while for negative values of B_{ref} and M_{ref} condition given in Eqn. (5.7) can be fulfilled. However Eqn. (5.9) sets a limit to negative values of M_{ref}, and for the case ω_a is set to infinity the boundary setting inequality is; $M_{ref} \geq -2\beta J_m$. Eqn. (5.8) also limits the lower bound of B_{ref} to negative values when both M_{ref} and B_{ref} are positive, since Eqn. (5.7) is always less conservative than the inequality $\frac{K_{\text{ref}}}{K\,(\alpha+1)} \text{-} \frac{1}{\alpha}$ due to the negative signed terms in Eqn. (5.7) as a result of positive M_{ref} and B_{ref}.

If controller gains are selected high, meaning $\alpha \to \infty$, Eqn. (5.8) and Eqn. (5.9) reduces to, $B_{ref} \geq 0$ and $M_{ref} \geq -B_{ref}/2\omega_a$ respectively. From this set of inequalities, it is observed that high controller gains eliminate the choice of negative B_{ref}; however, this does not mean that the system damping can not be compensated. In fact, if the controller gains are high, the rendered damping becomes B_{ref} directly, and a selection of B_{ref}=0 results in rendered damping being equal to zero. Choice of a positive B_{ref}, enables negative choice of M_{ref}, and if B_{ref} is chosen as zero, negative M_{ref} can not be chosen. Designing an SEA with high stiffness increases maximum passively selectable values of K_{ref} as well as B_{ref} and M_{ref}.

We will further study combinations of parallel mass-spring-damping virtual environments in order to draw clearer conclusions on stability robustness haptic rendering performance trade-offs.

5.3 Passivity of SEA under VSIC during Viscous Damper Rendering with Impedance Reference Roll-off

We continue our study by considering viscous damping rendering, by setting K_{ref} and M_{ref} in Theorem 5.3, to zero. Given the measured end effector position θ_{end} and assuming SEA under VSIC when both controllers are taken as proportional gains, and setting the desired impedance to $Z_d = B_{ref}s$, even though the resulting system is not implementable in real-time due to the non-causal nature of differentiation, studying the unfiltered case is still important to further study the effects of the bandwidth limitation of the filtering that is used to roll off the high-frequency component of the reference input. The interaction port impedance for the unfiltered case, $Z_d = B_{ref}s$, can be derived as following;

$$\frac{J_m K s + K(\beta + B_{\text{ref}}\alpha)}{J_m s^2 + \beta s + K(1+\alpha)} \tag{5.13}$$

The following conditions, derived by the invoke of Theorem 2.1, constitute the necessary and sufficient conditions for the passivity of damping rendering when the end effector velocity is available without filtering, $Z_{D_{\omega_{end}}}^{SEA^{P-P}}(s)$:

$$-\frac{\beta}{\alpha} \leq B_{\text{ref}} \leq 0 \tag{5.14}$$

The rendered damping at low frequencies, B_{vir}, is equal to $\frac{\beta+B_{ref}\alpha}{(1+\alpha)}$. It is observed that maximum passively renderable damping is limited to system damping itself, $\frac{\beta}{(1+\alpha)}$, since $Z_{D_{\omega_{end}}}^{SEA^{P-P}}(s)$ is non-passive for positive B_{ref} values. The system is further studied with the bandwidth-limiting filter to observe stability robustness and haptic rendering trade-offs.

Given the measured end effector position θ_{end} and assuming SEA under VSIC when both controllers are taken as proportional gains, and setting the reference impedance to $Z_d = B_{\text{ref}}\frac{s\,\omega_a}{s+\omega_a}$, the resulting interaction port impedance of the system is derived as the following:

$$\frac{J_m\,K\,s^2 + K\,(\beta + J_m\,\omega_a)\,s + K\,\omega_a\,(\beta + B_{\text{ref}}\,\alpha)}{J_m\,s^3 + (\beta + J_m\,\omega_a)\,s^2 + (\beta\,\omega_a + K\,(\alpha+1))\,s + K\,\omega_a\,(\alpha+1)} \tag{5.15}$$

The passivity of damper rendering of SEA under VSIC is established as the following.

Corollary 5.4. *Consider SEA under VSIC as in Figure 2.2 with* $Z_d = B_{ref}\,\frac{s\,\omega_a}{s+\omega_a}$, *where the torque and velocity controllers consist of proportional gains* P_t *and* P_m. *The following expression provides the necessary and sufficient conditions for the passivity of* $Z_D^{SEA^{P-P}}(s)$*:*

$$-\frac{\beta}{\alpha} \leq B_{ref} \leq \frac{K\,\beta\,(\alpha+1)}{\alpha\,\omega_a\,(\beta + J_m\,\omega_a)} \tag{5.16}$$

Proof. The proof of Corollary 5.4, necessary and sufficient conditions for the passivity of damper rendering of SEA under VSIC, can be recovered from the proof

provided in Subsection 5.2. When M_{ref} and K_{ref} are substituted as zero the resulting transfer function does not contain any right-hand side poles and the single pole at $s = 0$ is removed. Furthermore, Eqn. (5.9) reduces zero and the left-hand side of Eqn. 5.16 can be recovered from Eqn. 5.8 and right-hand side can be recovered from Eqn. (5.7), by substituting K_{ref}=0 and M_{ref}=0. □

The rendered damping low frequencies, B_{vir}, of $Z_D^{SEA^{P-P}}(s)$ is derived as $\frac{\beta+B_{ref}\alpha}{\alpha+1}$. Through the lower bound given in Eqn. (5.16), it is observed that B_{vir} can be passively set to zero if B_{ref} is set as $-\frac{\beta}{\alpha}$, therefore passivity enforces the constraint that damping compensation can not exceed the system damping.

If the cut-off frequency ω_a of the filter is chosen large, $\omega_a \to \infty$ then the upper bound in Eqn. (5.16) reduces to zero, recovering the unfiltered case given in Eqn. (5.14), however negative B_{ref} values can be chosen to compensate for the system damping. As ω_a decreases the upper bound given in Eqn. (5.16) increases, resulting in higher levels of passively renderable damping.

Designing an SEA with high stiffness K results in an increase in the maximum passively renderable damping, while a high plant inertia J_m decreases the maximum passively renderable damping. If P_t is chosen large, then the rendered damping, $\frac{\beta+B_{ref}\alpha}{\alpha+1}$, reduces to B_{ref}, while the lower bound given in Eqn. (5.16) reduces to zero and the maximum passively renderable damping decreases. As P_t decreases rendered damping can increase as well due to the decrease of the denominator of the low frequency rendered damping,$B_{vir} = \frac{\beta+B_{ref}\alpha}{\alpha+1}$.

5.4 Passivity of SEA under VSIC while Voigt Model Rendering with Impedance Reference Roll-off

Next, we consider Voigt model rendering, by setting M_{ref} in Theorem 5.3, to zero. Given the measured end effector position θ_{end} and assuming SEA under VSIC

when both controllers are taken as proportional gains, and setting the reference impedance to $Z_d = K_{ref} + B_{ref}s$ where no upper bandwidth limits are subjugated via impedance reference roll-off, the interaction port impedance can be derived as follows;

$$\frac{J_m\,K\,s^2 + K\,(\beta + B_{\mathrm{ref}}\,\alpha)\,s + K\,K_{\mathrm{ref}}\,\alpha}{J_m\,s^3 + \beta\,s^2 + K\,(\alpha+1)\,s} \tag{5.17}$$

The following conditions are the necessary and sufficient conditions for the passivity of Voigt model rendering when the end effector velocity is available, $Z_{SD_{\omega_{end}}}^{SEA^{P-P}}(s)$:

$$B_{ref} \geq \beta\left(\frac{K_{\mathrm{ref}}}{K\,(\alpha+1)} - \frac{1}{\alpha}\right) \tag{5.18}$$

$$B_{ref} \leq 0 \tag{5.19}$$

It is observed that this implementation of Voigt model rendering allows negative B_{ref}, while positive values of B_{ref} violate the passivity criteria. The B_{vir}, rendered damping of the system at low frequencies can be derived as follows:

$$\frac{\beta + B_{\mathrm{ref}}\,\alpha}{\alpha+1} - \frac{K_{\mathrm{ref}}\,\alpha\,\beta}{K\,(\alpha+1)^2} \tag{5.20}$$

Rendered damping at low frequencies, B_{vir}, is equal to zero when $B_{ref}=\frac{K_{ref}\beta}{K(\alpha+1)} - \frac{\beta}{\alpha}$, which is the lower bound of passivity condition, given in Eqn. (5.18). When B_{ref} is equal to zero, Eqn. (5.18) recovers the necessary and sufficient condition for passivity during spring rendering, $K \geq K_{ref}\frac{\alpha}{\alpha+1}$. In this case, when B_{ref}=0, an increase in K_{ref} will decrease the rendered damping of the system, given in Eqn. (5.20). However, the necessary and sufficient conditions for the passivity of rendering of the Voigt model are less conservative if the system is modeled with the inclusion of filtering for impedance reference roll-off and when only the end effector position is measured and velocity is estimated in real-time.

Given the measured end effector position θ_{end} and assuming SEA under VSIC when both controllers are taken as proportional gains, and setting the reference impedance to $Z_d = K_{ref} + B_{\mathrm{ref}}\frac{s\,\omega_a}{s+\omega_a}$ where the filtering limits the bandwidth of the reference impedance via roll-off, the resulting interaction port impedance of the system is derived as the following:

$$\frac{J_m\,K\,s^3 + K\,(\beta + J_m\,\omega_a)\,s^2 + K\,(\beta\,\omega_a + \alpha\,(K_{\text{ref}} + B_{\text{ref}}\,\omega_a))\,s + K\,\omega_a\,K_{\text{ref}}\,\alpha}{J_m\,s^4 + (\beta + J_m\,\omega_a)\,s^3 + (\beta\,\omega_a + K\,(\alpha+1))\,s^2 + K\,\omega_a\,(\alpha+1)} \tag{5.21}$$

The passivity of Voigt Model rendering of SEA under VSIC is established as follows:

Corollary 5.5. *Consider SEA under VSIC as in Figure 2.2 with* Z_d=K_{ref} + $B_{ref}\frac{s\,\omega_a}{s+\omega_a}$, *where the torque and motion controllers consist of proportional gains* P_t *and* P_m *respectively. The following expressions are the necessary and sufficient conditions for the passivity of* $Z_{SD}^{SEA^{P-P}}(s)$*:*

$$B_{ref} \geq \beta\left(\frac{K_{ref}}{K\,(\alpha+1)} - \frac{1}{\alpha}\right) \tag{5.22}$$

$$B_{ref} \leq \frac{\beta\,(K\,(\alpha+1) - K_{ref}\alpha)}{\alpha\,\omega_a\,(\beta + J_m\,\omega_a)} \tag{5.23}$$

Proof. The proof of Corollary 5.5, the necessary and sufficient condition for the passivity of Voigt model rendering of SEA under VSIC can be recovered from Subsection 5.2. When M_{ref} is substituted as 0, the resulting transfer function does not contain any right-hand side poles and the residue of the single pole at s=0 is $K_{ref}\alpha/(\alpha+1)$, which is positive and real. Furthermore Eqn. (5.9) reduces zero, Eqn. 5.22 is same as Eqn. 5.8 and Eqn. 5.23 can be recovered from Eqn. (5.7), by substituting M_{ref}=0. □

It is observed that Eqn. (5.22) is identical to Eqn. (5.18) however, Eqn. (5.23) differs from Eqn. (5.19) since B_{ref} can be chosen positive. The rendered damping is the same as the system in which velocity is measured, given in Eqn. (5.20).

It is observed that designing an SEA with high stiffness, K, will increase the maximum renderable damping for any arbitrary rendered stiffness amount. If the rendered amount of stiffness is equal to SEA stiffness itself such that K_{ref}=$K\frac{\alpha+1}{\alpha}$, then the upper bound on Eqn. (5.23) reduces to zero. The effect of the filter cut-off frequency ω_a and plant inertia J_m are similar to what has been discussed in Section 5.3. As the cutoff frequency of the filter and plant inertia decrease, the upper bound on maximum renderable damping increases.

If K_{ref} is equal to zero then Eqn. (5.22) is identical to the lower bound of Eqn. (5.16) and an increase in K_{ref} results in a higher lower bound. However, this effect can be negated with a design of a less compliant SEA. If controller gains are selected high then the lower bound reduces to zero. As the damping coefficient β increases the minimum passively selectable B_{ref} decreases; however, this does not translate to rendered damping since when B_{ref} is equal to the lower bound such that B_{ref}=β $\left(\frac{K_{ref}}{K(\alpha+1)} - \frac{1}{\alpha}\right)$, the rendered damping given in Eqn. (5.20) is always equal to zero.

5.5 Passivity of SEA under VSIC while Mass Rendering with Impedance Reference Roll-off

Next, we consider mass rendering, by setting B_{ref} and K_{ref} in Theorem 5.3, to zero. Given the measured end effector acceleration α_{end} with no roll-off of the impedance reference present on the reference impedance model, and assuming SEA under VSIC when both controllers are taken as proportional gains, and setting the reference impedance model to Z_d= $M_{ref}s^2$, the interaction port impedance can be derived as follows;

$$\frac{(J_m\,K + K\,M_{\mathrm{ref}}\,\alpha)\,s + K\,\beta}{J_m\,s^2 + \beta\,s + K + K\,\alpha} \tag{5.24}$$

The following conditions constitute the necessary and sufficient conditions for the passivity of $Z^{SEA^{P-P}}_{M_{\alpha_{end}}}(s)$:

$$M_{ref} \geq 0 \tag{5.25}$$

The rendered mass at low frequencies, M_{vir}, of the system can be derived as the following:

$$\frac{J_m + M_{\mathrm{ref}}\,\alpha}{\alpha + 1} - \frac{\beta^2}{K\,(\alpha+1)^2} \tag{5.26}$$

It can be easily seen that this system can render any amount of positive mass; however, it can not compensate the system mass. Moreover, $\frac{\beta^2}{K(\alpha+1)^2}$, might dominate

the rest of the terms in Eqn. (5.26) if M_{ref} is chosen small. A selection of high control gains, solves this issue and results in direct rendering of M_{ref}, meaning the rendered amount of mass, M_{vir}, being equal to M_{ref} and the rendered amount of damping, $B_{vir} = \frac{\beta}{\alpha+1}$ being equal to zero. However when the end effector acceleration can not be measured and filtering is required for numerical estimation of acceleration from end effector position and impedance reference is designed with a high-frequency roll-off, the necessary and sufficient conditions for the passivity of mass rendering of SEA under VSIC are altered.

Given the measured end effector position θ_{end} and assuming SEA under VSIC when both controllers are taken as proportional gains, and when the reference impedance is bandwidth limited with a high-frequency roll-off; $Z_d = M_{\text{ref}} \frac{s^2\,\omega_a^2}{(s+\omega_a)^2}$, the resulting interaction port impedance is $Z_M^{SEA^{P-P}}(s) = N_1/N_2$ where

$$\begin{aligned} N1 = {} & J_m\,K\,s^3 + K\,(\beta + 2\,J_m\,\omega_a)\,s^2 \\ & + K\,\omega_a\left(2\,\beta + \omega_a\left(M_{ref}\,\alpha\,{\omega_a}^2 + J_m\right)\right)s + K\,\beta\,{\omega_a}^2 \end{aligned} \tag{5.27}$$

$$\begin{aligned} N2 = {} & J_m\,s^4 + (\beta + 2\,J_m\,\omega_a)\,s^3 \\ & + \left(J_m\,{\omega_a}^2 + 2\,\beta\,\omega_a + K\,(\alpha+1)\right)s^2 \\ & + \left(\beta\,{\omega_a}^2 + 2\,\omega_a\,K\,(\alpha+1)\right)s + K\,{\omega_a}^2\,(\alpha+1) \end{aligned} \tag{5.28}$$

where β=P_m+B_m and α=$P_m P_t$.

The passivity of mass rendering of SEA under VSIC can be established according to the following theorem

Corollary 5.6. *Consider mass rendering for SEA under VSIC as in Figure 2.2 with $Z_d = M_{ref}(\frac{s\omega_a}{s+\omega_a})^2$, where the torque and velocity controllers consist of proportional gains P_t and P_m respectively. The following expressions are the necessary and sufficient conditions for the passivity of $Z_M^{SEA^{P-P}}(s)$:*

$$M_{ref} \leq \frac{K\,\beta\,(\alpha+1)}{\alpha\,{\omega_a}^2\,(\beta + 2\,J_m\,\omega_a)} \tag{5.29}$$

$$M_{ref} \geq -\frac{2\,K\,\beta\,(\alpha+1) + 2\,\sqrt{\eta}}{\alpha\,\omega_a\,(2\,K(\alpha+1) + \beta\,\omega_a)} \tag{5.30}$$

where

$$\eta = K^3\,\beta\,{\omega_a}^4\,(\alpha+1)\left(-M_{ref}(\alpha+\beta)\,{\omega_a}^2 + 2\,J_m\,\alpha\,\omega_a + K\,\beta\,(\alpha+1)\right)$$

Proof. The proof of mass rendering of SEA under VSIC can be recovered from Subsection 5.2. When B_{ref} and K_{ref} are substituted as 0, the resulting transfer function does not contain any right-hand side poles and the residue of the single pole at s=0 is removed. Furthermore Eqn. (5.29) can be recovered from Eqn. (5.7) and Eqn. (5.30) can be recovered from Eqn. (5.9). □

The rendered mass at low frequencies, M_{vir}, of the system, is the same as the system with the measured acceleration with no high frequency impedance reference roll-off, given in Eqn.(5.26). It can be seen from this equation, that a high selection of controller gains will result in rendered mass being M_{ref} with zero rendered damping. Eqn. (5.29). reveals that designing an SEA with low compliance increases the upper bound on maximum selectable M_{ref} and decreases the effect of negative signed term in Eqn. (5.26), resulting in a higher passively renderable M_{vir}. On the other hand a high cut-off frequency and plant mass will decrease the upper bound of M_{ref}.

Eqn. (5.30) can be made more intuitive with the sufficient case of η=0. It is observed that a low selection of the cut-off frequency expands the lower bound of M_{ref}, allowing for more mass compensation and expanding maximum M_{vir}. As controller gains increase the bound gets more conservative decreasing the maximum M_{vir} range. If SEA is designed with a low compliance the bound reduces to less conservative case of $M_{ref} \geq (-\beta/\alpha\omega_a)$.

5.6 Passivity of SEA under VSIC while Rendering Mass-Damper with Impedance Reference Roll-off

Next, we consider parallel mass-damper rendering, by setting K_{ref} in Theorem 5.3, to zero. Given the measured end effector velocity ω_{end} and end effector acceleration α_{end}, and assuming SEA under VSIC when both controllers are taken as proportional gains, and setting the reference impedance to $Z_d = M_{ref}s^2 + B_{ref}s$ where no bandwidth limit via high-frequency roll-off is subjugated to the reference impedance model, the interaction port impedance is derived as the following;

$$\frac{K\left(J_m + M_{\text{ref}}\,\alpha\right)s + K\left(\beta + B_{\text{ref}}\,\alpha\right)}{J_m\,s^2 + \beta\,s + K\left(1 + \alpha\right)} \tag{5.31}$$

The following conditions are the necessary and sufficient conditions of $Z_{MD_{\alpha_{end}}}^{SEA^{P-P}}(s)$:

$$-\frac{\beta}{\alpha} \leq B_{\text{ref}} \tag{5.32}$$

$$B_{\text{ref}} \leq \frac{M_{\text{ref}}\,\beta}{J_m} \tag{5.33}$$

The rendered damping at low frequencies, B_{vir}, is equal to $\frac{\beta + B_{ref}\alpha}{\alpha+1}$. The rendered mass at low frequencies, M_{vir} is derived as the following:

$$\frac{J_m + M_{\text{ref}}\,\alpha}{\alpha + 1} - \frac{\beta^2 + B_{ref}\alpha\beta}{K\left(\alpha+1\right)^2} \tag{5.34}$$

Eqns. (5.32 and 5.33) show that the selection of positive B_{ref} is restricted if compensation of system mass is desired. When $B_{ref}{=}-\beta/\alpha$, Eqn. (5.33) reduces to $M_{ref} \geq -J_m/\alpha$, this results in compensation of both system mass and damping. When $M_{ref} = -J_m/\alpha$, Eqn. (5.34) reduces to $-\frac{\beta^2 + B_{ref}\alpha\beta}{K\left(\alpha+1\right)^2}$, and substituting $B_{ref}{=}-\beta/\alpha$ reduces this equation to zero, meaning $M_{vir}{=}0$. Next, we consider only when the reference impedance model is filtered. Given the measured end effector position θ_{end} and assuming SEA under VSIC when both controllers are taken as proportional gains, and setting the desired impedance to $Z_d = M_{\text{ref}}\frac{s^2\,\omega_a^2}{(s+\omega_a)^2} + B_{ref}(\frac{s\omega_a}{s+\omega_a})$, the resulting interaction port impedance is $Z_{MD}^{SEA^{P-P}}(s)$

$= B_1/B_2$ where

$$\begin{aligned}B_1 =&(J_m\,K)\,s^3 + (K\,\beta + 2\,J_m\,K\,\omega_a)\,s^2 + \left(2\,K\,\beta\,\omega_a + J_m\,K\,{\omega_a}^2 + K\,M_{\text{ref}}\,\alpha\,{\omega_a}^2 + B_{\text{ref}}\,K\,\alpha\,\omega_a\right)s \\ &+ K\,\beta\,{\omega_a}^2 + B_{\text{ref}}\,K\,\alpha\,{\omega_a}^2 \\ B_2 =&J_m\,s^4 + (\beta + 2\,J_m\,\omega_a)\,s^3 + \left(J_m\,{\omega_a}^2 + 2\,\beta\,\omega_a + K + K\,\alpha\right)s^2 \\ &+ \left(2\,K\,\omega_a + \beta\,{\omega_a}^2 + 2\,K\,\alpha\,\omega_a\right)s + K\,{\omega_a}^2 + K\,\alpha\,{\omega_a}^2\end{aligned}$$

where, β=P_m+B_m and α=I_tP_m. The passivity of parallel mass-damper rendering of SEA under VSIC with proportional torque and impedance reference roll-off can be checked with the following corollary.

Corollary 5.7. *Consider parallel mass-damper rendering for SEA under VSIC as in Figure 2.2 with* $Z_d = M_{ref}(\frac{s\omega_a}{s+\omega_a})^2 + B_{ref}(\frac{s\omega_a}{s+\omega_a})$, *where the torque and velocity controllers consist of proportional gains* P_t *and* P_m, *respectively. The following expressions constitute the necessary and sufficient conditions for the passivity of* ${Z_{MD}^{SEA}}^{P-P}(s)$*:*

$$B_{ref} \leq \frac{1}{\beta + J_m\omega_a}\left(\frac{K\,\beta\,(\alpha+1)}{\alpha\,\omega_a} - M_{ref}\omega_a\,(\beta + 2\,J_m\,\omega_a)\right) \tag{5.35}$$

$$B_{ref} \geq -\frac{\beta}{\alpha} \tag{5.36}$$

$$\begin{aligned}M_{ref} \geq &\frac{B_{ref}(\,\omega_a\,(\beta + J_m\,\omega_a) - K\,(\alpha+1)) - 2\,K\,\beta\,(\alpha+1)}{\alpha\omega_a\,(\beta\,\omega_a + 2\,K\,(\alpha+1))} \\ &- 2\sqrt{\chi}/(\alpha\omega_a\,(\beta\,\omega_a + 2\,K\,(\alpha+1)))\end{aligned} \tag{5.37}$$

where

$$\begin{aligned}\chi =& -K^3\,{\omega_a}^4\,(\alpha+1)\,(\beta + B_{ref}\,\alpha)\,(B_{ref}\left(J_m\,\alpha\,{\omega_a}^2 + \alpha\,\beta\,\omega_a\right) \\ &+ M_{ref}\left(2\,J_m\,\alpha\,{\omega_a}^3 + \alpha\,\beta\,{\omega_a}^2\right) - K\,\beta\,(\alpha+1))\end{aligned} \tag{5.38}$$

Proof. The proof of Corollary 5.7, the necessary and sufficient conditions for the passivity of parallel mass damper rendering of SEA under VSIC can be recovered from Subsection 5.2. When K_{ref} is substituted as 0, the resulting transfer function does not contain any right-hand side poles and the residue of the single pole at s=0 is removed. Furthermore Eqn. (5.35), Eqn. (5.36) and Eqn. (5.37) can be recovered from, in order, Eqn. (5.7), Eqn. (5.8) and Eqn. (5.9) by substituting K_{ref}=0. □

Due to the complexity of the resulting equations, the effects of the system parameters are further argued on the sufficient case of χ=0. The rendered damping of this system is equal to B_{vir}=$\frac{\beta+B_{ref}\alpha}{(1+\alpha)}$, and rendered mass is equal to;

$$\frac{J_m + M_{\text{ref}}\,\alpha}{(1+\alpha)} - \frac{\beta(\beta + B_{ref}\alpha)}{K\,(1+\alpha)^2} - \frac{B_{ref}\alpha}{\omega_a(1+\alpha)}$$

It is observed that the minimum amount of renderable damping, B_{vir}, can be made zero when B_{ref} is chosen as the lower bound given in Eqn. (5.36).

Eqn. (5.37) shows that the selection of a negative B_{ref} will result in a less conservative lower bound of M_{ref} and Eqn. (5.35) shows that selection of a negative M_{ref} will result in less conservative upper bound of B_{ref}. Therefore it is observed that compensation of system damping increases maximum renderable mass, M_{vir} and compensation of system mass increases maximum renderable damping, B_{vir}.

If controller gains are high, meaning $\alpha \to \infty$, B_{vir} becomes equal to B_{ref} and M_{vir} becomes equal to M_{ref}-$B_{ref}(1/\omega_a)$ and the upper bound of B_{ref} given in Eqn. (5.35) becomes more conservative. A design of an SEA with high stiffness will result in a less conservative upper bound of B_{ref} given in Eqn. (5.35) and will allow for a higher B_{vir}.

As the cut-off frequency of the filter ω_a increases the upper bound of B_{ref}, given in Eqn. (5.35), becomes less conservative, increasing maximum renderable damping B_{vir}.

5.7 Passivity of SEA under VSIC with Integral Torque and Proportional Motion Controllers for Mass Rendering

In this section, we present an alternative controller structures that increase the haptic rendering performance of mass rendering of SEA under VSIC. Even though VSIC with proportional torque and motion controller gains can result in safe and high-fidelity rendering of mass, the rendered virtual environment also contains damping that is being rendered as a side product as it will be argued more in-depth in Subsection 6.4. This behavior can be negated if the torque controller gain is selected high. However alternative controller structures of VSIC can result in better rendering fidelity with the choice of different controllers.

Given the end effector position θ_{end}, when torque and motion controllers are taken as, integral gain I_t and proportional gain P_m, and if the impedance controller is set to $Z_d = \frac{M_{\text{ref}}\, s^2\, {\omega_a}^2}{(s+\omega_a)^2}$ where the reference impedance model is rolled-off at high-frequencies, the resulting interaction port impedance of the system is derived as the following: the interaction port impedance transfer function of SEA under VSIC, $Z_M^{SEA^{I-P}}(s)$ is M_1/M_2 in which:

$$
\begin{aligned}
M_1 =& (J_m\, K)\, s^4 + (K\, (\delta + 2\, J_m\, \omega_a))\, s^3 + (K\, \omega_a\, (2\, \delta + J_m\, \omega_a))\, s^2 + \left(K\, {\omega_a}^2\, (\delta + M_{\text{ref}}\, \gamma)\right) s \\
M_2 =& J_m\, s^5 + (\delta + 2\, J_m\, \omega_a)\, s^4 + (K + \omega_a\, (\delta + J_m\, \omega_a))\, s^3 + \left(K\, (\gamma + 2\, \omega_a) + \delta\, {\omega_a}^2\right) s^2 \\
& + \left(K\, \left({\omega_a}^2 + 2\, \gamma\, \omega_a\right)\right) s + K\, \gamma\, {\omega_a}^2
\end{aligned}
$$

where, $\delta = P_m + B_m$ and $\gamma = I_t P_m$.

The passivity of SEA under VSIC with integral torque and proportional motion controllers while mass rendering is established with the following theorem.

Theorem 5.8. *Consider mass rendering for SEA under VSIC as in Figure 2.2 with $Z_d = M_{ref}(\frac{s\omega_a}{s+\omega_a})^2$, where the torque and motion controllers consist of integral gain I_t/s and proportional gain P_m respectively. The following expression*

constitutes sufficient conditions for the passivity of $Z_{Mass}^{SEA^{I-P}}(s)$*:*

$$I_t \leq \frac{\delta}{J_m P_m} \tag{5.39}$$

$$M_{ref} \geq \frac{K}{\omega_a^2}\left(1 - \frac{\delta}{J_m \gamma}\right) \tag{5.40}$$

$$M_{ref} \leq \frac{2\,K\,(\delta - J_m\,\gamma)}{\gamma\,(2\,\delta\,\omega_a + K + J_m\,\omega_a^2)} \tag{5.41}$$

$$M_{ref} \geq \frac{\omega_a\,(J_m\,\gamma - \delta)}{\gamma\,(2\,\gamma + \omega_a)} \tag{5.42}$$

Proof.

• Through Routh-Hurwitz stability criterion it can be shown that the system does not have any right-hand side poles if:

$$\begin{aligned}
&K\,(\delta - J_m\,\gamma) + \omega_a\left(\delta\,(2\,\delta + 4\,J_m\,\omega_a) + 2\,J_m\,{\omega_a}^2\right) \geq 0\\
&\left(2\,{J_m}^2\,\delta\right){\omega_a}^5 + \left(4\,J_m\,\delta^2\right){\omega_a}^4\\
&+ \left(2\,\delta^3 + 4\,J_m\,K\,(\delta - J_m\,\gamma)\right){\omega_a}^3 + \left(4\,K\,\delta^2\,(\delta - J_m\,\gamma)\right){\omega_a}^2\\
&+ \left(2\,K^2\,(\delta - J_m\,\gamma)\right)\omega_a + K^2\,\gamma\,(\delta - J_m\,\gamma) \geq 0\\
&2\,K\,\omega_a\left({\omega_a}^2\,(\delta + J_m\,\omega_a) + K\,(\gamma + \omega_a)\right)^2(\delta - J_m\,\gamma) \geq 0
\end{aligned}$$

Eqn. (5.39) fulfills the stability conditions presented above.

• Through Routh-Hurwitz stability criterion it is shown that there are no poles on the imaginary axis since Eqn. (5.39) ensures left-hand side of stability conditions are always greater than zero.

• The sign of $Re\{Z_{Mass}^{SEA^{I-P}}(s)\}$ can be checked as follows:

$$S_4\,\omega^4 + S_2\,\omega^2 + S_0 \;\geq 0 \quad \omega \in (-\infty, \infty) \tag{5.43}$$

where

$$S_0 = K^2\omega_a^3\left(\gamma\left(2M_{ref}\left(\omega_a+\gamma\right)-J_m\omega_a\right)+\delta\omega_a\right)$$
$$S_2 = K\,{\omega_a}^2\left(2\,K\left(\delta-J_m\,\gamma\right)-M_{\mathrm{ref}}\,\gamma\left(J_m\,{\omega_a}^2+2\,\delta\,\omega_a+K\right)\right)$$
$$S_4 = K\left(J_m\,M_{\mathrm{ref}}\,\gamma\,{\omega_a}^2+K\left(\delta-J_m\,\gamma\right)\right)$$

Eqns. (5.40, 5.41, and 5.42) dictate that $S_4 \geq 0 \wedge S_2 \geq 0 \wedge S_0 \geq 0$, respectively, resulting in positiveness of $Re\{Z_{Mass}^{SEA^{I-P}}(s)\}$. □

At low frequencies the system renders pure mass, meaning the rendered damping of the system is zero when $\lim_{w\to 0} Z_M^{SEA^{I-P}}(jw)$ and rendered mass of $Z_M^{SEA^{I-P}}(s)$ at low frequencies, M_{vir}, is equal to:

$$M_{ref} + \frac{\delta}{\gamma} \tag{5.44}$$

If M_{ref} is selected as $-\delta/\gamma$, the system mass, $\frac{\delta}{\gamma}$ can be compensated. However, it can be easily shown that M_{ref} can not be chosen as -δ/γ by substituting it to Eqns. (5.42), and simplifying the equation results in the inequality $\delta \leq$ -$J_m\omega_a/2$. Since δ itself is bound to be a positive value, the inherent system mass can not be compensated fully. The minimum value M_{vir} can have, and the ruling minimum renderable mass condition, that is conservativeness of either Eqn. (5.40) or Eqn. (5.42), heavily depends on the cut-off frequency of the filter. As the cut-off frequency increases Eqn. (5.40) becomes more conservative than Eqn. (5.42).

If the cut-off frequency is high such that, Eqn. (5.40) is the valid lower bound, the minimum renderable mass can be derived by substituting Eqn. (5.40) in to Eqn. (5.44). In this case M_{vir} becomes equal to $\frac{\delta}{\gamma}\left(1-\frac{K}{J_m\omega_a^2}\right)+\frac{K}{\omega_a^2}$. As ω_a goes to infinity, this bound stays valid and rendered mass amount becomes equal to $M_{vir} = \delta/\gamma$ since Eqn. (5.40) reduces to $M_{ref} \geq 0$. The right hand side of Eqn. (5.40) is always negative due to the constraint caused by Eqn. (5.39). Since the right hand side is always negative, It can be said that a less compliant SEA will result in Eqn. (5.40) being less conservative and resulting in Eqn. (5.42) becoming

the ruling condition. A selection of the highest possible I_t value in the confine of Eqn. (5.39), meaning $\gamma = \delta/J_m$, and substituting γ in to $\frac{\delta}{\gamma}\left(1 - \frac{K}{J_m\omega_a^2}\right) + \frac{K}{\omega_a^2}$, results in lowest passively renderable mass, $M_{vir} = J_m$, while Eqn. (5.40) is the more conservative lower bound.

When Eqn. (5.42) is the more conservative lower bound, substituting Eqn. (5.42) to Eqn. (5.44) shows that the minimum renderable mass is equal to, $M_{vir} = \frac{2\delta + J_m\omega_a}{2\gamma + \omega_a}$. With Eqn. (5.39) the minimum renderable mass of this system can be shown to be the plant mass, J_m. Since Eqn. (5.39) dictates: $\gamma \leq \delta/J_m$, substituting $\gamma = \delta/J_m$ in to $\frac{2\delta + J_m\omega_a}{2\gamma + \omega_a}$ results in $M_{vir} = J_m$. A decrease in I_t will result in a higher rendered mass than J_m. If ω_a is high and Eqn. (5.42) is more conservative than Eqn. (5.40), the rendered mass $M_{vir} = \lim_{\omega_a \to \infty} \frac{2\delta + J_m\omega_a}{2\gamma + \omega_a}$ will again be equal to J_m.

Eqn. (5.41) sets the upper bound on maximum passively renderable mass. It is observed that a high cut-off frequency will decrease the maximum passively renderable M_{vir}. If $\gamma{=}\delta/J_m$ then right hand side of Eqn. (5.41) reduces to zero. Since γ is equal to δ/J_m and M_{ref} is confined to be zero, through Eqn. (5.44), maximum passively renderable mass M_{vir} becomes equal to J_m. As discussed previously, if $\gamma{=}\delta/J_m$ the minimum amount of passively renderable mass is also equal to J_m, therefore if right hand and left hand side of Eqn. (5.39) are equal to each other only plant mass, J_m can be passively rendered.

Chapter 6

Passive Physical Equivalents of Mass-Spring-Damper Rendering with SEA under VSIC

In this chapter, we present passive physical equivalents of combinations of parallel mass-spring-damper rendering of SEA under VSIC when the impedance reference model has a high-frequency roll-off.

6.1 Passive Physical Equivalent of SEA under VSIC During Parallel Mass-Spring-Damper Rendering

Figure 6.1a is a passive physical equivalent of the mass-spring-damper rendering of SEA under VSIC system argued in Subsection 5.2. $K2_{MSD}$ is equal to $K - K_{ref}\frac{\alpha}{1+\alpha}$. $K1_{MSD}$ is the rendered stiffness, K_{vir}=$K1_{MSD}$=$K_{ref}\frac{\alpha}{1+\alpha}$, and $C1_{MSD}$ is the rendered damping, B_{vir}=$C1_{MSD}$=$\frac{\beta+B_{\text{ref}}\,\alpha}{\alpha+1} - \frac{K_{\text{ref}}\,\alpha\,\beta}{K\,(\alpha+1)^2}$. The rest of the terms are given in the Matlab script [1] . The rendered mass of the system is given in the

[1]The Matlab script including the parameters of the realization in Figure 6.1a is available at `https://hmi.sabanciuniv.edu/SEA_VSIC_MSD`.

matlab file with the rest of the terms. If the rendered mass, M_{vir}, of the system is less than 0, it is accepted as M_{vir}=0.

When M_{ref}=0, $K3_{MSD}$ and $C3_{MSD}$ reduce to zero and the passive physical equivalent of voigt model rendering, given in Figure 6.1b, is recovered. When M_{ref}=0 $\wedge$ K_{ref}=0, $K1_{MSD}$, $K3_{MSD}$ and $C3_{MSD}$ reduce to zero and the passive physical equivalent of damping rendering, given in Figure 6.1d, is recovered. When K_{ref}=0 $\wedge$ B_{ref}=0, $K1_{MSD}$ reduces to zero and the passive physical equivalent of mass rendering, given in Figure 6.1e, is recovered. When K_{ref}=0, $K1_{MSD}$ reduces to zero and the passive physical equivalent of parallel mass-damper rendering, given in Figure 6.1c, is recovered.

An analytical analysis shows that $C1_{MSD}$ is always positive as long as the condition given in Eqn. (5.8) is fulfilled. It is also observed that Eqn. (5.7) is more conservative than the condition that guarantees the positiveness of $K2_{MSD}$, when both B_{ref} and M_{ref} are positive, meaning the fulfillment of Eqn. (5.7) gurantees positiveness of $K2_{MSD}$. On the other hand, if both B_{ref} and M_{ref} are negative, then Eqn. (5.7) becomes less conservative than the condition which guarantees the positiveness of $K2_{MSD}$, therefore positiveness of $K2_{MSD}$ guarantees the fulfilment of Eqn. (5.7). A numerical analysis, in the region passive physical equivalent is feasible shows that fulfillment of the sufficient case, meaning $\zeta = 0$, of the condition given in Eqn. (5.9), results in $C2_{MSD}$, $K3_{MSD}$ and $B2_{MSD}$ being positive and if the condition given in Eqn. (5.9) is not fulfilled while the conditions in Eqn. (5.7,5.8) are fulfilled, $C2_{MSD}$, $K3_{MSD}$ and $B2_{MSD}$ become negative.

It is observed that in the region where the passive physical equivalent is feasible, an increase in the cut-off frequency, ω_a results in an increase in $B1_{MSD}$. An increase in $B1_{MSD}$ results in haptic rendering performance enhancement due to the counter element effect to the SEA stiffness K, meaning a convergence to the physical spring dynamics at a higher interaction frequency. Since $B1_{MSD}$ contains a free plant inertia term, J_m, it is observed that an increase in J_m would increase the performance of damping rendering by lagging the convergence to the SEA stiffness.

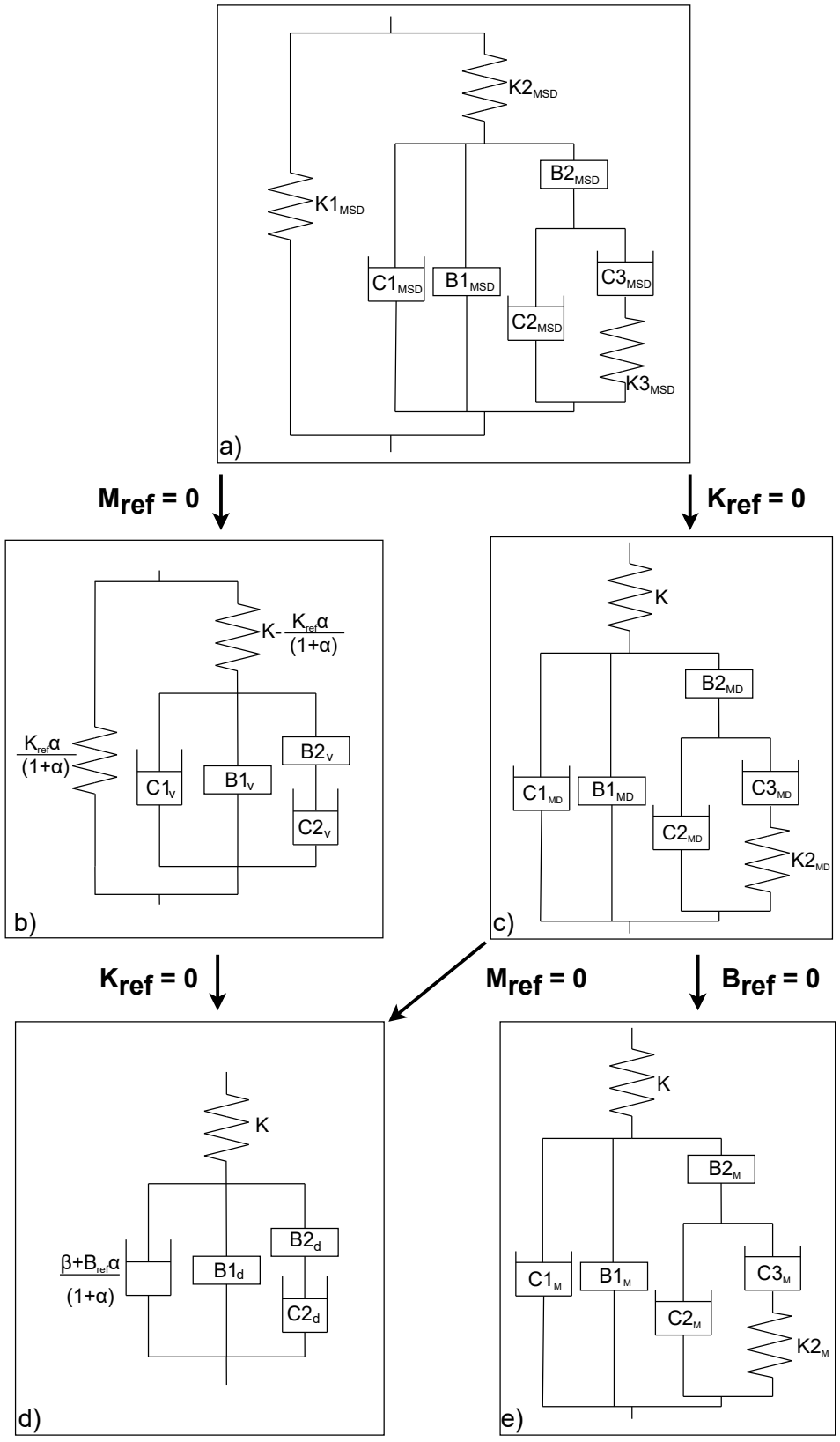

FIGURE 6.1: Passive Physical Equivalents of a) Mass-Spring-Damper model, b) Voigt model, c)Mass-Damper Model, d)Damper, e) Mass, rendering of SEA under VSIC while the torque and motion controller consists of proportional controller gains.

6.2 Passive Physical Equivalent of SEA under VSIC During Damper Rendering

Figure 6.1d is a passive physical equivalent of the damping rendering SEA under VSIC system argued in Subsection 5.3. K is the series elastic actuator stiffness and $(\beta + B_{ref}\alpha)/(\alpha + 1)$ is the rendered damping, B_{vir} of the system. The rest of the elements $C2_d$, $B1_d$ and $B2_d$ are given in the Matlab scriot [2].

For positiveness of the damping element, $(\beta + B_{ref}\alpha)/(\alpha + 1)$, the lower bound in Eqn. (5.16) must be fulfilled. The B1 inerter term is equal to $\frac{J_m K}{K(\alpha+1)-B_{\text{ref}}\alpha\omega_a}$, positiveness of $B1_d$ is achieved if the upper bound in Eqn. (5.16) is fulfilled. For positive values of B_{ref}, it is observed that, as ω_a increase, inerter term $B1_d$ increase and for negative values of B_{ref}, as ω_a increase, inerter term $B1_d$ decrease. For positive values of B_{ref}, if ω_a is chosen large then the feasibility of passive physical equivalent becomes invalid since $C2_d$'s highest order ω_a terms are negative.

If controller gains P_m and P_t are selected high such that $\alpha \to \infty$, the low frequency rendered damping $C1_d$ reduces to B_{ref} and $B1_d$ diminishes furthermore, $B2_d$ reduces to $B_{ref}\left(\frac{B_{ref}}{K} - \frac{1}{\omega_a}\right)$.

The value of inerter $B1_d$ can be altered with the selection of cut-off frequency ω_a without changing the rendered damping, B_{vir}. Even though $B1_d$ interferes with the rendering of damping by converging to inerter dynamics, it can be set as an counter element to SEA stiffness and an increase in $B1_d$ results in an increase in haptic rendering performance, as it will be discussed more in the numerical evaluations, Subsection 7.2.

[2]The Matlab script including the parameters of the realization in Figure 6.1d is available at `https://hmi.sabanciuniv.edu/SEA_VSIC_Damping`.

6.3 Passive Physical Equivalent of SEA under VSIC During Voigt Model Rendering

Figure 6.1b is a passive physical equivalent of the Voigt model rendering SEA under VSIC system argued in Subsection 5.4. $K_{ref}\frac{\alpha}{\alpha+1}$ is the rendered stiffness of the system and $C1_v$=$\frac{\beta+B_{\mathrm{ref}}\,\alpha}{\alpha+1}$ − $\frac{K_{\mathrm{ref}}\,\alpha\,\beta}{K\,(\alpha+1)^2}$ is the rendered damping of the system. The rest of the terms, $K1_v$, $C2_v$, $B1_v$ and $B2_v$ are given in the Matlab script [3]. The passive physical equivalent of Voigt model rendering recovers the realization of damping rendering when K_{ref} is equal to zero.

The criteria for positiveness of $C1_v$ is same as the passivity criteria given in Eqn.(5.22). The inerter term $B1_v$ is derived as the following:

$$\frac{J_m\,(K_{\mathrm{ref}}\,\alpha - K\,(\alpha+1))^2}{-K\,(\alpha+1)^2\,(K_{\mathrm{ref}}\,\alpha - K\,(\alpha+1) + B_{\mathrm{ref}}\,\alpha\,\omega_a)} \tag{6.1}$$

If Eqn. (5.23) is fulfilled $B1_v$ is bound to be positive since the positiveness criteria of $B1_v$ is more conservative than the condition given in Eqn. (5.23).

If controller gains are selected high such that $\alpha \to \infty$ then K_{ref} and B_{ref} becomes the rendered stiffness and damping while $B1_v$ reduces to zero. If the filter cut-off frequency is high, $\omega_a \to \infty$ and controller gains are selected high $\alpha \to \infty$, $K_{ref}\frac{\alpha}{\alpha+1}$ reduces to K_{ref}, $C1_v$ reduces to B_{ref}, $C2_v$ reduces to -B_{ref} and $B2_v$ reduces to $\frac{{B_{\mathrm{ref}}}^2}{K-K_{\mathrm{ref}}}$. This shows us the passive physical equivalent in this case is only valid when B_{ref}=0.

[3]The Matlab script including the parameters of the realization in Figure 6.1b is available at `https://hmi.sabanciuniv.edu/SEA_VSIC_Voigt`.

6.4 Passive Physical Equivalent of SEA under VSIC During Mass Rendering

Figure 6.1e is a passive physical equivalent of the mass rendering system of SEA under VSIC with both proportional gains argued in Subsection 5.5. K is the SEA stiffness. $C1_{M^P}$=$\frac{\beta}{1+\alpha}$ is the damping byproduct of the system and the inerter $B1_{M^P}$ is equal to $\frac{J_m K}{K(\alpha+1)-M_{ref}\alpha\omega_a^2}$ and $B2_{M^P}$ is equal to

$$\frac{M_{ref}\,\alpha\left(K\,(\alpha+1)-{\omega_a}^2\,(J_m+M_{ref}\,\alpha)\right)}{(K\,(\alpha+1)-M_{ref}\,\alpha\,{\omega_a}^2)\,(\alpha+1)}$$

The rest of the elements are given in the attached Matlab script [4].

At low frequencies the series elastic element, K, and the system damping, $\frac{\beta}{\alpha+1}$, interferes with pure mass rendering, meaning the rendered dynamics not only contains mass but also damper. The addition of two inerter elements, $B1_{M^P}$ and $B2_{M^P}$ are equal to $\frac{J_m+M_{\mathrm{ref}}\,\alpha}{\alpha+1}$, the positive element of M_{vir} given in Eqn. (5.26). If the series elastic actuator is a stiff element meaning $K \to \infty$ the impedance transfer function of the parallel connection of $C1_{M^P}$, $B1_{M^P}$ and $B2_{M^P}$ is equal to

$$\frac{(J_m + M_{ref}\alpha)s + \beta}{\alpha + 1} \tag{6.2}$$

the resultant effective mass of the system is equal to $\frac{J_m+M_{ref}\alpha}{\alpha+1}$ which is the addition of the inerter terms $B1_{M^P}$ and $B2_{M^P}$. However if the series elastic element gets more compliant the rendered mass becomes more interfered by the system damping and SEA stiffness. When the SEA stiffness K is a finite value, a series connection of spring K to the parallel connection of $C1_{M^P}$, $B1_{M^P}$ and $B2_{M^P}$ yields the following impedance transfer function:

$$\frac{(J_m\,K + K\,M_{\mathrm{ref}}\,\alpha)\,s + K\,\beta}{(J_m + M_{\mathrm{ref}}\,\alpha)\,s^2 + \beta\,s + K + K\,\alpha} \tag{6.3}$$

[4]The Matlab script including the parameters of the realization in Figure 6.1e is available at `https://hmi.sabanciuniv.edu/SEA_VSIC_Mass`.

In return, the effective mass of the impedance transfer function becomes equal to Eqn. (5.26). From this equation, it can also be observed that as the series elastic stiffness K increases, the effective mass increases as well.

The positiveness of $B1_{M^p}$ is guaranteed if the passivity condition is given in Eqn. (5.29) is fulfilled. A numerical analysis in the region where passive physical equivalent is feasible shows that the positiveness criteria of elements $B2_{M^p}$, $C3_{M^p}$ and $K3_{M^p}$ are more conservative than the passivity criteria given in Eqn. (5.29).

If the cut-off frequency of the filter is high such that $\omega_a \to \infty$, $B1_{M^p}$ reduces to zero and $B2_{M^p}$ reduces to $\frac{J_m+M_{ref}\alpha}{\alpha+1}$. If controller gains are selected high such that $\alpha \to \infty$ then $C1_{M^p}$ and $B1_{M^p}$ reduce to zero. In that case the rendered dynamics become the inerter, $B2_{M^p}$, which is equal to M_{ref} therefore it is observed that an increase in controller gains reduce the damping interference and increase haptic rendering performance.

6.5 Passive Physical Equivalent of SEA under VSIC During Parallel Mass-Damper Rendering

Figure 6.1c is a passive physical equivalent of the mass-damper rendering of SEA under VSIC with both proportional gains argued in Subsection 5.6. The selection of B_{ref}=0 recovers the realization of SEA under VSIC while mass rendering argued in Subsection 6.4. K is the SEA stiffness, $C1_{MD}$=$\frac{\beta+\alpha B_{ref}}{1+\alpha}$ is the rendered damping of the system. Rest of the elements are provided in the Matlab script [5]. The addition of the two inerter terms, $B1_{MD}$+$B2_{MD}$, is derived as the following:

$$\frac{J_m + M_{\text{ref}}\,\alpha}{(1+\alpha)} + \frac{B_{ref}\alpha(\beta + B_{ref}\alpha)}{K\,(1+\alpha)^2} - \frac{B_{ref}\alpha}{\omega_a(1+\alpha)} \tag{6.4}$$

[5]The Matlab script including the parameters of the realization in Figure 6.1c is available at `https://hmi.sabanciuniv.edu/SEA_VSIC_MD`.

The effective mass of a parallel connection of the damper $C1_{MD}$, and inerters $B1_{MD}$ and $B2_{MD}$ is equal to Eqn. (6.4). However as argued in Subsection 6.4 the connection of the series stiffness alters the rendered mass. The effective mass M_{vir} of series connection of SEA stiffness K with parallel connection of the damper $C1_{MD}$, and inerters $B1_{MD}$ and $B2_{MD}$ results in effective mass, M_{vir} being equal to Eqn. (5.6).

Fulfilment of Eqn. (5.36) guarantees positiveness of $C1_{MD}$. If ω_a is chosen high such that, $\omega_a \to \infty$, $B1_{MD}$ reduces to zero and $B2_{MD}$ reduces to $\frac{J_m+M_{\text{ref}}\,\alpha}{(1+\alpha)} + \frac{B_{ref}\alpha(\beta+B_{ref}\alpha)}{K\,(1+\alpha)^2}$, in turn effective mass becomes equal to

$$\frac{J_m + M_{\text{ref}}\,\alpha}{(1+\alpha)} - \frac{\beta(\beta + B_{ref}\alpha)}{K\,(1+\alpha)^2} \tag{6.5}$$

the special case of the effective mass given in Eqn. (5.6) when the negatively signed $\frac{B_{ref}\alpha}{\omega_a(1+\alpha)}$ reduces to zero.

If controller gains are selected high such that $\alpha \to \infty$, $B1_{MD}$ reduces to zero, $C1_{MD}$ reduces to B_{ref}, $B2_{MD}$ reduces to $M_{\text{ref}} - \frac{B_{\text{ref}}}{\omega_a} + \frac{{B_{\text{ref}}}^2}{K}$. However if α is infinite then the realization is only valid for B_{ref}=$[-\infty\ 0]$, otherwise $C2_{MD}$ is guaranteed to be negative signed.

Systematic numerical analysis in the feasible range of passive physical equivalent shows that a decrease in cut-off frequency increases the spring, $K2_{MD}$, resulting in an increased dominance of $B2_{MD}$ over the parallel $C2_{MD}$ and resulting in increased haptic rendering performance.

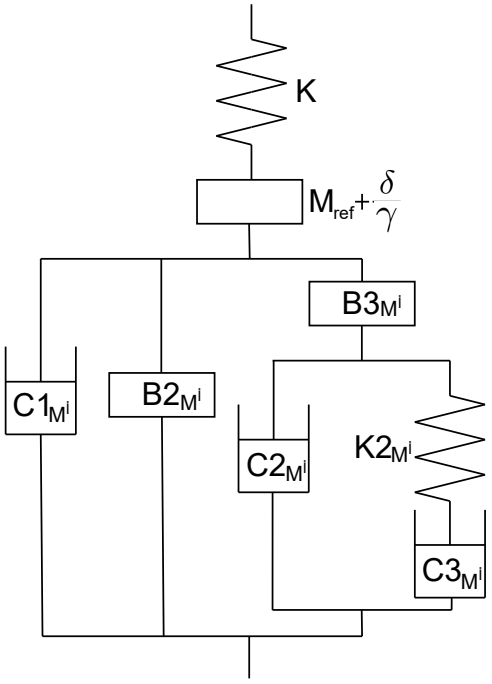

FIGURE 6.2: Passive Physical Equivalent of Mass Rendering of SEA Under VSIC with Filtered Impedance Reference Model when the Torque Controller Consists of an Integral Gain

6.6 Passive Physical Equivalent of SEA under VSIC During Mass Rendering with Integral Torque Gain

Figure 6.2 is a passive physical equivalent of the mass rendering of SEA under VSIC with integral torque and proportional motion controllers argued in Subsection 5.5. K is the SEA stiffness and $B1_{M^i}$=$M_{ref} + \delta/\gamma$ is the low frequency rendered mass. Rest of the elements of the passive physical equivalent are provided in the Matlab script [6].

If (5.42) is satisfied the resultant $C1_{M^i}$ and $B2_{M^i}$ are found to be positive. For positive M_{ref} values, fulfilment of Eqn. (5.39) also guarantees positiveness of $C1_{M^i}$ and $B2_{M^i}$. As $\omega_a \to \infty$, $C2_{M^i}$ is guaranteed to converge to positive infinity, resulting in rendering of damping. The damping $C1_{M^i}$ can be made less effective

[6]The Matlab script including the parameters of the realization in Figure 6.2 is available at `https://hmi.sabanciuniv.edu/SEA_VSIC_M_IP`.

with design choices such as designing an SEA system with a low plant inertia and damping J_m and B_m, respectively, however it must be noted that this method has are very limited effect on haptic rendering performance.

As $\gamma \to \infty$, such that controller gains are selected high, $B1_{M^i}$ reduces to M_{ref} and results in direct rendering of M_{ref}. $C1_{M^i}$ in turn reduces to $\frac{M_{\text{ref}}\omega_a}{2}$ and $B2_{M^i}$ reduces to $\frac{M_{ref}J_m}{M_{ref}-J_m}$.

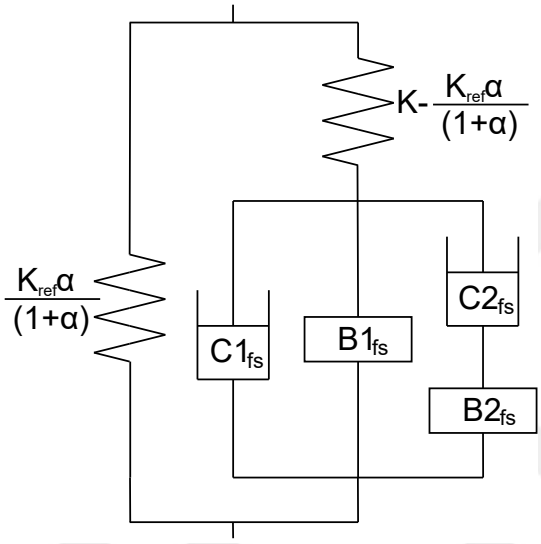

FIGURE 6.3: Passive Physical Equivalent of Spring Rendering of SEA Under VSIC with Filtered End Effector Velocity Feedback

6.7 Passive Physical Equivalent of Spring Rendering with the Impedance Reference Roll-off

Figure 6.3 is a passive physical equivalent of the spring rendering of SEA under VSIC with filtered impedance reference where both controllers consist of proportional gains, argued in Subsection 5.1. The low frequency rendered stiffness of the system is $K_{ref}\alpha/(1+\alpha)$. The rest of the terms are provided in the Matlab script [7]. Fulfilment of Eqn. (5.2) results in positiveness of $K1_{fs}$ and $B1_{fs}$ and Eqn. (5.2)

[7]The Matlab script including the parameters of the realization in Figure 6.3 is available at `https://hmi.sabanciuniv.edu/SEA_VSIC_Spring_Fil`.

is fulfilled if and only if $C1_{fs}$ is positive. If controller gains are selected high such that $\alpha \to \infty$, the low frequency rendered stiffness of the system becomes equal to K_{ref}, and the seriel spring, $K - K_{ref}\frac{\alpha}{\alpha+1}$ becomes equal to K-K_{ref}. On the other hand, unlike the unfiltered case, $C1_{fs}$ becomes equal to -K_{ref}/ω_a which breaks down the validity of the passive physical equivalent.

The selection of the cut-off frequency heavily impacts the performance of the system. If the aim is rendering a pure spring without the system damping, ω_a can be set to a value that reduces $C1_{fs}$ to zero. For pure spring rendering without damping interference, the cut-off frequency can be chosen as the following.

$$\omega_a = \frac{KK_{ref}\alpha(1+\alpha)}{\beta(K(1+\alpha) - K_{ref}\alpha)} \tag{6.6}$$

Chapter 7

Numerical Evaluations of Mass-Spring-Damper Rendering with SEA under VSIC

In this chapter, we study the effects of the plant parameters and controller gains on the rendering performance through a comprehensive numerical analysis. We compare our results with the understanding we have acquired through passivity analysis and passive physical equivalents.

Table 7.1 presents the physical plant parameters and controller gains used in our simulations, unless stated otherwise.

TABLE 7.1: System parameters used for the simulations of mass-spring-damper rendering of SEA

Parameter	J	B	K
Value	0.00052 kg-m^2	0.0111 Nm s/rad	252 Nm/rad
Parameter	P_t	P_m	ω_a
Value	10 rad/(s Nm)	10 Nm s/rad	400 s$^-$1

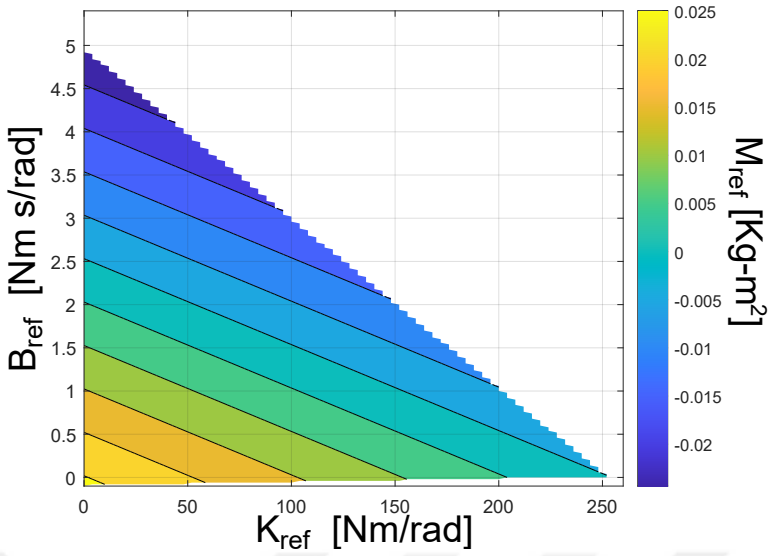

FIGURE 7.1: KBM plot of SEA under VSIC while rendering Mass-Spring-Damper model with a cut-off frequency of ω_a=100.

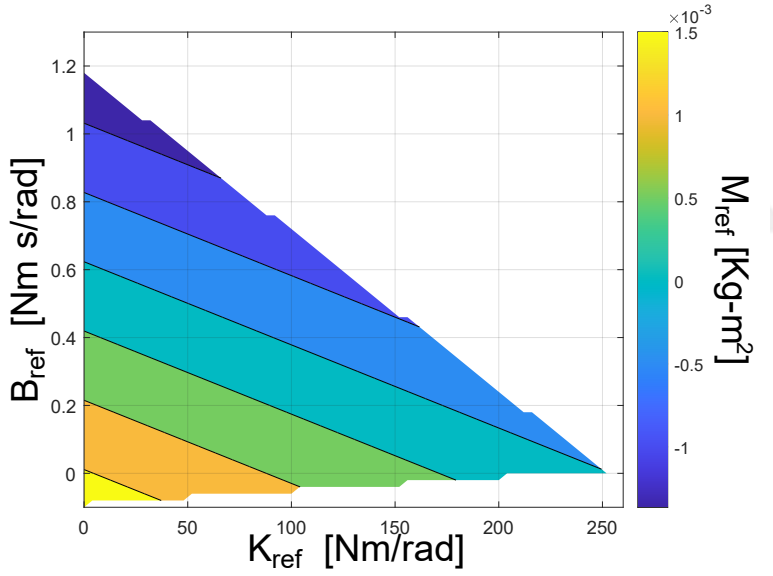

FIGURE 7.2: KBM plot of SEA under VSIC while rendering Mass-Spring-Damper model with a cut-off frequency of ω_a=400.

7.1 Parallel Mass-Spring-Damper Rendering

We first start our numerical evaluations with the parallel mass-spring-damper rendering of SEA under VSIC, studied in subsection 5.2. The plots are given with K_{ref}, B_{ref} and M_{ref} parameters instead of rendered spring, K_{vir}, damper B_{vir}, mass ,M_{vir}, due to effective impedance range of spring and mass rendering can not

be defined together.[46]

Figure 7.2 and Figure 7.1 show the maximum M_{ref} values, at each unique K_{ref} and B_{ref} point without violating the passivity criteria.It can be observed that as the cut-off frequency ω_a increases, the maximum M_{ref} value decreases as discussed in subsection 5.2.

Figure 7.2 and Figure 7.1 show that a selection of negative M_{ref} increases maximum passively selectable B_{ref} and a selection of negative B_{ref} increases maximum passively selectable M_{ref}. Looking into Figure 7.2, when K_{ref}=0 and B_{ref}=0, maximum passively selectable M_{ref} is equal to 1.5 $10^{-3} Kg\text{-}m^2$ however when B_{ref}=$-0.1 Nms/rad$, which is the minimum passively selectable B_{ref} accordingly to Eqn. (5.8) when K_{ref}=0, maximum selectable M_{ref} becomes equal to 1.77 $10^{-3} Kg - m^2$. Likewise when K_{ref}=0 and M_{ref}=0, maximum passively selectable B_{ref} is equal to $0.62 Nms/rad$ however when M_{ref} is chosen as $-1.3\ 10^{-3} Kg\text{-}m^2$ for mass compensation, maximum passively selectable B_{ref} value becomes equal to $1.18 Nms/rad$.

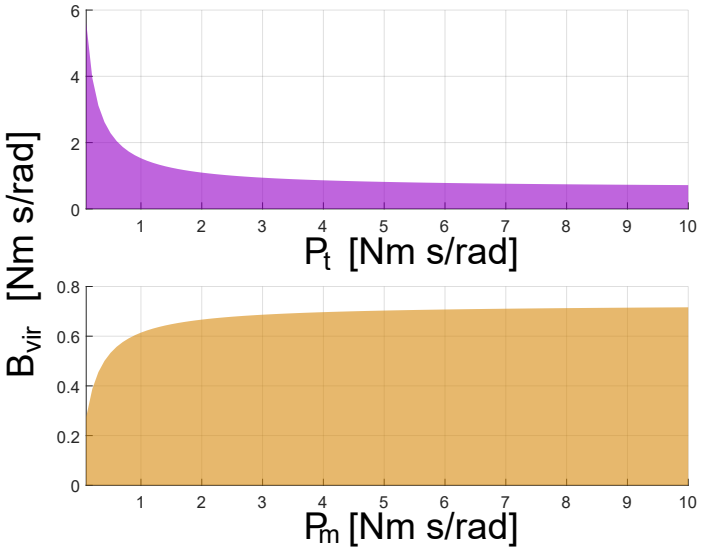

FIGURE 7.3: Maximum passively renderable damping of $Z_D^{SEA^{P-P}}(s)$ at distinct controller gains.

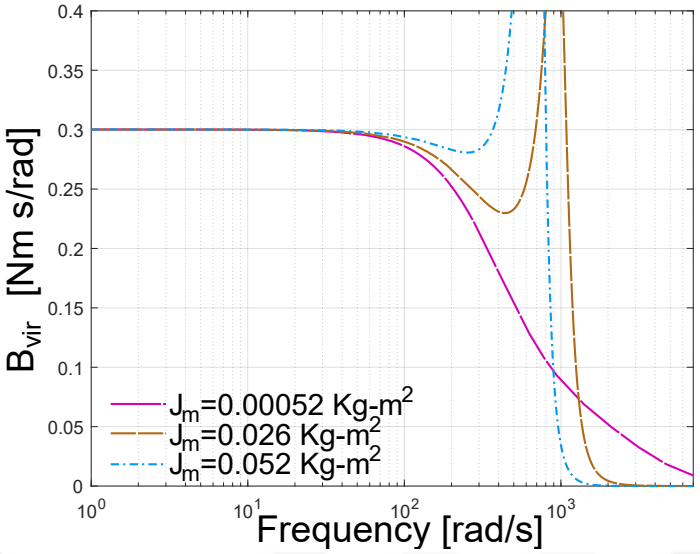

FIGURE 7.4: Effective damping versus interaction frequency at various J_m, of damping rendering of SEA under VSIC with impedance reference roll-off.

7.2 Damper Rendering

We continue our study for numerical evaluations for damper rendering, the system given in Subsection 5.3.

Figure 7.3 presents the maximum passively renderable damping values at distinct controller gains. As argued in Subsection 5.3, increasing P_t lowers the maximum passively renderable damping and decreasing P_t results in higher maximum passively renderable damping, however it must be noted a small P_t also results in performance loss. It is also observed that an increase in P_m also increases the maximum passively renderable damping.

Figure 7.5 and Figure 7.4 presents, effective damping plots at distinct ω_a and J_m values, respectively. It is observed that as both of these parameters increase the haptic rendering performance increase. This behaviour is due to increase in $B1$ and $C2$ argued in Section 6.2. As $B1$ and $C2$ increase the convergence to spring dynamics lags from the dynamics of parallel damper,mass and seriel damper mass, resulting in an enhanced rendering performance.

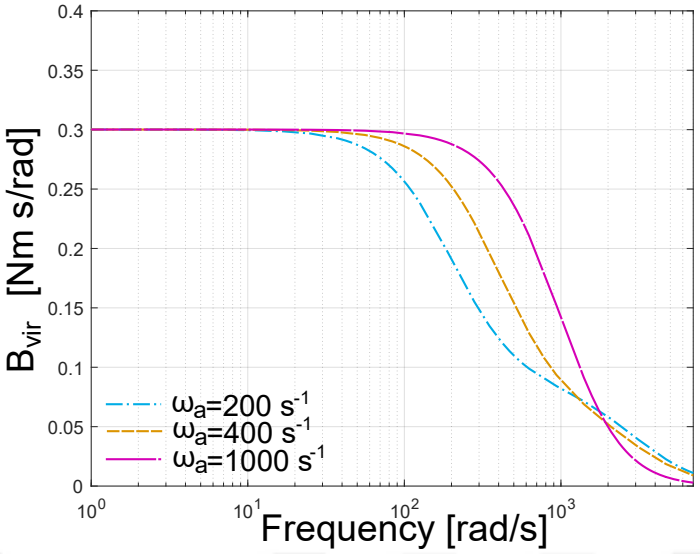

FIGURE 7.5: Effective damping versus interaction frequency at various ω_a, of damping rendering of SEA under VSIC with impedance reference roll-off.

7.3 Voigt Model Rendering

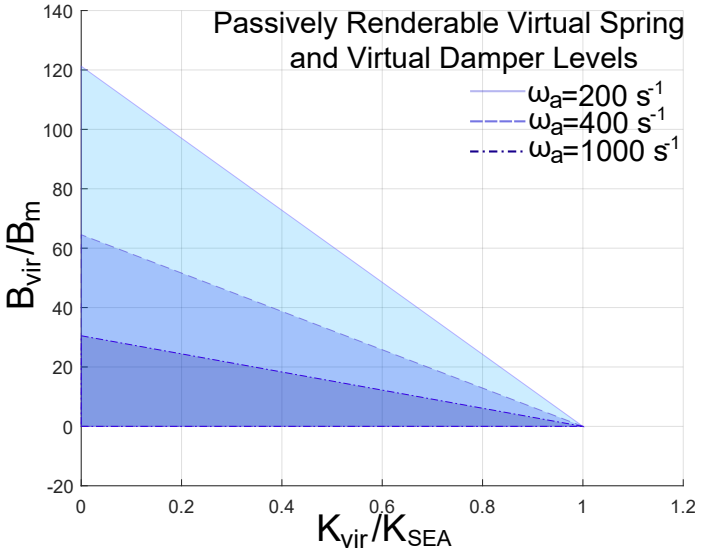

FIGURE 7.6: KB plot of SEA under VSIC while rendering Voigt model at various cut-off frequencies, with impedance reference roll-off.

We continue our study with numerical evaluations for Voigt model rendering, the system studied in Subsection 5.4.

Figure 7.6 shows K-B plots, the maximum and minimum passively renderable damping at each unique rendered stiffness point at distinct cut-off frequencies ω_a.

It can be observed that as ω_a decreases, the maximum passively renderable damping increases while the minimum passively renderable damping does not change and is equal to zero. As ω_a goes to infinity, the bounds in Eqns. (5.18,5.19) are recovered and B_{vir} cannot exceed the system damping, $\beta/(\alpha+1)$, however compensation of the system damping is still possible.

Figure 7.7 shows the effective stiffness and effective damping plots of Voigt model rendering at two distinct cut-off frequencies. An increase in ω_a results in increase in haptic rendering performance due to an increase in $B1$, the same reason argued in Subsection 7.2.

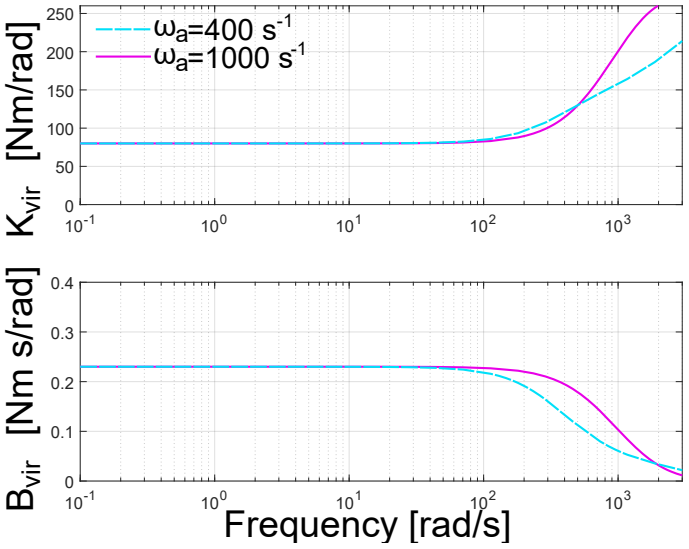

FIGURE 7.7: Effective stiffness and damping versus interaction frequency at various ω_a.

7.4 Mass Rendering and Parallel Mass-Damper Rendering

We continue our study with numerical evaluations for mass rendering of SEA under VSIC, studied in Subsection 5.5. Figure 7.8 shows the M-width plot of SEA under VSIC, when both controllers consist of proportional gains, the maximum and minimum passively renderable mass range. It is observed that an increase in

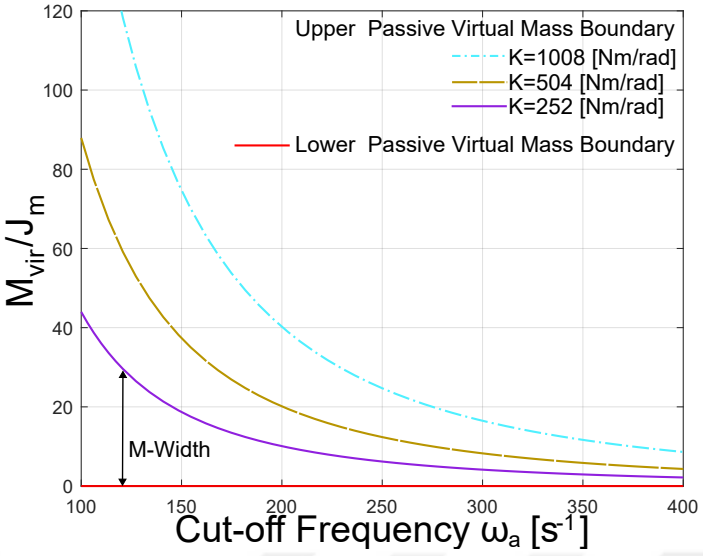

FIGURE 7.8: M-width plot of SEA under VSIC.

the cut-off frequency ω_a results in a smaller passively renderable mass range. It is also observed that a change in ω_a does not change the lower bound on passively renderable mass. An SEA with higher stiffness will not change the lower bound of passively renderable mass, that is because the fact that the lower bound of M_{ref} results in a system phase of $[-\pi/2\ 0]$, in which the effective mass is not defined. The upper bound of M-width on the other hand, increases with an increase in SEA stiffness.

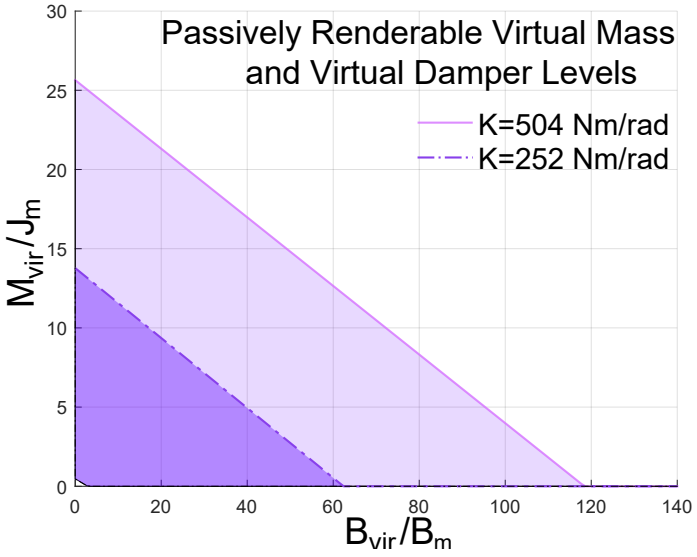

FIGURE 7.9: MD plot, maximum renderable mass at each distinct rendered damping, at various SEA stiffnesses when ω_a=200 s^{-1}.

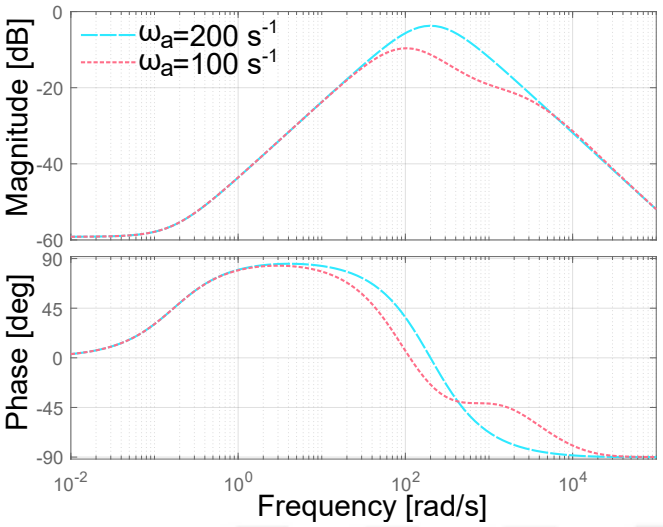

FIGURE 7.10: Bode plot of parallel mass-damper rendering with B_{vir}=0.0011 Nms/rad and M_{vir}=0.0065 $Kg - m^2$ at distinct cut-off frequencies.

We continue our study with numerical evaluations for parallel mass-damper rendering, studied in Subsection 5.6. Figure 7.9 shows the maximum and minimum passively renderable mass at each distinct rendered damping point. It is observed if either M_{ref} or B_{ref} is chosen negative such that M_{vir} or B_{vir} is made zero, in order, the upper bound on B_{vir} or M_{vir} increase. It is also shown that as SEA stiffness K increase the upper bound on maximum renderable M_{vir} and B_{vir} increase while the lower bound does not change.

Figure 7.10 shows Bode plots of parallel mass-damper rendering while rendering a B_{vir} of 0.0011 Nms/rad and a M_{vir} of 0.0065 $Kg-m^2$ at cut-off frequencies ω_a=100 s^{-1} and ω_a=200 s^{-1}. It is observed that the increase in the cut-off frequency increases the performance as the system tracks desired dynamics for a longer period of interaction frequency, however the increase in cut-off frequency also results in more conservative passivity bounds as argued in Subsection 5.6.

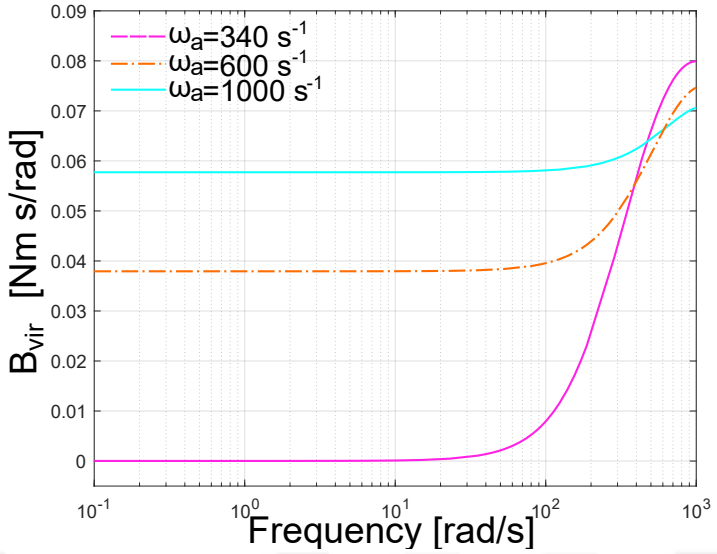

FIGURE 7.11: Effective damping of spring rendering with impedance reference roll-off at various cut-off frequencies.

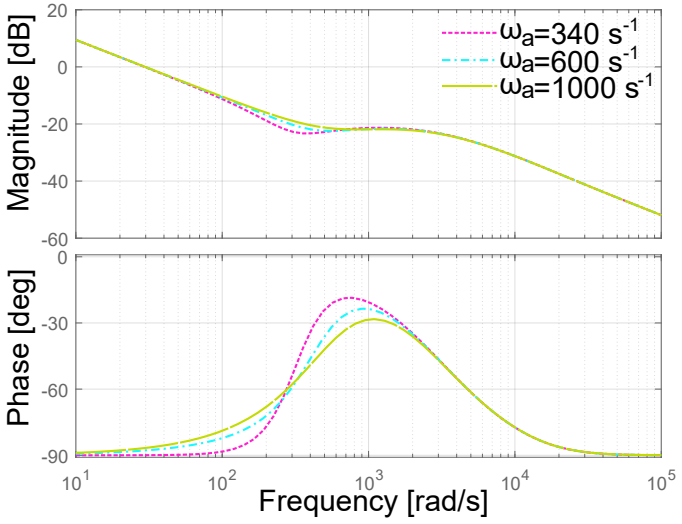

FIGURE 7.12: Bode plots of spring rendering with impedance reference roll-off at various cut-off frequencies.

7.5 Spring Rendering with Impedance Reference Roll-off of SEA under VSIC

We continue our study with numerical evaluations for spring rendering with impedance reference roll-off, the system studied in Subsection 5.1.

Figure 7.11 is the effective damping plot of spring rendering with low-pass filtered end effector position feedback, while rendering a spring of 29.7 Nm/rad at various filter cut-off frequencies. It is observed that when the filtering frequency is selected as given in the equation 6.6, that is the minimizing value of $C1_{fs}$ which is given in the passive physical equivalent presented in Figure 6.3, the effective damping of the system reduces to 0. As the cut-off frequency increases effective damping of the system increases as well. Therefore it is shown that filtering the impedance reference results in increased haptic rendering performance.

The performance enhancement can also be shown through Bode plots. Figure 7.12 presents the Bode plots of spring rendering with impedance reference roll-off at various cut-off frequencies while rendering a spring of 29.7 Nm/rad. It is observed that the cut-off frequency that minimizes the effective damping also results in the widest range of spring rendering bandwidth as larger cut-off frequencies result in drifts from the required dB per decade at smaller frequencies.

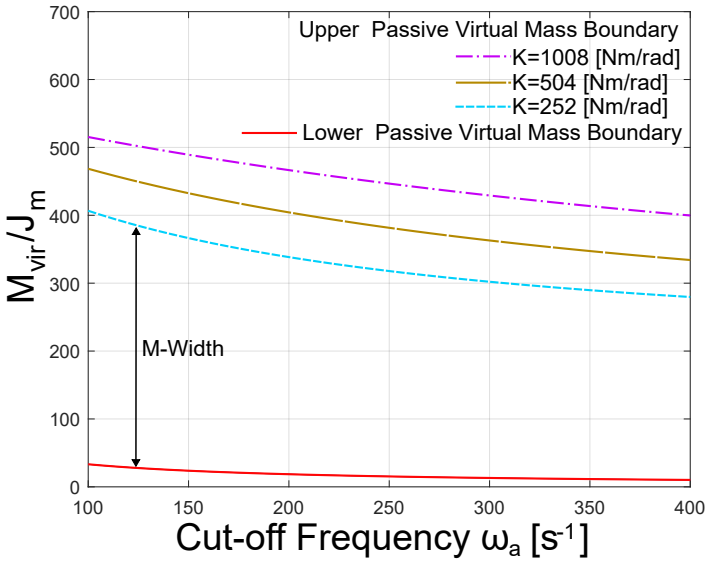

FIGURE 7.13: Upper and lower bounds of passive virtual mass boundary through cut-off frequency, M-width with distinct stiffness level of SEA.

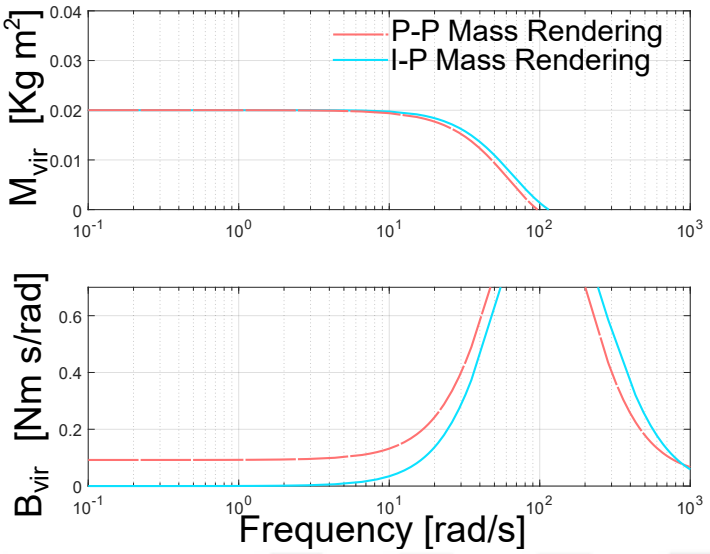

FIGURE 7.14: Mass rendering performance of P-P and I-P system, effective mass and damping when I_t=10 $rad/(s^2Nm)$, P_t=10 $rad/(sNm)$, P_m=1 Nms/rad and ω_a=100 s^{-1}.

7.6 Mass Rendering of SEA when the Torque Controller Consists of an Integral Gain

Figure 7.14 shows the performance of mass rendering of SEA under VSIC when both controllers are proportional gains and when torque controller is integral gain and motion controller is proportional gain. Figure 7.14 shows effective mass and damping plots while rendering a mass of 0.02 Kg-m^2. As argued in Section 5.5, mass rendering of SEA under VSIC when both controllers are proportional gains, maintains the system damping, $\beta/(\alpha+1)$, while SEA under VSIC when torque controller is integral gain and motion controller is proportional gain, fully compensates the system damping. The figure shows that the effective damping is a finite value when both controllers are proportional gains and zero when only the torque controller is an integral gain.

Chapter 8

Experimental Evaluations of Mass-Spring-Damper Rendering with SEA under VSIC

This chapter presents the experimental validation of the theoretical passivity bounds and haptic rendering performance of SEA using a single degree of freedom series elastic actuator break pedal presented in [44]. The series elastic actuator break pedal is equipped with a brushless DC motor utilizing an optical encoder and Hall-effect sensor. The torque of the motor is amplified with a gearbox and a capstan with a total transmission ratio of 1:38.1. The series elastic element, in between the capstan pulley and the end effector, is used to estimate user induced torques with a linear encoder sensing the deflection of the cross-flexure. Controllers are implemented in real-time at 1 kHz using an industrial PC utilizing EtherCAT bus.

8.1 Identification of Plant Parameters

The stiffness of the cross-flexure joint is determined by locking the actuator and applying pre-determined torques and measuring the deflections that occurs on the

cross-flexure. The SEA stiffness is found to be K=252 N-m/rad with, a least square fit to the experimental data with R^2=0.99.

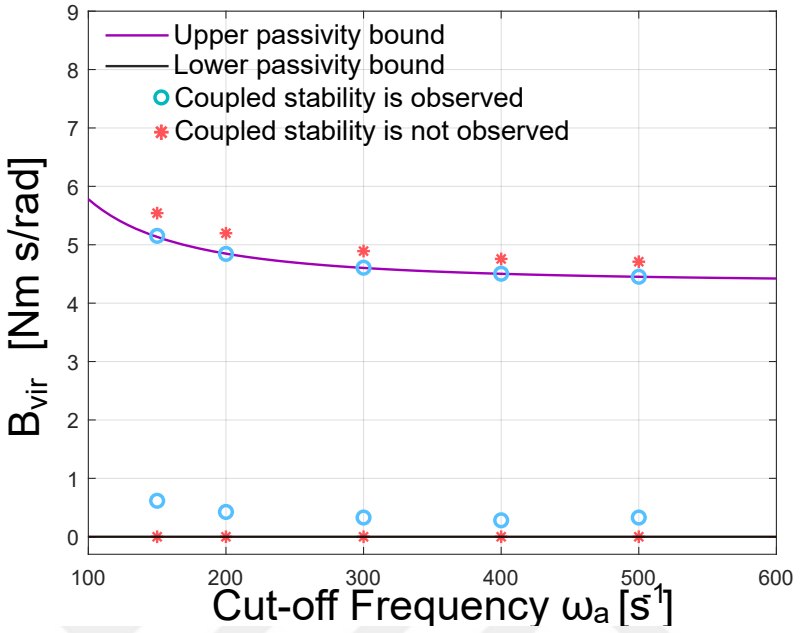

FIGURE 8.1: Coupled Stability Experiments of Damper Rendering

To determine system parameters related to the motor and power transmission, closed-loop system identification is utilized. Closed-loop identification results in accurate prediction of the system parameters due to robust motion controller compensating parasitic nonlinear effects. To determine the reflected inertia and damping of the plant, the system identification is carried out with motion controller, P_m=0.0576 N-ms/rad. A chirp velocity reference signal with a range of 0.01-10 Hz is applied and the experimental data is saved. A first-order transfer function is fitted with R^2=0.95 and the plant parameters are identified as J_m=0.00052 $Kg\text{-}m^2$ and B_m=0.0111$N\text{-}ms/rad$. Due to the transmission ratio n, the following mappings are applied to the system parameters: $J_{m_{eq}}$=n^2J_m, $B_{m_{eq}}$=n^2B_m, $P_{m_{eq}}$=n^2P_m, $P_{t_{eq}}$=$\frac{P_t}{n}$. Controller gains are selected as P_t=10 $rad/(sNm)$ and P_m=0.0576 Nms/rad and the filter cut-off frequency is set as w_a=200 s^{-1} unless stated otherwise.

8.2 Experimental Validation of Passivity Bounds

In this section we present experimental validation of the derived necessary and sufficient conditions for the passivity of haptic rendering. Coupled stability experiments of interaction controllers when the system is coupled to most destabilizing environments have been established in the literature. [8] Validation of passivity bounds for spring rendering of SEA are studied by coupling inertia to the interaction port while validation of passivity bounds for mass rendering of SEA are studied by coupling stiffness to the interaction port. End effector is applied a human induced impact to check coupled stability. If chatter is observed the system is concluded to be not passive while no chatter is observed after numerous trials the system is concluded to be passive.

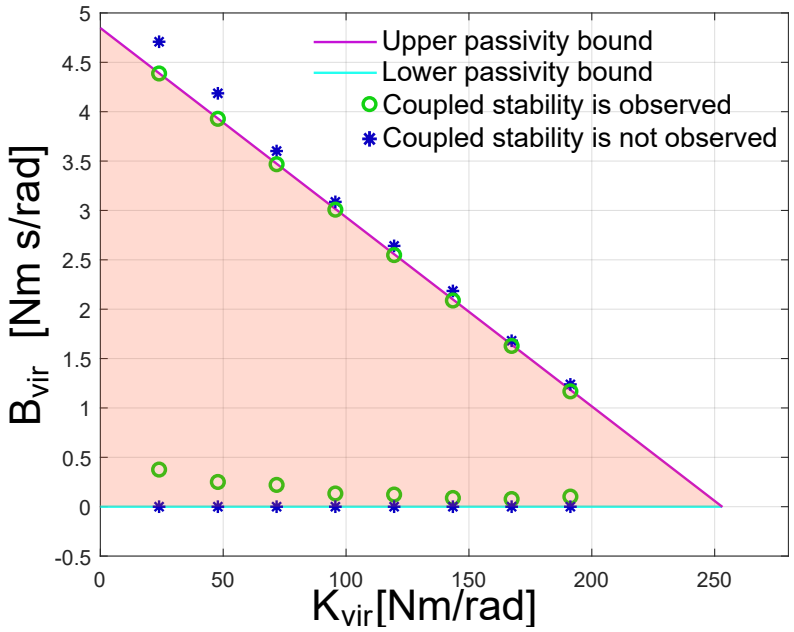

FIGURE 8.2: Coupled Stability Experiments of Voigt Model Rendering.

8.2.1 Validation of Passivity Bounds of Viscous Damping Rendering

In this experiment, coupled stability of SEA under VSIC while damper rendering, $Z_D^{SEA^{P-P}}(s)$, is investigated. Figure 8.1 shows the experimentally verified passive

B_{vir} values and the necessary and sufficient conditions for the passivity, given as in the right hand side and the left hand side of Eqn. (5.16), respectively. Rendered damping at low frequencies, B_{vir} is equal to $\frac{\beta+B_{ref}\alpha}{\alpha+1}$. The sample points shown with signs "*" and "o" mark the points where the coupled stability is violated and obtained respectively.

The cut-off frequency of the filter, that is to ensure causality of estimation of the velocity through end effector position, is increased at each sample point. As discussed in Section 5.3, a decrease in the filter cut-off frequency increases the maximum passively renderable damping. The upper passivity bounds for passivity are found to be more conservative than the experimentally verified passivity limits while the lower bound is found to be less conservative than the experimentally verified passivity limits. The average error is found to be 7.4%, indicating the experimentally verified passivity limits of B_{vir} and our theoretical results are in good agreement.

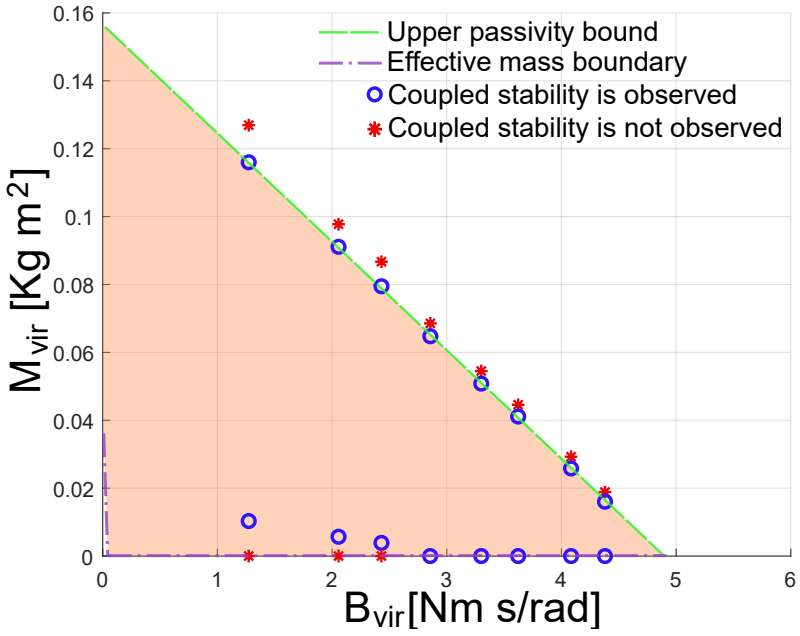

FIGURE 8.3: Coupled Stability Experiments of Parallel Mass-Damper Rendering.

8.2.2 Validation of Passivity Bounds of Voigt Model Rendering

In this experiment, coupled stability of SEA under VSIC while Voigt model rendering, $Z_{SD}^{SEA^{P-P}}(s)$, is investigated. Figure 8.2 shows the experimentally verified passive B_{vir} and K_{vir} values. The necessary and sufficient conditions for the passivity, given in Eqns. (5.22,5.23), are the lower and upper passivity bounds, respectively. Rendered stiffness at low frequencies is equal to K_{vir}=$K_{ref}\frac{\alpha}{\alpha+1}$ and rendered damping at low frequencies is given in Eqn. (5.20). The sample points shown with signs "*" and "o" mark the points where the coupled stability is violated and obtained respectively.

This experiment investigates maximum and minimum passively renderable damping at various rendered stiffness levels. The cut-off frequency is chosen as ω_a=200 s^{-1} and K_{vir} is increased after data collection in each point. It is observed that the experimentally verified maximum passively renderable damping is less conservative than our theoretical bounds while experimentally verified minimum passively renderable damping is more conservative than our theoretical bounds. The average error for this experiment is found to be 7.11%.

8.2.3 Validation of Passivity Bounds of Parallel Mass-Damper Rendering

In this experiment, coupled stability of SEA under VSIC while parallel mass-damper rendering, $Z_{MD}^{SEA^{P-P}}(s)$, is investigated. Figure 8.3 shows the experimentally verified passive B_{vir} and M_{vir} values. The necessary and sufficient conditions for the passivity, given in Eqns. (5.35,5.37), are the upper and lower passivity bounds, respectively. The lower bound is named effective mass boundary due to negative mass not being defined and being projected as zero. Rendered damping at low frequencies is equal to B_{vir}=$\frac{\beta+B_{ref}\alpha}{\alpha+1}$ and rendered mass at low frequencies is given in Eqn. (5.34). The sample points shown with signs "*" and "o" mark the points where the coupled stability is violated and obtained respectively.

This experiment investigates maximum and minimum passively renderable mass at various rendered damping levels. The cut-off frequency is chosen as ω_a=150 s^{-1} while the motion controller gain is set as P_m=0.0176 $Nm\ s/rad$ and B_{vir} is increased after data collection at each point. Theoretical results are found to be more conservative than experimentally found values for the upper passivity bound while theoretical results are found to be less conservative than experimentally founds values for the lower passivity bound. The average error for parallel mass-damper rendering of SEA under VSIC is found to be 8.89%.

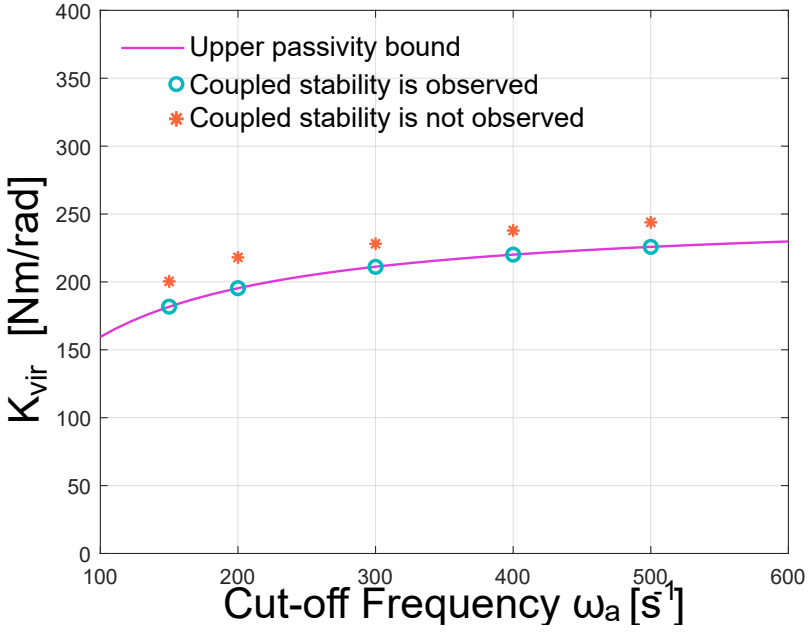

FIGURE 8.4: Coupled Stability Experiments of Spring Rendering with Low-Pass Filtered End-Effector Position Feedback

8.2.4 Validation of Passivity Bounds of Spring Rendering

In this experiment, coupled stability of SEA under VSIC while spring rendering with low-pass filtered end effector position feedback, $Z_{FS}^{SEA^{P-P}}(s)$, is investigated. Figure 8.4 shows the experimentally verified passive K_{vir} values at distinct filter cut-off frequencies. The necessary and sufficient conditions for the passivity, given in Eqn. (5.2), is the upper passivity bound. The rendered stiffness at low frequencies is equal to K_{vir}=$K_{ref}\frac{\alpha}{\alpha+1}$. The sample points shown with signs "*" and "o" mark the points where the coupled stability is violated and obtained respectively.

The experiment shows that as filter cut-off frequency increases the maximum passively renderable stiffness value increases as well. Theoretical results are found to be more conservative than experimentally found values for the upper passivity bound. The average error for spring rendering of SEA under VSIC with low-pass filtered end effector position feedback is found to be 9.1%.

8.3 Experimental Validation of Rendering Fidelity

In this subsection, we present systemic haptic rendering performance experiments of SEA under VSIC for damping rendering, Voigt model rendering, mass rendering, parallel mass-damper rendering and spring rendering when the end-effector position feedback is low-pass filtered.

The end-effector of the SEA break pedal is rigidly coupled to an ideal motion source and the system is excited with a sine wave with distinct interaction frequencies. At each frequency point the resultant torque on the SEA, τ_{SEA} and the end effector position is saved. The end-effector position is fitted to a sine wave and the fitted sine wave is differentiated in post processing to calculate end effector velocity, ω_{end}. The impedance at the interaction port can be experimentally found as $\frac{\tau_{sea}}{\omega_{end}}$. The resultant impedance at each interaction port excitation frequency is than plotted on to magnitude bode plots. Errors in this experiment is calculated with the difference between the expected torque on the SEA and the actual measured torques on the SEA.

8.3.1 Experimental Validation of Fidelity of Viscous Damping Rendering

Figure 8.5 presents the haptic performance of damping rendering of SEA under VSIC at nine distinct interaction frequencies while rendering B_{vir}=4.35 Nms/rad and B_{vir}=1.95 Nms/rad. It is observed that the experimentally found rendered

damping, B_{vir}=4.35 has an error of 9.1% and B_{vir}=1.95 has an error of 10%when compared to simulation data of the bode magnitude plot of the system.

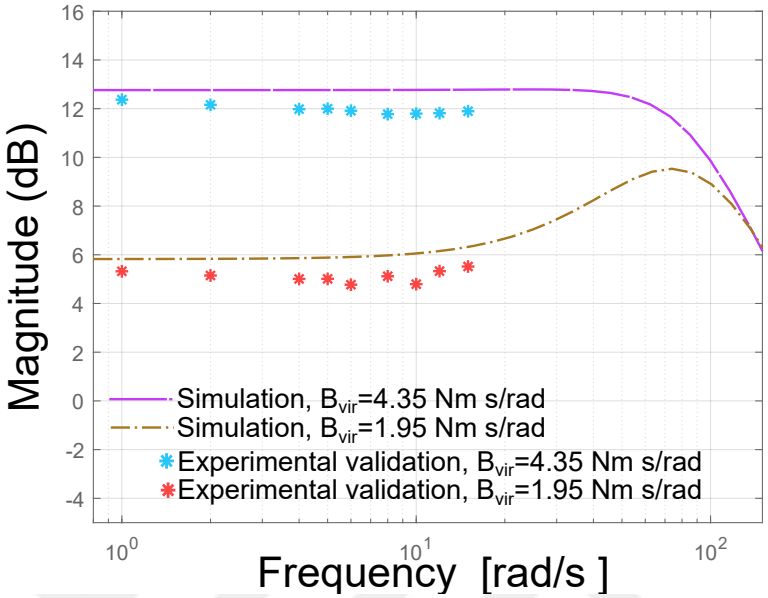

FIGURE 8.5: Excitation Experiment of Damper rendering

8.3.2 Experimental Validation of Fidelity of Voigt Model Rendering

Figure 8.6 presents the haptic performance of voigt model rendering of SEA under VSIC at nine distinct interaction frequencies while rendering K_{vir}=25 Nm/rad, B_{vir}=5.94 Nms/rad and K_{vir}=25 Nm/rad, B_{vir}=2.2 Nms/rad. For this set of experiment the proportional torque controller is set to P_t=7 $rad/(s\ Nm)$. It is observed that a decrease in B_{vir} increases the spring rendering performance as the spring rendering bandwidth with respect to interaction frequency increase. The error for this experiment is equal to 8.5% when B_{vir}=5.94$Nm\ s/rad$ and 5.3 % when B_{vir}=2.2$Nm\ s/rad$. When B_{vir}=5.94$Nm\ s/rad$, the system converges to rendered damping when the interaction frequency exceeds approximately 8 rad/s, while the system with B_{vir}=2.2 $Nm\ s/rad$ does not converge to damping with in the frequency range which the experiment is conducted, therefore it is observed that the error is higher when the system dynamics converge to rendered damping.

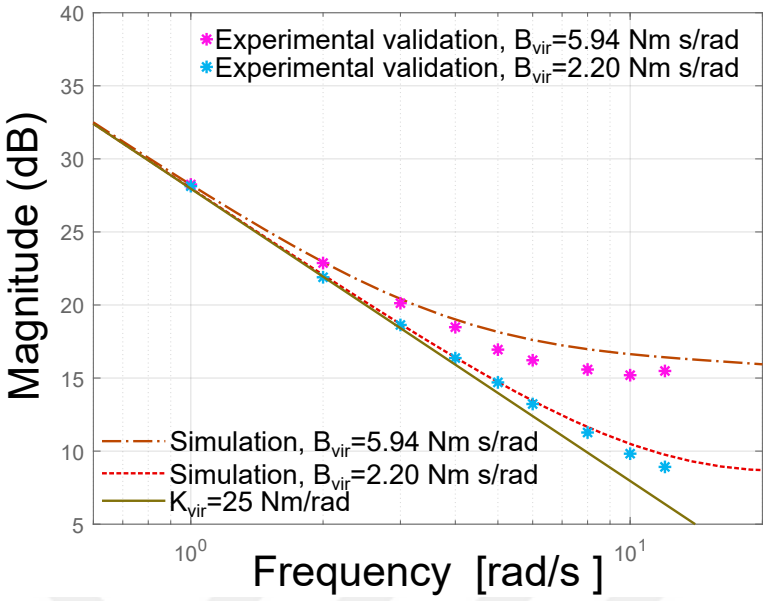

FIGURE 8.6: Excitation Experiment of Voigt Model Rendering

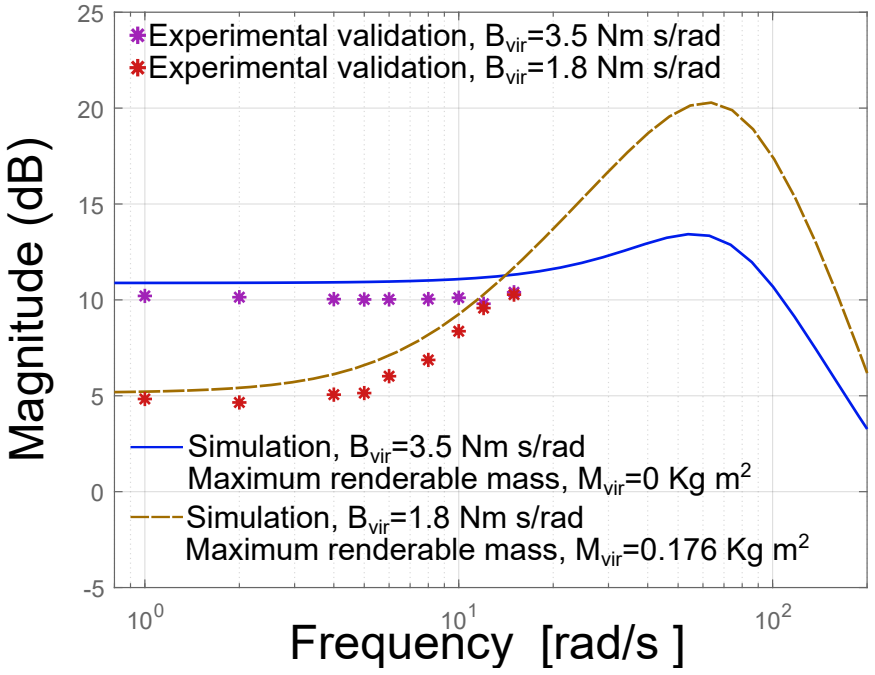

FIGURE 8.7: Excitation Experiment of Parallel Mass-Damper Rendering

8.3.3 Experimental Validation of Fidelity of Parallel Mass-Damper Rendering

Figure 8.7 presents the haptic performance of parallel mass-damper rendering of SEA under VSIC at nine distinct interaction frequencies while rendering the maximum passively renderable mass of 0 $Kg\,m^2$ and 0.176 $Kg\,m^2$ while B_{vir}=3.5 $Nm\ s/rad$ and B_{vir}=1.8 $Nm\ s/rad$, respectively, with a proportional motion controller gain of P_m=0.01 $Nm\ s/rad$ and a low-pass filter cut-off frequency of w_a=150 s^{-1}. Figure 8.7 shows that compensation of the system damping enables rendering higher values of passive mass as mentioned in subsection 5.6. For this set of experiments the error is calculated as 10.2 % and 11 % for B_{vir}=3.5 $Nm\ s/rad$ and B_{vir}=1.8 $Nm\ s/rad$ respectively.

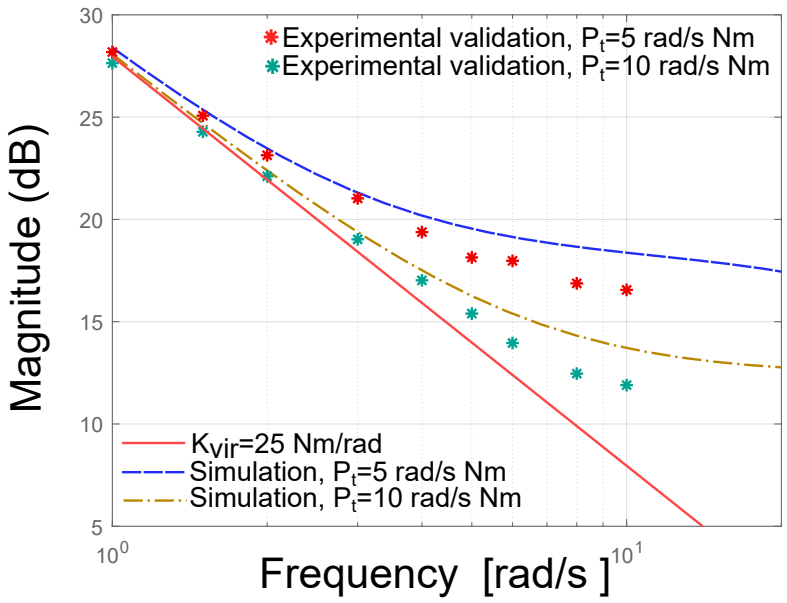

FIGURE 8.8: Excitation Experiment of Spring Rendering with Low-Pass Filtered End-Effector Position Feedback

8.3.4 Experimental Validation of Fidelity of Spring Rendering with Filtered Impedance Reference

Figure 8.8 presents the haptic rendering performance of spring rendering of SEA under VSIC when the impedance reference is filtered, at nine distinct interaction frequencies while rendering a stiffness of K_{vir}=25 Nm/rad with proportional torque controller gains of P_t=10 $rad/(s\ Nm)$ and P_t=5 $rad/(s\ Nm)$. The errors for this set of experiment is 8.21 % and 8.54 % for P_t=10 $rad/(s\ Nm)$ and P_t=5 $rad/(s\ Nm)$ respectively. It is observed that as the proportional torque controller gain increase the spring rendering performance of the system increase. The increase in performance is due to the decrease of rendered damping in the system which can be shown through the passive physical equivalent of the system, presented in Figure 6.3. The $C1_{fs}$ damper term decreases from 7.41 $Nm\ s/rad$ to 3.78 $Nm\ s/rad$ as P_t increases to 10 $rad/(s\ Nm)$ from 5 $rad/(s\ Nm)$, resulting in enhancement of haptic rendering performance.

Chapter 9

Conclusion

We have presented stability robustness and haptic rendering performance trade-offs of SEA under VSIC, that are induced by utilization of filters for: (i) attenuation of the high frequency sensor noise, (ii) shaping the phase response of the haptic system by introducing filters as compensators and (iii) o shape the dynamics of the reference model to ensure its trackability and causality by introducing high-frequency roll-off characteristics. We have derived necessary and sufficient conditions for the passivity of SEA during haptic rendering of combinations of virtual environments consisting of combinations of linear parallel mass-spring-damper and studied the haptic rendering performance alterations caused by filters with passive physical equivalents. We have compared the resultant stability robustness and haptic rendering performance trade-offs with the earlier results in the literature [13, 20].

The effects of filtering on the actuator velocity feedback to attenuate either the analog sensor noise, or to attenuate the quantization noise amplification caused by the real-time estimation of the velocity has been studied for linear spring and null impedance rendering of SEA. We have shown that filtering the actuator velocity feedback increases the haptic rendering performance of SEA, by reducing the parasitic damping while the passively realizable virtual stiffness range is not negatively impacted. On the other hand we have shown that, through a rearrangement of the block diagram, utilization of a low-pass filter on the actuator velocity feedback

results in noise amplification on the torque controller of the VSIC by introducing a derivative gain. When an additional low-pass filter is introduced to the torque loop of the VSIC to attenuate the noise in the torque controller, haptic rendering performance is further enhanced at the cost of introducing a lower bound to the passively realizable virtual stiffness range, resulting in a stability robustness and haptic rendering performance trade-off. Our contributions include extending the sufficient conditions for the passivity given in [17], by deriving the necessary and sufficient conditions for the passivity, providing intuitive understanding through the rearrangement of the block diagram to why if the actuator velocity feedback is filtered then the force controller is also required to be filtered as shown numerically in [16] and we conclude that the upper bound on the range of passively renderable stiffness levels improve as the cut-off frequency of the low-pass filter increases while the lower bound can be improved as the time constant of the controller approaches the mechanical time constant of the system.

We study the phase response of haptic rendering of SEA by introducing phase altering filters to the torque loop of the VSIC. We utilize lag compensators to introduce negative phase and lead compensators to introduce positive phase to the system. On both cases it has been observed that the passively realizable stiffness levels are lower than the case where no positive or negative phase is introduced to the system. Through the derived passive physical equivalents we show that for linear spring rendering of SEA under VSIC, lead compensation results in a decrease in haptic rendering performance while lag compensation results in an increase in haptic rendering performance by respectively increasing and decreasing the parasitic damping. Previously it had been shown that addition of negative phase via an integral gain to the torque controller of VSIC results in increased haptic rendering performance [20], however requires an additional integral gain in the motion control loop resulting in over-complications in the implementation process. By disposing of the integral gain on the motion controller and introducing roll-off characteristics to the torque controller similar to [4], the proposed system results in favorable stability robustness and haptic rendering performance characteristics.

We study the reference shaping to ensure trackability and causality by introducing roll-off characteristics to the impedance model. We study the stability robustness and haptic rendering performance trade-offs of SEA under VSIC while rendering linear combinations of linear parallel mass-spring-damper. For the virtual environment that consists of a linear spring that is filtered to roll off the high-frequency content of the reference input, it is observed that cut-off frequency can be chosen such that the parasitic damping becomes equal to zero, without inducing more conservative passivity criteria. Next we study the case where the reference virtual envoirnment consists of parallel mass-spring-dampers and the high frequency content of the reference impedance converges to a linear spring, the open-loop response of the SEA, as studied in [22]. Through rigorously derived necessary and sufficient conditions for the passivity we show that rolling-off of the reference damper and mass models and a decreasing of the cut-off frequency, increases passively realizable mass and damper levels, extending the safe region for human-robot interaction as studied for the case of explicit force control in [21]. Through the passive physical equivalents we also show that the decrease in the cut-off frequency decreases the haptic rendering performance, resulting in a stability robustness and haptic rendering performance trade-off. We further showed that with filtering damping rendering and Voigt model rendering of SEA under VSIC becomes passively realizable which otherwise only allows for passive compensation [30]. We also showed that the minimum passively renderable mass is equal to mass of the plant without the inclusion of mass in the rendered virtual envoirnment, however reducing the passively renderable mass is possible by including damping to the rendered virtual environment.

We performed systematic simulations to show stability robustness and haptic rendering performance trade-offs induced by filtering for: (i) attenuation of the high frequency sensor noise, (ii) shaping the phase response of the haptic system by introducing filters as compensators and (iii) o shape the dynamics of the reference model to ensure its trackability and causality by introducing high-frequency roll-off characteristics. We experimentally validated our results through real-time experiments utilizing a single degree-of-freedom haptic interface. We conduct a

psycho-physics experiment to showcase how phase addition through filtering increases the performance of perception of haptic interaction.

As a part of our ongoing work, we study the effects of non-collocation in SEA as the sensor stiffness increases, we study the effects of feed-forward terms in haptic rendering performance and we study stability robustness and haptic rendering performance of other controllers [47].

We plan to extend our understanding of haptic rendering to admittance type controllers [36] and study the fundamental limitations of haptic rendering [28].

Bibliography

[1] S. Eppinger and W. Seering, "Understanding bandwidth limitations in robot force control," in *Proceedings. 1987 IEEE International Conference on Robotics and Automation*, vol. 4, pp. 904–909, 1987.

[2] W. S. Newman, "Stability and Performance Limits of Interaction Controllers," *Journal of Dynamic Systems, Measurement, and Control*, vol. 114, pp. 563–570, 12 1992.

[3] R. D. Howard, *Joint and actuator design for enhanced stability in robotic force control*. PhD thesis, MIT, 1990.

[4] G. A. Pratt and M. M. Williamson, "Series elastic actuators," in *IEEE Int. Conf. on Intelligent Robots and Systems*, vol. 1, pp. 399–406, 1995.

[5] J. W. Sensinger and R. F. Weir, "Unconstrained impedance control using a compact series elastic actuator," in *2006 2nd IEEE/ASME International Conference on Mechatronics and Embedded Systems and Applications*, pp. 1–6, 2006.

[6] D. Robinson, J. Pratt, D. Paluska, and G. Pratt, "Series elastic actuator development for a biomimetic walking robot," in *1999 IEEE/ASME International Conference on Advanced Intelligent Mechatronics (Cat. No.99TH8399)*, pp. 561–568, 1999.

[7] G. Wyeth, "Demonstrating the safety and performance of a velocity sourced series elastic actuator," in *2008 IEEE International Conference on Robotics and Automation*, pp. 3642–3647, 2008.

[8] J. E. Colgate and N. Hogan, "Robust control of dynamically interacting systems," *International Journal of Control*, vol. 48, no. 1, pp. 65—-88, 1988.

[9] N. Colonnese and A. M. Okamura, "M-width: Stability, noise characterization, and accuracy of rendering virtual mass," *The International Journal of Robotics Research*, vol. 34, no. 6, pp. 781–798, 2015.

[10] J. Mehling, J. Colgate, and M. Peshkin, "Increasing the impedance range of a haptic display by adding electrical damping," in *First Joint Eurohaptics Conference and Symposium on Haptic Interfaces for Virtual Environment and Teleoperator Systems. World Haptics Conference*, pp. 257–262, 2005.

[11] Y. Aydin, O. Tokatli, V. Patoglu, and C. Basdogan, "A computational multicriteria optimization approach to controller design for physical human-robot interaction," *IEEE Transactions on Robotics*, vol. 36, no. 6, pp. 1791–1804, 2020.

[12] E. Colgate and N. Hogan, "An analysis of contact instability in terms of passive physical equivalents," in *Proceedings, 1989 International Conference on Robotics and Automation*, pp. 404–409 vol.1, 1989.

[13] C. U. Kenanoglu and V. Patoglu, "Passive realizations of series elastic actuation: Passivity and effects of plant and controller dynamics on haptic rendering performance," *CoRR*, 2022.

[14] R. Volpe and P. Khosla, "The equivalence of second order impedance control and proportional gain explicit force control: Theory and experiments," in *Experimental Robotics II*, pp. 1–24, Springer, 1993.

[15] R. Volpe and P. Khosla, "A theoretical and experimental investigation of explicit force control strategies for manipulators," *IEEE Trans. on Automatic Control*, vol. 38, no. 11, pp. 1634–1650, 1993.

[16] M. Dohring and W. Newman, "The passivity of natural admittance control implementations," in *IEEE Int. Conf. on Robotics and Automation*, vol. 3, pp. 3710–3715, 2003.

[17] H. Vallery, R. Ekkelenkamp, H. Van Der Kooij, and M. Buss, "Passive and accurate torque control of series elastic actuators," in *IEEE/RSJ Int. Conf. on Intelligent Robots and Systems*, pp. 3534–3538, 2007.

[18] R. Volpe, *Real and artificial forces in the control of manipulators: theory and experiments*. PhD thesis, Carnegie Mellon, 1990.

[19] F. Sergi and M. K. O'Malley, "On the stability and accuracy of high stiffness rendering in non-backdrivable actuators through series elasticity," *Mechatronics*, vol. 26, pp. 64–75, 2015.

[20] F. E. Tosun and V. Patoglu, "Necessary and sufficient conditions for the passivity of impedance rendering with velocity-sourced series elastic actuation," *IEEE Trans. on Robotics*, vol. 36, no. 3, pp. 757–772, 2020.

[21] H. Qian and J. De Schutter, "Stabilizing robot force control through low pass filtering with low cut off frequency," in *[1992] Proceedings of the 31st IEEE Conference on Decision and Control*, pp. 1893–1896 vol.2, 1992.

[22] W. S. Newman, "Stability and performance limits of interaction controllers," *Journal of Dynamic Systems, Measurement, and Control*, vol. 114, no. 4, pp. 563—-570, 1992.

[23] I. Kolmanovsky, E. Garone, and S. Di Cairano, "Reference and command governors: A tutorial on their theory and automotive applications," in *2014 American Control Conference*, pp. 226–241, 2014.

[24] A. M. . S. G. Kapasouris, P., "Design of feedback control systems for unstable plants with saturatingactuators," in *IFAC IEEE Symposium Nonlinear Control System Design*, pp. 302–307, 1990.

[25] E. Gilbert, I. Kolmanovsky, and K. T. Tan, "Nonlinear control of discrete-time linear systems with state and control constraints: a reference governor with global convergence properties," in *Proceedings of 1994 33rd IEEE Conference on Decision and Control*, vol. 1, pp. 144–149 vol.1, 1994.

[26] M. N. Emanuele Garone and L. Ntogramatzidis, "Explicit reference governor for linear systems," *International Journal of Control*, vol. 91, no. 6, pp. 1415–1430, 2018.

[27] K. Merckaert, B. Vanderborght, M. M. Nicotra, and E. Garone, "Constrained control of robotic manipulators using the explicit reference governor," in *2018 IEEE/RSJ International Conference on Intelligent Robots and Systems (IROS)*, pp. 5155–5162, 2018.

[28] P. G. Griffiths, R. B. Gillespie, and J. S. Freudenberg, "A fundamental linear systems conflict between performance and passivity in haptic rendering," *IEEE Transactions on Robotics*, vol. 27, no. 1, pp. 75–88, 2011.

[29] H. Vallery, J. Veneman, E. Van Asseldonk, R. Ekkelenkamp, M. Buss, and H. Van Der Kooij, "Compliant actuation of rehabilitation robots," *IEEE Robotics and Automation Magazine*, vol. 15, no. 3, pp. 60–69, 2008.

[30] N. L. Tagliamonte and D. Accoto, "Passivity constraints for the impedance control of series elastic actuators," *Institution of Mechanical Engineers, Part I: Journal of Systems and Control Engineering*, vol. 228, no. 3, pp. 138–153, 2014.

[31] A. Calanca, R. Muradore, and P. Fiorini, "Impedance control of series elastic actuators: Passivity and acceleration-based control," *Mechatronics*, vol. 47, pp. 37–48, 2017.

[32] U. Mengilli, U. Caliskan, Z. O. Orhan, and V. Patoglu, "Two-port analysis of stability and transparency in series damped elastic actuation," *CoRR*, 2020.

[33] U. Mengilli, Z. O. Orhan, U. Caliskan, and V. Patoglu, "Passivity of series damped elastic actuation under velocity-sourced impedance control," in *IEEE World Haptics Conference*, pp. 379–384, 2021.

[34] E. Colgate and N. Hogan, "An analysis of contact instability in terms of passive physical equivalents," in *International Conference on Robotics and Automation*, vol. 1, pp. 404–409, 1989.

[35] J. S. Hart and G. Niemeyer, "Absolutely stable model-based 2-port force controller for telerobotic applications," *Int. J. Robotics Res.*, vol. 33, no. 6, pp. 847–865, 2014.

[36] A. Q. Keemink, H. van der Kooij, and A. H. Stienen, "Admittance control for physical human–robot interaction," *The International Journal of Robotics Research*, vol. 37, no. 11, pp. 1421–1444, 2018.

[37] J. J. Gil, Rubio, and J. Savall, "Decreasing the apparent inertia of an impedance haptic device by using force feedforward," *IEEE Transactions on Control Systems Technology*, vol. 17, no. 4, pp. 833–838, 2009.

[38] G. Aguirre-Ollinger, J. E. Colgate, M. A. Peshkin, and A. Goswami, "Inertia compensation control of a one-degree-of-freedom exoskeleton for lower-limb assistance: Initial experiments," *IEEE Transactions on Neural Systems and Rehabilitation Engineering*, vol. 20, no. 1, pp. 68–77, 2012.

[39] I. Desai, A. Gupta, and D. Chakraborty, "Rendering mass using model matching framework," in *IEEE Haptics Symposium*, pp. 46–51, 2018.

[40] S. Haykin, *Active network theory*. Addison-Wesley Pub. Co., 1970.

[41] M. Z. Chen, C. Papageorgiou, F. Scheibe, F.-c. Wang, and M. C. Smith, "The missing mechanical circuit element," *IEEE Circuits and Systems Magazine*, vol. 9, no. 1, pp. 10–26, 2009.

[42] R. M. Foster, "A reactance theorem," *The Bell System Technical Journal*, vol. 3, no. 2, pp. 259–267, 1924.

[43] O. Brune, "Synthesis of a finite two-terminal network whose driving-point impedance is a prescribed function of frequency," 1931.

[44] U. Caliskan, A. Apaydin, A. Otaran, and V. Patoglu, "A series elastic brake pedal to preserve conventional pedal feel under regenerative braking," in *2018 IEEE/RSJ International Conference on Intelligent Robots and Systems (IROS)*, pp. 1367–1373, 2018.

[45] J. Mehling, J. Colgate, and M. Peshkin, "Increasing the impedance range of a haptic display by adding electrical damping," in *IEEE World Haptics Conf.*, pp. 257–262, 2005.

[46] N. Colonnese, A. F. Siu, C. M. Abbott, and A. M. Okamura, "Rendered and characterized closed-loop accuracy of impedance-type haptic displays," *IEEE Trans. on Haptics*, vol. 8, no. 4, pp. 434—446, 2015.

[47] C. U. Kenanoglu and V. Patoglu, "Passivity of series elastic actuation under model reference force control during null impedance rendering," *IEEE Transactions on Haptics*, vol. 15, no. 1, pp. 51–56, 2022.